# The role of HMGB1 in the innate immune response to *Listeria monocytogenes*

Dissertation
to obtain the academic degree of
Doctor of Natural Sciences (Dr. rer. nat.)

submitted to the Department of Biology of the Faculty of Mathematics, Informatics and Natural Sciences at the University of Hamburg

by
**Annika Volmari**
from Hamburg

Hamburg, December 2019

This doctoral dissertation was supervised by Dr. med. Peter Hübener and performed at the I. Department of Internal Medicine, University Medical Center Hamburg-Eppendorf, in Hamburg, Germany from May 2015 until May 2019.

Vorsitzender der Prüfungskommission: Prof. Dr. rer. nat. Jörg Ganzhorn
1. Gutachter: Prof. Dr. rer. nat. Johannes Herkel
2. Gutachter: Prof. Dr. rer. nat. Wolfgang Streit
weiteres Mitglied der Prüfungskommission: PD Dr. rer. nat. Hartwig Lüthen

Termin der Disputation: 09.12.2022

## Abstract

High-mobility group box 1 (HMGB1), a paradigmatic damage-associated molecular pattern (DAMP), is a major proinflammatory factor following tissue damage. Release following necroptotic cell death or active secretion by immunocompetent cells induces the infiltration of immune cells and inflammatory responses. HMGB1 has repeatedly been suggested as a potent therapeutic target for inflammatory and infectious diseases like polymicrobial abdominal sepsis or bacterial and viral infections. However, it has not been clearly established from which cells HMGB1 originates during inflammation and whether relevant functions arise from extracellular HMGB1 or the involvement in intracellular processes like autophagy. Due to the recent availability of cell-specific knockouts, these analyses are now possible. Therefore, the aim of this thesis was to investigate the role and cellular origin of HMGB1 in the initiation of the innate immune response following infection with *Listeria monocytogenes*, a well-established model for gram-positive bacterial infection, in order to further elucidate the cell-specific function of HMGB1 and its applicability as a therapeutic target.

Using cell-specific knockout mice of HMGB1, this study could show that while hepatocyte-derived HMGB1 is dispensable for the innate immune response to a controlled infection with *Listeria monocytogenes*, antibody-mediated neutralization and myeloid cell-specific ablation of HMGB1 (*Hmgb1*$^{\Delta LysM}$) led to uncontrolled infection and exacerbated hepatic inflammation, which is characterized by increased gene expression of proinflammatory mediators and aggravated tissue damage. Previous postulations that HMGB1 ablation caused defects in phagocyte autophagy, resulting in impaired bacterial clearance and attenuated immune responses, were largely ruled out as the cause for uncontrolled *Listeria* infection in the experimental settings in this work. Instead, it was observed that myeloid cell-specific ablation of HMGB1 resulted in increased hepatic infiltration of neutrophils and decreased infiltration of proinflammatory monocytes into the liver early after infection. Proinflammatory monocytes have been shown to differentiate into tumor necrosis factor and inducible nitric-oxide synthase-producing dendritic cells (Tip-DCs) and type 1 (M1) monocyte-derived macrophages in the liver and the reduced number of these cells presumably results in the hampered containment of *Listeria*, which likely accounts for the more severe infection in *Hmgb1*$^{\Delta LysM}$ mice. While this early effect of HMGB1 depletion could be the reason for increased hepatic bacterial titers, the subsequent accumulation of dead cells within the granulomas of *Hmgb1*$^{\Delta LysM}$ mice could then lead to the exacerbation of inflammation and infection by enhancing bacterial pathogenesis. Adoptive transfer of *Hmgb1*-deleted cells demonstrated that tissue-resident and circulating immune cells contribute to infection control in the liver.

Overall, this study demonstrates the critical importance of HMGB1 signaling originating from myeloid cells during the systemic infection with *Listeria monocytogenes*, while establishing the highly context-dependent nature of HMGB1 activity during infection and inflammation.

# Zusammenfassung

High-mobility group box 1 (HMGB1), ein paradigmatisches damage-associated molecular pattern (DAMP), ist ein wichtiger proinflammatorischer Faktor nach Gewebeschäden. Die Freisetzung nach nekrotischem Zelltod oder die aktive Sekretion durch immunkompetente Zellen induziert die Infiltration von Immunzellen und anschließende Entzündungsreaktionen. HMGB1 wurde wiederholt als wirksames therapeutisches Ziel für entzündliche und infektiöse Erkrankungen wie polymikrobielle abdominelle Sepsis oder bakterielle und virale Infektionen vorgeschlagen. Es ist jedoch nicht eindeutig geklärt, welches die Ursprungszellen von HMGB1 während der Entzündung sind und ob die Funktion von HMGB1 eher extrazellulär besteht oder aus der Beteiligung an intrazellulären Prozessen wie der Autophagie resultiert. Aufgrund der kürzlichen Verfügbarkeit von zellspezifischen Knockout-Mäusen sind Analysen zur Klärung dieser Fragen jetzt möglich. Ziel dieser Arbeit war es daher, die Rolle und den zellulären Ursprung von HMGB1 bei der Auslösung der angeborenen Immunantwort nach einer Infektion mit *Listeria monocytogenes*, einem etablierten Modell für eine grampositive bakterielle Infektion, zu untersuchen, um die zellspezifische Funktion von HMGB1 und seine Eignung als Ziel therapeutischer Interventionen zu untersuchen.

Unter Verwendung von zellspezifischen Knockout-Mäusen von HMGB1 konnte diese Studie zeigen, dass HMGB1 aus Hepatozyten für die angeborene Immunantwort auf eine kontrollierte Infektion mit *Listeria monocytogenes* entbehrlich ist. Im Gegensatz dazu führte die durch Antikörper vermittelte Neutralisierung bzw. die Depletion von HMGB1 in myeloiden Zellen (*Hmgb1*$^{\Delta LysM}$) zu einer unkontrollierten Infektion sowie Leberentzündung, die sich durch erhöhte Genexpression proinflammatorischer Mediatoren und verstärkte Gewebeschädigung auszeichnete. Frühere Annahmen, dass die Depletion von HMGB1 zellintrinsische Defekte in der Induktion von Autophagie in Phagozyten im Kontext von Infektionen verursacht und die Immunantwort beeinträchtigt, wurden als Ursache für eine erhöhte Listerien-Infektion in dieser Arbeit weitgehend ausgeschlossen. Stattdessen wurde beobachtet, dass die zellspezifische Deletion von HMGB1 in myeloiden Zellen zu einer erhöhten Infiltration von Neutrophilen und zusätzlich zu einer verminderten Infiltration von proinflammatorischen Monozyten führte. Proinflammatorische Monozyten differenzieren im Zielgewebe zu tumor necrosis factor and inducible nitric-oxide synthase-producing dendritic cells (Tip-DCs) und type 1 (M1) monocyte-derived macrophages, und die verringerte Anzahl dieser Zellen führt potentiell zu einer beeinträchtigten bakteriellen Eindämmung und liefert daher eine Begründung für die schwerwiegendere Infektion bei den *Hmgb1*$^{\Delta LysM}$ Mäusen. Während dieser frühe Effekt der HMGB1-Depletion der Grund für eine verminderte frühe immunologische Kontrolle der

Infektion sein könnte, könnte die anschließende Akkumulation toter Zellen innerhalb der Granulome von *Hmgb1*$^{\Delta LysM}$ Mäusen zu einer Verschärfung der Entzündung und Infektion führen. Der adoptive Transfer von Hmgb1-deletierten Zellen zeigte zusätzlich, dass sowohl Gewebe-residente als auch zirkulierende Immunzellen zur Infektionskontrolle in der Leber beitragen.

Zusammenfassend konnte diese Studie die entscheidende Bedeutung der HMGB1-Signalübertragung ausgehend von myeloiden Zellen während der systemischen Infektion mit *Listeria monocytogenes* belegen, während gleichzeitig die kontextabhängige Aktivität von HMGB1 während der Infektion und Entzündung gezeigt wurde.

# Table of content

# Table of figures

# Table of tables

# Abbreviations

| | |
|---|---|
| ACK | ammonium-chloride-potassium |
| ActA | actin assembly-inducing protein |
| APC | antigen presenting cell |
| BCA | bicinchoninic acid |
| BH3 | B cell lymphoma 2 (Bcl-2) homology domain 3 |
| BMDM | bone marrow-derived macrophage |
| BSA | bovine serum albumin |
| CCL2 | chemokine (C-C motif) ligand 2; monocyte chemoattractant protein 1 (MCP1) |
| CCR2 | C-C chemokine receptor type 2; CD192 |
| CD | cluster of differentiation |
| CD11b | integrin alpha M (ITGAM) |
| CD11c | integrin alpha X (ITGAX) |
| CDH1 | cadherin-1 |
| cDNA | complementary DNA |
| CFU | colony forming unit |
| $C_T$ | cycle threshold |
| Ctrl | control |
| CXCL12 | C-X-C motif chemokine 12; stromal cell-derived factor 1 |
| CXCR4 | C-X-C chemokine receptor type 4; fusin; CD184 |
| DAMP | damage-associated molecular pattern |
| DC | dendritic cell |
| $ddH_2O$ | double-distilled water |
| DNA | deoxyribonucelic acid |
| EDTA | ethylenediaminetetraacetic acid |
| ELISA | enzyme-linkes immunosorbent assay |
| EtOH | ethanol |
| FACS | fluorescence-activated cell sorting, flow cytometry |
| FBS | fetal bovine serum |
| FDR | false discovery rate |
| h.p.i. | hours post infection |
| $H_2O_2$ | hydrogen peroxide |

| | |
|---|---|
| HCV | hepatitis C virus |
| HKLM | heat-killed *Listeria monocytogenes* |
| HMGB1 | high mobility group box 1 |
| HRP | horseradish peroxidase |
| IFN-γ | interferon gamma |
| IgG | immunoglobulin G |
| IL | interleukin |
| InlA | Internalin A |
| InlB | Internalin B |
| iNOS | inducible nitric-oxide synthase |
| INS | infectious-nonself model |
| $KHCO_3$ | potassium bicarbonate |
| LC3 | microtubule-associated protein 1A/1B-light chain 3 |
| LLO | Listeriolysin O |
| Lm | *Listeria monocytogenes* |
| LPS | lipopolysaccharide |
| Ly6C | lymphocyte antigen 6 complex, locus C |
| Ly6G | lymphocyte antigen 6 complex, locus G |
| M-CSF | macrophage colony-stimulating factor |
| MAPK | mitogen-activated protein kinase |
| MD2 | myeloid differentiation factor-2 |
| MEM | minimum essential medium |
| MET | tyrosine-protein kinase Met |
| mM | millimolar |
| MOI | multiplicity of infection |
| NaCl | sodium chloride |
| NF-κB | nuclear factor kappa-light-chain-enhancer of activated B cells |
| $NH_4Cl$ | ammonium chloride |
| NLS | nuclear localization sequence |
| NO | nitric oxide |
| PAMP | pathogen-associated molecular pattern |
| PBS | phosphate buffered saline |
| PBS-T | phosphate-buffered saline-Tween20 |
| PI3K | phosphoinositide 3-kinase |
| PMN | polymorphonuclear leukocytes; granulocyte |
| PMSF | phenylmethylsulfonyl fluoride |

| | |
|---|---|
| PRR | pattern recognition receptor |
| PVDF | polyvinylidene fluoride |
| qRT-PCR | qualitative real-time polymerase chain reaction |
| RAGE | receptor for advanced glycation endproducts |
| RIPA | radioimmunoprecipitation |
| RNA | ribonucleic acid |
| RPMI | Roswell Park Memorial Institute |
| RT | room temperature |
| SEM | standard error of the mean |
| SNS | self-nonself model |
| SPF | specific pathogen-free |
| SQSTM1 / p62 | sequestosome 1 |
| TBS-T | tris-buffered saline-Tween20 |
| TGF-β | transforming growth factor beta |
| Th1 cell | type 1 T helper cell |
| Tip-DC | TNF- and iNOS-producing dendritic cells |
| TLR | toll-like receptor |
| TNF | tumor necrosis factor |
| TRAIL | TNF-related apoptosis-inducing ligand |
| Tris/HCl | tris(hydroxymethyl)aminomethane hydrochloride |
| TSB | tryptic soy broth |
| TUNEL | terminal deoxynucleotidyl transferase dUTP nick and labeling |
| UNG | uracil-DNA glycosylase |

# I. Introduction

## 1. The Danger Model

For 60 years, a general concept in immunology was that the immune system differentiates between 'self' and 'non-self' for the induction of an immune response. This 'self-nonself model' (SNS), first proposed by F. M. Burnet, suggested that any foreign entity (non-self) induces an immune response in an organism, whereas endogenous factors (self) are not recognized by the immune system, and therefore do not lead to an immune response. Surface receptors on lymphocytes were stated to recognize foreign entities, thereby initiating immune responses. Self-reactive lymphocytes, on the other hand, would be eliminated at an early time point [1]. This theory was modified several times to accommodate new findings in immunology research, i.e., adding co-stimulatory signals by T helper cells [2] and antigen presenting cells (APCs) [3] in order to account for the possibility of autoimmunity by B and T cells. In 1989, C. A. Janeway proposed that otherwise dormant APCs are activated upon recognizing conserved pathogen-associated molecular patterns (PAMPs), common components on bacteria or viruses (e.g. lipopolysaccharide, LPS), via pattern recognition receptors (PRRs) and are thereby able to differentiate between 'infectious-nonself' and 'noninfectious-self'. This was termed the 'infectious-nonself model' (INS) [4]. And even though these models underwent multiple revisions to address several unanswered problems, inflammatory phenomena associated with autoimmunity, transplant rejection or the immunological clearance of cancer cells were not sufficiently explained by this model. These questions led to the development of the 'Danger Model' by P. Matzinger [5].

The 'Danger Model' proposes that the immune system is actually less focused on foreign entities but has evolved to respond to factors conferring non-physiological cell death, damage or stress. This means that the immune system, rather than differentiating whether an entity is foreign or not, reacts to alarm signals released by damaged tissue. Any intracellular component can potentially act as a danger signal (damage-associated molecular pattern, DAMP) upon active or passive release. In the absence of infection or tissue damage, DAMPs have physiological functions associated with the cell, and during controlled cell death (apoptosis), cellular components are degraded and endogenous damage signals are not released into the surroundings of dying cells. In contrast, during necrosis, a form of uncontrolled cell death, cellular components are released into the surroundings and alarm signals can subsequently activate adjacent immune cells. DAMPs are therefore not released by healthy cells or cells undergoing physiological cell death [6]. Both the 'INS model' and the 'Danger Model' assume

that APCs are activated by signals in their surroundings, either PAMPs or DAMPs, respectively, by binding to PRRs like toll-like receptors (TLRs), which induce signaling cascades within the cell that ultimately lead to the induction of an immune response. Using the Danger Model, several issues could be addressed by connecting cell death to the initiation of an immune response. For example, during ischemia and reperfusion injury, due to the absence of microorganisms termed 'sterile inflammation', DAMPs are released following tissue damage and elicit adverse effects [6]. This induction of an immune response in the absence of PAMPs could previously not be explained by the 'INS model'.

## 2. High-mobility group box 1

Damage-associated molecular patterns are defined as molecules that during homeostasis are immunologically inert, however, following tissue damage induce an immune response. Based on this, High-mobility box group 1 (HMGB1), a highly conserved nucleoprotein, has been described as a paradigmatic DAMP. Within the nucleus, HMGB1 functions as a DNA chaperone by transiently binding and bending DNA, and thereby enabling assembly of nucleosomes and regulating gene expression [7,8]. During necrotic cell death, but not apoptosis, HMGB1 is released into the extracellular milieu, where it induces an immune response (Fig. 1). HMGB1 adjuvanticity was demonstrated through its ability to activate dendritic cells (DCs) *in vitro* [9] as well as promote macrophage migration and reprogramming *in vivo* [10].

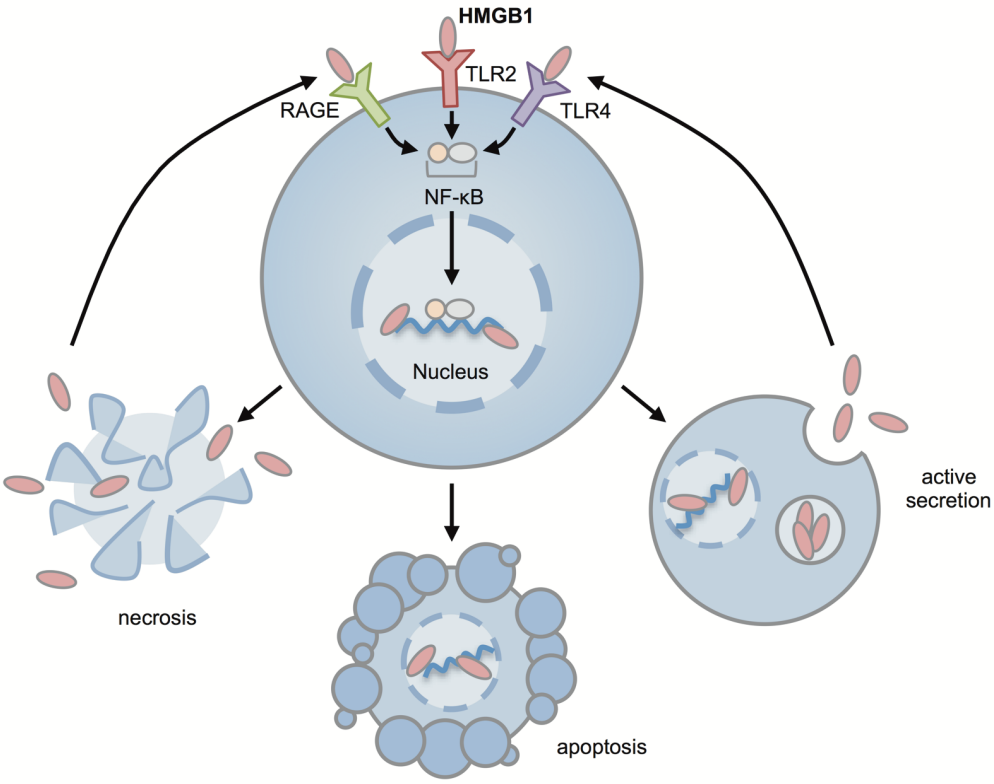


**Figure 1 | Roles of HMGB1.** During homeostasis, HMGB1 transiently binds DNA in the nucleus, thereby regulating gene expression. During necrotic cell death, HMGB1 is passively released into the extracellular space. Inflammation can induce active secretion of HMGB1 by immunocompetent cells. Extracellular HMGB1 then binds to pattern recognition receptors (e.g. RAGE, TLR2, TLR4) and induces gene expression of inflammatory mediators via NF-κB. In contrast to its inflammatory role, HMGB1 is retained during apoptotic cells death, resulting in non-immunogenic cell death. Adapted from Lotze and Tracey (2005) [11].

## 2.1. Regulation of HMGB1

HMGB1 consists of two DNA binding motifs, Box A and Box B, as well as an acidic C tail (Figure 2) [12]. Analysis of truncated forms of HMGB1 showed, that Box B elicits pro-inflammatory activity [13], whereas Box A displayed anti-inflammatory properties [14]. During homeostasis, HMGB1 is localized within the nucleus, where it is transiently bound to DNA. Due to two nuclear localization sequences (NLSs), HMGB1 is able to shuttle between the cytoplasm and the nucleus. Acetylation of HMGB1 at the NLS sites is necessary for active secretion, but it does not seem to change binding specificities or signaling activity of HMGB1 once it is released [15].

Whereas passive release of HMGB1 due to necrosis is a direct effect, active release via a specific secretory pathways is much slower [16]. Hyperacetylation of lysine residues within the two NLS sites prevents HMGB1 from shuttling back into the nucleus and leads to the accumulation of

HMGB1 in the cytoplasm [17]. Afterwards, HMGB1 is released into the extracellular space via programmed, pro-inflammatory cell death called pyroptosis [18,19] or via secretory lysosomes [16]. Acetylation of HMGB1 has been defined as a molecular signature of actively secreted HMGB1. Differentiation of passively and actively released HMGB1 in the serum still relies on mass spectrometry analysis. The differentiation of passive and active release of HMGB1 demonstrated that cell death is not necessary for the presence of extracellular HMGB1, but rather that its active secretion can also signal severe cell stress or the presence of PAMPs during an infection [8].

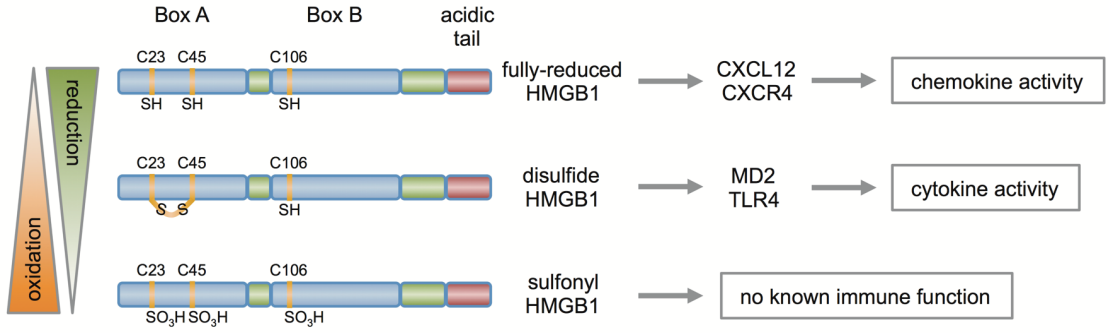


**Figure 2 | Regulation of HMGB1.** HMGB1 exists in three distinct isoforms with differing functions. Fully-reduced HMGB1, which has three cysteine thiol residues, forms a heterocomplex with CXCL12, binding to CXCR4 and resulting in chemotactic activity. Disulfide HMGB1 has a disulfide bond between cysteine residues C23 and C45 and signals via the TLR4/MD2 complex to induce inflammation. The third form, sulfonyl HMGB1, which possesses a sulfonyl-group on each of the three cysteine residues, does not have a known function in inflammation. Adapted from Antoine et al. (2014) [20].

The redox status of each of its three cysteine residues (C23 and C45 in Box A, and C106 in Box B), though, plays an essential role in receptor binding and biological activity. The nucleus und cytosol have a reducing redox potential, therefore HMGB1 within the cell is mainly the fully-reduced form, which has three cysteine thiol residues [21,22]. In contrast, the extracellular milieu has a more oxidizing potential, which is even further increased during inflammation. This leads to the formation of a disulfide bond between cysteines C23 and C45 upon release of HMGB1. Reactive oxygen species can then further oxidize the cysteines to sulfonates [22] (Fig. 2). These distinct molecular conformations result in different functions of each redox-form of HMGB1. Fully-reduced HMGB1 forms a heterocomplex with CXCL12, which binds CXCR4 and thereby elicits chemotactic activity, promoting cell migration and tissue invasion [23]. Similar to LPS, disulfide HMGB1 binds and signals via the TLR4/myeloid differentiation factor-2 (MD2) complex to induce NF-κB activation and subsequent cytokine expression and release [24-26].

Sulfonyl HMGB1 does not have an identified function within inflammation. The first identified receptor for HMGB1 was the receptor for advanced glycation endproducts (RAGE) [27]. By binding to this receptor, HMGB1 induces the nuclear translocation of NF-κB and a transient phosphorylation of MAP kinases, and the subsequent production of tumor necrosis factor (TNF) and nitric oxide (NO) [28,29]. Another study showed that signaling via RAGE leads to HMGB1 endocytosis and subsequent cell pyroptosis, leading to the release of pro-inflammatory factors, both *in vitro* and *in vivo* [30]. Additionally, activation of RAGE signaling is responsible for the secretion of chemokines, among others CXCL12 [31], which can subsequently form a heterocomplex with HMGB1 and induce a positive feedback loop within inflammation development.

### 2.2. HMGB1 in inflammation and regeneration

HMGB1 has been shown to initiate post-necrotic inflammation in various tissues, for example the skin [32], liver [33,34] and pancreas [35,36]. For instance, following ischemia and reperfusion injury in the liver, HMGB1 released from necrotic hepatocytes initiated neutrophil infiltration, which greatly amplified liver injury [34]. Neutralization of extracellular HMGB1 reduced the development of severe acute pancreatitis [35], LPS-induced septic shock [37] and lethality in polymicrobial abdominal sepsis [14]. In addition, studies have also suggested roles for HMGB1 during viral [38,39] and bacterial [40] infections. For example, secreted HMGB1 has been proposed to protect hepatocytes from Hepatitis C virus (HCV) infection by acting as an early warning signal for uninfected cells [39]. At an early time-point after infection with *Staphylococcus aureus*, antibody-mediated neutralization of HMGB1 resulted in attenuated lung pathology [40]. It has therefore been suggested that HMGB1 would be a potent therapeutic target for inflammation and infection.

In contrast to its role during sterile inflammation, HMGB1 has also been shown to confer tissue regeneration by stimulating stem cell migration and proliferation as well as angiogenesis [41,42]. H. Yanai et al. demonstrated a protective effect of intracellular HMGB1 for endotoxemia and bacterial infection [43]. Similarly, genetic ablation of HMGB1 did not alleviate inflammation or lethality following LPS-induced shock[34].

These differences in the effect of HMGB1 in varying settings may potentially be explained by the different redox forms of HMGB1. The three mutually exclusive isoforms of HMGB1 have been proposed to have sequential functions during inflammation. The initial release of fully-reduced HMGB1 leads to the infiltration of immune cells. The heterocomplex of CXCL12 and disulfide HMGB1 then activates these cells and induces the production and secretion of proinflammatory

cytokines and chemokines. Further oxidation of HMGB1 will then produce sulfonyl HMGB1 which inactivates the pro-inflammatory function of HMGB1 and enables regeneration of the tissue and return to homeostasis [22,44].

## 3. *Listeria monocytogenes*

Infection with *Listeria monocytogenes*, a Gram-positive bacterium first described in 1926 [45], which in the 1980s was identified as a food-borne pathogen [46], is a paradigmatic model of Gram-positive bacterial infection. The number of infections with *Listeria monocytogenes* per year is relatively low, but the mortality rate among *Listeria*-infected individuals is very high (20 - 30 %) [47]. *Listeria monocytogenes* is able to cross the blood-brain barrier and fetoplacental barrier, which makes it especially hazardous for pregnant women, where it can lead to abortion of the pregnancy or life threatening infection of the newborn [48].

After ingestion of *Listeria*-contaminated food by the host, the pathogen reaches the gastrointestinal tract, traverses the epithelial barrier and is then able to disseminate via the lymph and blood into its target organs, liver and spleen [49]. The bacteria are then either phagocytized by macrophages or enter epithelial cells by binding to cell surface molecules. Within the cells, *Listeria* are able to proliferate and thereby forego the recognition by the humoral immune system.

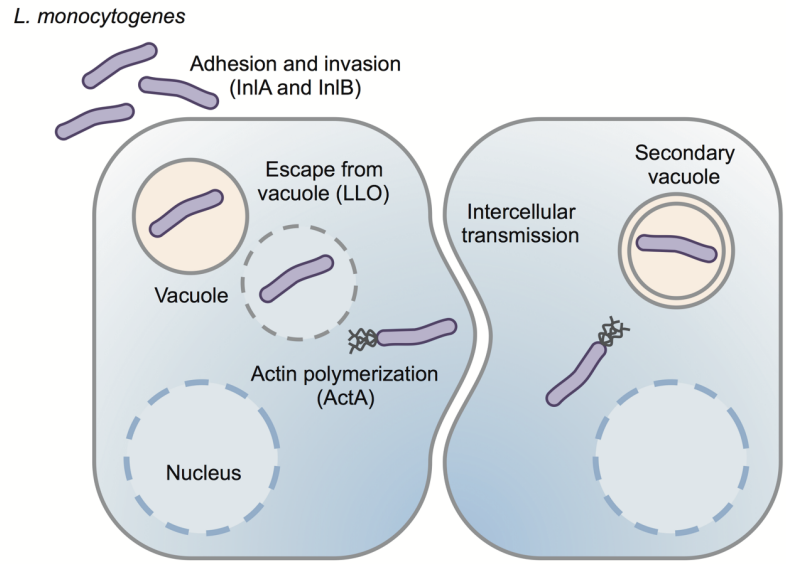


**Figure 3 | *Listeria monocytogenes* infection.** After reaching their target organs, *Listeria* enter their target cells either via phagocytosis or by binding to receptors with Internalin A (InlA) and Internalin B (InlB). Within the cell, Listeriolysin O (LLO) is then employed by the bacteria to physically disrupt the phagosome, enabling the escape of the bacteria into the cytoplasm. *Listeria* are then able to proliferate in the cytoplasm and use actin-based motility to move within the cell and spread from one cell to the next. Adapted from Pamer (2004) [50].

For the receptor-mediated entry into epithelial cells, *Listeria monocytogenes* employs the cell surface molecules Internalin A (InlA) and Internalin B (InlB). InlA binds Cadherin-1 (CDH1) on epithelial cells and induces changes in the cytoskeleton, which are essential for bacterial entry into the cell [51]. Whereas InlA has a high affinity for the human CDH1, it does not bind well to the murine version, which explains the low infection rate via the oral transmission route in mice [52]. InlB binds the tyrosine-protein kinase Met (MET) on hepatocytes, which subsequently activates phosphoinositide 3-kinase (PI3K) and mitogen-activated protein kinase (MAPK) [53]. Similar to the mechanism induced by InlA, activation of these kinases leads to changes in the actin-cytoskeleton, mediating vacuole formation and internalization of bacteria.

After phagocytosis or receptor-mediated entry into the cell, *Listeria monocytogenes* escapes from the phagosome into the cytoplasm by physically rupturing the vacuolar membrane via Listeriolysin O (LLO) [54]. *Listeria* within the cytosol proliferate and by exploiting actin-based motility are able to spread to neighboring cells, like hepatocytes. Actin assembly-inducing protein (ActA) polymerizes Actin on the bacterial cell surface, propelling bacteria through the cytoplasm and enabling cell-to-cell spread [55,56].

Since mice are not very susceptible to oral infection with *Listeria monocytogenes*, most studies employ intravenous injection of bacteria and therefore analyze immune responses to systemic

listeriosis, which is a well-characterized model of Gram-positive bacterial infection and therefore used in this study to analyze infectious inflammation.

## 4. Innate immune response following *Listeria* infection

Following infection with *Listeria monocytogenes*, initial immune responses are elicited via innate immune cells like macrophages, monocytes and neutrophils, which are essential for the survival of the host organism. Mice lacking both T cell and humoral immunity were shown to be able to control the initial infection, but were unable to clear the infection in the long run, demonstrating the importance of innate immunity in the early phase of infection [57].

The innate immune response is the first line of defense against pathogens, which is immediately activated upon infection. It is a very fast, relatively non-specific defense mechanism that induces inflammation. Cells of the innate immune response, for example macrophages, monocytes and neutrophils, are able to phagocytize and destroy pathogens. This initial control of the infection allows for the development of antigen-specific lymphocytes during the subsequent adaptive immune response, that are then able to fully eliminate pathogens and confer protective immunity, preventing reinfection [58].

After reaching the liver, *Listeria* are taken up by the liver-resident macrophages, called Kupffer cells. Phagocytosis of *Listeria* induces Kupffer cell necroptosis, which leads to the rapid infiltration of pro-inflammatory monocytes, expressing high levels of Ly6C (Ly6C$^{hi}$ monocytes), and neutrophils. At the site of infection, infiltrating neutrophils initially form microabscesses [59]. Infiltrating monocytes subsequently replace the dying neutrophils and form granulomas, which are characteristic for Listeriosis [60,61]. Histomorphologically, these granulomas correlate with the cell-mediated immune response to *Listeria monocytogenes*, and presumably act as a physical barrier, constraining the infectious foci and preventing further cell-to-cell spread of bacteria [62].

Recruitment of monocytes is controlled by the chemokine CCL2, which is produced during the early phase of *Listeria* infection in the liver. Binding to its receptor CCR2 on the surface of monocytes prompts their egress from the bone marrow and migration into the liver. After infiltrating the infected tissues, Ly6C$^{hi}$ monocytes differentiate into tumor necrosis factor and inducible nitric-oxide synthase-producing dendritic cells (Tip-DCs) and type 1 (M1) monocyte-derived macrophages.

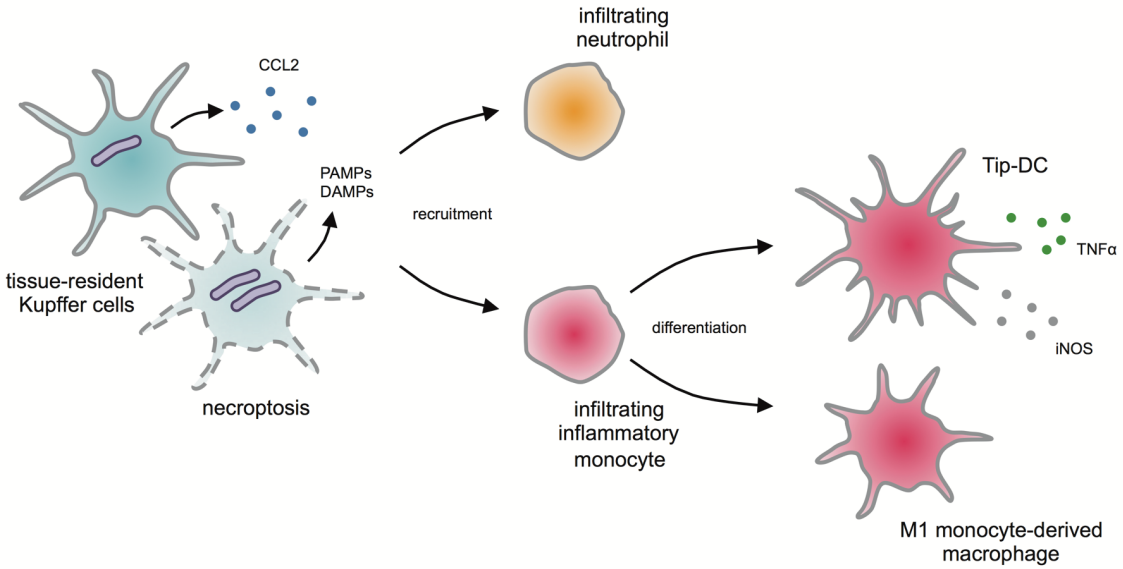


**Figure 4 | Innate immune responses following *Listeria monocytogenes* infection.** Tissue-resident Kupffer cells are the main targets of *Listeria monocytogenes* in the liver and infection leads to necroptotic cell death of these cells. Secretion of the chemokine CCL2 and the release of PAMPs and DAMPs triggers the infiltration of neutrophils and inflammatory monocytes, which initially differentiate into Tip-DCs and M1 monocyte-derived macrophages required for the immunological control of the infection, by producing TNFα and iNOS, among others.

Tip-DCs have been shown to play an integral part in increasing bacterial clearance [63-65] by producing tumor necrosis factor (TNF) and inducible nitric-oxide synthase (iNOS). TNF induces the activation of macrophages and monocytes and the production of further pro-inflammatory cytokines like interleukin-1β (IL-1β), interleukin-6 (IL-6) and interferon-γ (IFN-γ). Similar to TNF [66], IFN-γ is also essential for the initial defense against *Listeria* [67] and mice that lack either TNF or IFN-γ, or their respective receptors, are not able to control the infection [68-70]. Nitric oxide, synthesized by the enzyme iNOS, is able to efficiently enter cells due to it small size and subsequently induce apoptosis. This is especially important for the elimination of intracellular *Listeria*.

Whereas the indispensable role of infiltrating monocytes was demonstrated by inhibiting the recruitment of monocytes to the sites of infection by blocking the surface protein CD11b or knocking out CCR2, which led to increased susceptibility to infection [71,72], the neutralization of neutrophils during *Listeria* infection led to conflicting results. Where Shi et al. postulate that, in contrast to monocytes, neutrophils are dispensable for the anti-bacterial defense against systemic listeriosis [73], Carr et al. state that neutrophils are essential for the TNF-mediated immune response [74]. More recently, a study proposed more efficient bacterial containment by neutrophils in comparison to monocytes during *in vitro* studies.[75] In an attempt to

accommodate these studies, it has been suggested, that neutrophils are especially important in mice infected with higher doses of *Listeria* [74,76] and that they contribute more to the containment of the bacteria, by phagocytizing *Listeria* and limiting the spread, than the actual killing [77].

Taken together, the innate immune response towards *Listeria* consists of the initial production of pro-inflammatory cytokines by tissue-resident Kupffer cells and infiltrating monocytes, which leads to the production of IFN-γ, subsequently promoting phagocytosis of bacteria and bactericidal activity.

### 4.1 Differentiation of type 1 and 2 macrophages

Macrophages are classified into different subtypes, according to their role during inflammation and their production of cytokines.

Differentiation of infiltrating monocytes into M1 pro-inflammatory macrophages is driven by IFN-γ [78] and signaling via PRRs like TLR2 and TLR5 [79]. The pro-inflammatory phenotype of these cells is characterized by increased phagocytosis of pathogens and increased nitric oxide production by iNOS, an important effector molecule with bactericidal properties [80]. By additional secretion of pro-inflammatory cytokines and promotion of Th1 development, M1 macrophages induce a highly microbicidal environment. In contrast, M2 macrophages are generally considered to be anti-inflammatory and regenerative, and are divided into three subtypes. Most M2 macrophages correspond to the M2a subtype. Differentiation of M2a macrophages is induced by the cytokines IL-4 [81] and IL-13 [82]. The main effector of these cells is the enzyme arginase, which converts the amino acid arginine to ornithine, which can induce cell proliferation and repair [83]. Since arginase and iNOS compete for the same substrate, M2a macrophages are able to counterbalance the pro-inflammatory phenotype of M1 macrophages and shift the immune response towards tissue regeneration. In contrast to the categorization of T cells, macrophages are highly plastic and therefore, a clear distinction between the subtypes is not always possible. It is currently assumed that over the course of the *Listeria* infection, monocytes initially differentiate into pro-inflammatory M1 macrophages to reduce the bacterial burden in the liver, followed by the development of M2 macrophages in order to return the tissue to homeostasis [84].

## 5. Impact of cell death and autophagy on inflammation

Tissue damage and inflammation is generally followed by infiltration of immune cells as well as controlled cell death in order to remove damaged cells and enable tissue regeneration. During infection with *Listeria monocytogenes*, several cell death pathways, including programmed and non-programmed, play a role in the progression of the infection and induction of the immune response. *Listeria* has an almost exclusively intracellular lifecycle and is therefore able to escape the cellular and humoral immune response [74,85,86]. Necroptosis, a form of programmed necrosis or inflammatory cell death, has been proposed as a defense mechanism against intracellular pathogens [87]. The necroptotic death of Kupffer cells in the liver following *Listeria* infection leads to the release of intracellular components, which initially triggers the differentiation of M1 macrophages for bacterial clearance, followed by the development of M2 macrophages for tissue regeneration [84].

Programmed cell death, apoptosis, also plays a critical role in the pathogenesis of *Listeria monocytogenes*. Apoptosis is defined morphologically by cell rounding and shrinkage, chromatin condensation and, nuclear fragmentation and membrane blebbing [88]. During apoptosis, cells also undergo DNA fragmentation and their plasma membranes are inverted, exposing membrane-bound phosphatidylserine. Both lymphocytes [89] and hepatocytes [90,91] undergo apoptosis over the course of the infection with *Listeria monocytogenes*. Production of type I interferons during the early infection leads to lymphocyte apoptosis [92], which favors pathogen growth, since it is associated with the induction of an immunosuppressive state [93]. Impaired defense mechanisms promote the infection by facilitating the dissemination of intracellular bacteria. Mice deficient of the pro-apoptotic B cell lymphoma 2 homology domain 3 (BH3)-only proteins [94] or TNF-related apoptosis-inducing ligand (TRAIL) [95], respectively, showed a more efficient anti-bacterial immune response compared to control mice. Dead cells, that underwent apoptosis, are usually rapidly cleared by phagocytes, which is considered an anti-inflammatory process, or they undergo secondary necrosis, which is then considered a pro-inflammatory process [96].

Cells also induce autophagy during inflammation, a pro-survival process during which damaged cellular components are degraded to generate metabolites needed for cellular functions under conditions of substrate depravation or cellular stress [97]. Apoptosis and autophagy compete and interact within the cell due to common protein effectors that are needed for both pathways [98]. Autophagy is a mechanism for the cell to cope with stress, and can ultimately also end in apoptosis of the cell [99]. During autophagy, cytoplasmic components are enclosed in autophagosomes, and are ultimately degraded in matured autolysosomes [100], a process that

relies on the interaction of over 30 different proteins [101]. Autophagy can be beneficial during an infection, since it can control the replication of intracellular pathogens and control cytokine production and release [102-104]. Intracellular pathogens, like *Listeria monocytogenes*, have evolved mechanisms to selectively suppress autophagy and autophagy-induced intracellular degradation to induce their pathogenesis [102]. *Listeria*, for example, use ActA to prevent identification by ubiquitin ligases and autophagy adaptors, thereby circumventing autophagy and favoring their intracellular survival [105].

## 6. Aim of the thesis

It is generally assumed that the immune system differentiates between 'self' and 'non-self' to detect infection and initiate an immune response. By contrast, the danger theory incorporates noninfectious inflammatory processes, and is conceptually based on the immunological sensing of danger signals (damage-associated molecular patterns, DAMPs) – cellular components released by distressed or disintegrating cells that indicate tissue damage and trigger inflammation. During the course of an infection, pathogens cause tissue damage, consequently leading to the release of DAMPs. The specific functions of these alarm signals in contrast to pathogen-derived signals (pathogen-associated molecular signals, PAMPs) during the course of an infection and the ensuing immune response are incompletely understood. Previous studies showed that neutralization of HMGB1, a prototypical DAMP, conferred protection in various animal models of inflammation and also greatly reduced lethality during LPS-induced septic shock. However, the early postnatal lethality of HMGB1-knockout animals has long precluded functional analyses of the molecule *in vivo*. Surprisingly, findings from recently available mice with conditional HMGB1 deficiency have demonstrate unexpected intracellular functions of HMGB1 that are beneficial for the host in the context of infection. Therefore, the aim of this work was to analyze the role of HMGB1 during the systemic infection with *Listeria monocytogenes*, and to specifically address the question how genetic and pharmacological disruption of HMGB1-mediated injury sensing would interfere with anti-bacterial immune responses.

Using antibody-mediated and several genetic deletion models, the aim was to investigate the role of HMGB1 during the initiation of innate immune responses towards *Listeria monocytogenes in vivo*. Bacterial burden, immune cell activation and expression of inflammatory factors were determined in order to assess the induction of bacterial clearance and hepatic inflammation. To further elucidate the role of different cellular subsets, *in vitro* studies and bone

marrow transfer experiments were performed. Activation and functionality of macrophages and neutrophils were analyzed *in vitro*, employing different experimental setups and readouts, i.e. bacterial degradation or induction of apoptosis. Together, these findings might contribute to a better understanding of the interplay between HMGB1 and the innate immune system following bacterial infection.

# II. Materials and Methods

## 1. Materials

### 1.1 Instruments

| Instrument | Producer |
|---|---|
| accu-jet® pro | Brand GmbH + Co. KG, Germany |
| BD LSRFortessa™ | BD Biosciences, USA |
| Biowizard Xtra Line Clean Bench | Kojair®, Finland |
| Centrifuge 5424R | Eppendorf AG, Germany |
| Centrifuge 5810 | Eppendorf AG, Germany |
| Centrifuge MC 6 | Sarstedt, Germany |
| $CO_2$ Incubator KM-CC17RU2 | Panasonic Industry Europe GmbH, Germany |
| Cooled Incubator MIR-154-PE | Panasonic Industry Europe GmbH, Germany |
| Cryotome SLEE CUT 5062 | Thermo Scientific™, USA |
| Fusion FX Imager | Vilber Lourmat, France |
| Improved Neubauer Chamber | Hartenstein, Germany |
| Infinite® F50 microplate reader | Tecan Trading AG, Switzerland |
| Microscope BZ-X710 | Keyence, Japan |
| Microscope DM IL LED | Leica, Germany |
| Microtome HM 550 | Thermo Scientific™, USA |
| Microwave HMT882L | Bosch, Germany |
| Mini-PROTEAN Tetra Cell | BioRAD Laboratories, USA |
| Multipette® E3 | Eppendorf AG, Germany |
| nCounter® SPRINT Profiler | NanoString Technologies, Inc., USA |
| ND-1000 spectrophotometer | NanoDrop Technologies, USA |
| peqSTAR Thermocycler 732-3242 | peqlab, Germany |
| PowerPac™ Basic Power Supply | BioRAD Laboratories, USA |
| Research plus pipettes | Eppendorf AG, Germany |
| Semi-dry blotter | peqlab, Germany |

| | |
|---|---|
| Surgical instruments | Fine Science Tools, Inc., USA |
| T3 Thermocycler | Biometra®, Germany |
| Thermomixer Comfort | Eppendorf AG, Germany |
| Tuberoller RS-TR5 | Phoenix Instrument, Germany |
| Viia™ 7 System | Applied Biosystems™, USA |

**Table 1 | List of instruments.**

### 1.2. Reagents

| **General reagents** | **Producer** |
|---|---|
| 10x Annexin V Binding Buffer | BD Biosciences, USA |
| Acrylamide, Rotiphorese® gel 40 | Carl Roth GmbH + Co. KG, Germany |
| Albumin Fraktion V, biotinfrei | Carl Roth GmbH + Co. KG, Germany |
| Ammoniumchlorid | Sigma-Aldrich, Germany |
| Antibiotika/Antimykotika-Lsg. (100x) | Gibco™, USA |
| Antibody Diluent | Dako (Agilent), USA |
| Aprotinin | Sigma-Aldrich, Germany |
| Ammonium persulfate (APS) | AppliChem GmbH, Germany |
| Benzamidine | Sigma-Aldrich, Germany |
| Distilled Water Dnase/Rnase free | Invitrogen™, USA |
| Dithiothreitol (DTT) | Sigma-Aldrich, Germany |
| Dulbecco's Phosphate Buffered Saline (DPBS) | Sigma-Aldrich, Germany |
| EDTA Dinatriumsalz Dihydrat >99% | Carl Roth GmbH + Co. KG, Germany |
| EDTA-solution pH 8.0 (0.5 M) | AppliChem GmbH, Germany |
| Entellan® neu | Sigma-Aldrich, Germany |
| Eosin G-Lösung 0,5% wässrig | Carl Roth GmbH + Co. KG, Germany |
| Ethanol vergällt ≥99,8% | Carl Roth GmbH + Co. KG, Germany |
| Fetal Bovine Serum, heat inactivated | Gibco™, USA |
| Fluorescent Mounting Medium | Dako (Agilent), USA |
| Formaldehyde solution for molecular biology | Sigma-Aldrich, Germany |
| Gentamicin (10 mg/ml) | Gibco™, USA |

| | |
|---|---|
| Glycerol ReagentPlus® ≥99% (GC) | Sigma-Aldrich, Germany |
| Goat Serum (Normal) | Dako (Agilent), USA |
| Hemalum solution acid cc. to Mayer | Carl Roth GmbH + Co. KG, Germany |
| Histopaque 1077 | Sigma-Aldrich, Germany |
| Histopaque 1119 | Sigma-Aldrich, Germany |
| Hoechst 33258 | Invitrogen™, USA |
| Hydrogenperoxide 30% EMSURE® | Merck KGaA, Germany |
| Leupeptin | Sigma-Aldrich, Germany |
| Liquid DAB+ Substrate Chromogen System | Dako (Agilent), USA |
| LPS from E. coli | Sigma-Aldrich, Germany |
| M-CSF (Animal Free), rec. murine | PeproTech, Inc., USA |
| MEM Alpha Medium (1x) | Gibco™, USA |
| Methanol z.A. >99,8% | ChemSolute® (Th. Geyer), Germany |
| PageRuler™ Plus Prestained Protein Ladder, 10 to 250 kDa | Thermo Scientific™, USA |
| PE Annexin V | BD Biosciences, USA |
| Percoll | GE Healthcare Life Sciences, UK |
| Phenylmethanesulfonyl fluoride (PMSF) | Sigma-Aldrich, Germany |
| Potassium bicarbonate | Sigma-Aldrich, Germany |
| Protein Block Serum-Free | Dako (Agilent), USA |
| Proteinase K, recombinant PCR Grade | Roche Diagnostics GmbH, Germany |
| Recombinant mouse IFN-gamma (carrier-free) | BioLegend, Inc., USA |
| Roti®-Histofix 4% | Carl Roth GmbH + Co. KG, Germany |
| RPMI medium 1640 (1x) + GlutaMAX™ | Gibco™, USA |
| Skimmed milk powder | Spinnrad GmbH, Germany |
| Sodium chloride >99,8% | Carl Roth GmbH + Co. KG, Germany |
| Sodium dodecyl sulfate (SDS) | BioRAD Laboratories, USA |
| Sodium orthovanadate | Sigma-Aldrich, Germany |
| Sucrose | Sigma-Aldrich, Germany |
| Sulfuric acid 1 mol/l – 2N Maßlösung | Carl Roth GmbH + Co. KG, Germany |

| | |
|---|---|
| TaqMan™ Fast Advanced PCR Master Mix | Applied Biosystems™, USA |
| TaqMan™ Universal PCR Master Mix | Applied Biosystems™, USA |
| Tetramethylethylenediamine (TEMED) | Sigma-Aldrich, Germany |
| Tissue-Tek O.C.T.™ Compound | Sakura Finetek, Japan |
| Tri-sodium citrate dihydrate for analysis EMSURE® | Merck KGaA, Germany |
| Triton™ X-100 | Sigma-Aldrich, Germany |
| Trizma® hydrochloride | Sigma-Aldrich, Germany |
| Trypan Blue solution 0.4% for microscopy | Sigma-Aldrich, Germany |
| TSB Agar | Sigma-Aldrich, Germany |
| Tween®20 for molecular biology | AppliChem GmbH, Germany |
| UltraComp eBeads | Invitrogen™, USA |
| Xylol z.A. | ChemSolute® (Th. Geyer), Germany |

**Table 2 | List of general reagents.**

### 1.3. Commercial Assays

| **Kit** | **Producer** |
|---|---|
| BCA Protein Assay Kit | Pierce, USA |
| High-Capacity cDNA Reverse Transcription Kit | Applied Biosystems™, USA |
| HMGB1 ELISA | IBL International / Tecan, Germany / Switzerland |
| In Situ Cell Death Detection Kit, TMR red | Roche, Germany |
| Mouse IFN-gamma DuoSet ELISA | R&D Systems, Inc., USA |
| Mouse IL-1 beta/IL-1F2 DuoSet ELISA | R&D Systems, Inc., USA |
| nCounter® mouse myeloid innate immunity panel V2 | Nanostring Technologies, Inc., USA |
| NucleoSpin® RNA | Macherey Nagel GmbH und Co. KG, Germany |
| Substrate Reagent Pack | R&D Systems, Inc., USA |
| Super Signal West Dura Chemiluminescent Substrate | Pierce, USA |

**Table 3 | List of commercial assays.**

### 1.4. Software

| Software | Producer |
|---|---|
| Adobe Photoshop CS5 | Adobe Systems, USA |
| BD FACSDive™ Software | BD Biosciences, USA |
| Evolution Capt | Vilber Lourmat, France |
| FlowJo Software | Tree Star, Inc., USA |
| GraphPad Prism 8 | GraphPad, USA |
| Image Lab | BioRAD Laboratories, USA |
| ImageJ | ImageJ, USA |
| Magellan™ | Tecan Trading AG, Switzerland |
| QuantityOne Software | BioRAD Laboratories, USA |
| ViiA™ 7 System | Applied Biosystems™, USA |

**Table 4 | List of software.**

## 2. Methods

### 2.1. Experimental Models

#### 2.1.1. Animal studies

Mouse experiments performed during the course of this study were approved by the Behörde für Gesundheit und Verbraucherschutz of the Freie und Hansestadt Hamburg (Nr. 42/15). All experiments were carried out in strict accordance with the state guidelines. Mice were bred and kept in the Animal Research Facility at the University Medical Center Hamburg-Eppendorf. All Animals were kept under specific pathogen-free (SPF) conditions in individually ventilated cages, with water and food *ad libitum*.

For the *in vivo* studies, female littermates, ages 8-12 weeks old, were used. During infection experiments, mice were monitored daily and mice with signs of severe distress were euthanized to minimize suffering.

### 2.1.2. Strains and organisms

*Hmgb1*$^{f/f}$ mice were kindly provided by Robert Schwabe at Columbia University, New York, USA [106].

| Name | Background | |
|---|---|---|
| C57BL/6J | | Control group |
| *Hmgb1*$^{f/f}$ | B6.129S-Hmgb1tmRfs/J | Exons 2-4 of HMGB1 flanked by loxP sites (Fig. 8A); control group |
| *Hmgb1*$^{\Delta hep}$ | B6.129S-Hmgb1tmRfs/J x B6.Cg-Tg(Alb-cre)21Mgn/J | Hepatocyte-specific ablation of HMGB1 |
| *Hmgb1*$^{\Delta LysM}$ | B6.129S-Hmgb1tmRfs/J x B6.129P2-*Lyz2*$^{tm1(cre)Ifo}$/J | Myeloid cell-specific ablation of HMGB1 |

**Table 5 | Genetic background of mice.**

Cell specific knockouts were generated by crossing *Hmgb1*$^{f/f}$ mice with albumin-Cre [107] and Lyz2-Cre [108] mice, resulting in hepatocyte- (*Hmgb1*$^{\Delta hep}$) and myeloid cell-specific (*Hmgb1*$^{\Delta LysM}$) ablation of HMGB1 (Fig. 8).

### 2.1.3. Bacterial infection

Female mice between 8 and 12 weeks old were infected with 2 × $10^4$ wild type *Listeria monocytogenes*, strain EGD (Lm) [45] in 200 µl sterile PBS via tail vein injection. Bacterial inocula were controlled by serial dilutions and plating on tryptic soy agar. Plates were incubated overnight at 37 °C and colony forming units (CFU) were counted the next day. Mice were euthanized and analyzed 24 and 72 hours post infection (h.p.i.) (Fig. 5).

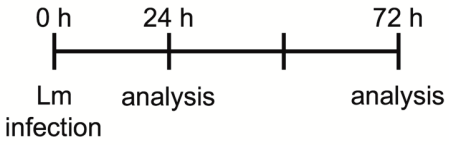


**Figure 5 | Experimental setup for *Listeria monocytogenes* infection.** Female mice were infected with 2 × $10^4$ wild type *Listeria monocytogenes* in 200 µl sterile PBS via i.v. injection. Bacterial burden and parameters of inflammation in the liver were analyzed 24 hours and 72 hours following infection.

As a readout for the infection, hepatic bacterial titers were determined. Small pieces of liver were mechanically homogenized in 0.1% Triton X-100 in $H_2O$. Suspensions were serially diluted and plated on TSB-agar plates. Plates were incubated at 37 °C overnight and CFUs were counted the next day to calculate the bacterial titer.

To inactivate the bacteria (heat-killed *Listeria monocytogenes*, HKLM), *Listeria* stock was incubated at 60 °C for 1 h. The sample was plated on TSB Agar to validate inactivation and subsequently stored at -80 °C.

### 2.1.4. *In vivo* depletion of HMGB1

Antibodies for the *in vivo* depletion of HMGB1 were kindly provided by Masahiro Nishibori and Hidenori Wake at Okayama University, Japan [109].

For the depletion of HMGB1, mice received daily doses of 100 µg of anti-HMGB1 antibodies or IgG control antibodies respectively for three consecutive days of the infection. Analysis was performed 72 hours after infection.

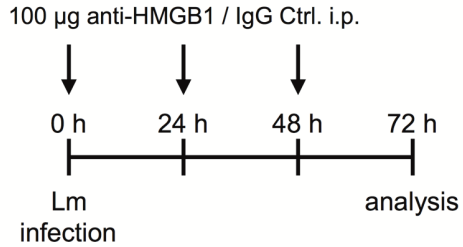


**Figure 6 | Experimental setup for antibody-mediated neutralization and *Listeria monocytogenes* infection.** Mice were infected with 2 × $10^4$ wild type *Listeria monocytogenes* in 200 µl sterile PBS via i.v. injection. Additionally, these mice received i.p. injections of 100 µg anti-HMGB1 or IgG control antibodies, respectively, on three consecutive days of the infection. Analysis was performed 72 hours post infection.

### 2.1.5. Bone marrow transplantation

For the generation of bone marrow chimera, bone marrow transfer was performed as described previously [106]. In short, bone marrow recipients were irradiated using 9 Gray for 10 min and received 4 × $10^6$ bone marrow cells (see section 2.2.4.) on the following day via tail vein injection. After 4 weeks of reconstitution, mice were infected with 2 × $10^4$ *Listeria monocytogenes*, as described previously (see section 2.1.3.).

## 2.2. Cellular biological methods

### 2.2.1. Isolation of intrahepatic immune cells

For the isolation of intrahepatic immune cells, the organ was passed through a 100 µm cell strainer into a 50 ml falcon tube, washed with PBS and placed on ice. The sample was brought to a total volume of 30 ml with cold PBS, centrifuged with 450 × g for 5 min at 4 °C, and the supernatant was discarded. The cells were then washed with 15 ml cold FACS buffer (2.5 % FBS in PBS), centrifuged with 450 × g for 5 min at 4 °C, and the supernatant was discarded. To isolate the immune cells from hepatocytes, the pellet was then resuspended in 37.5 % Percoll in FACS Buffer and the sample was centrifuged with 450 × g with the off-brake setting (accelerate: 2; decelerate: 0) for 30 min at RT. The supernatant was then carefully taken off without disturbing the pellet. The leukocyte-containing pellet was resuspended in 1 ml ACK Lysing Buffer (150 mM $NH_4Cl$, 10 mM $KHCO_3$, 0.1 mM EDTA) and incubated at room temperature for up to 10 min with frequent inversion in order to lyse the red blood cells in the sample. Afterwards, 10 ml FACS Buffer was added to the sample and it was centrifuged at 450 × g for 5 min at 4 °C. The supernatant was again discarded and the pellet was resuspended in 1 ml FACS Buffer for the subsequent cell counting and staining. In order to determine the cell number, samples were diluted using trypan blue and cells were counted using an improved Neubauer Chamber (Hartenstein, Germany).

### 2.2.2. FACS staining

For the extracellular FACS staining, samples were washed with 200 µl FACS buffer and centrifuged with 1700 rpm at RT for 3 min in FACS tubes. Supernatants were then discarded by decanting. The cells were resuspended in 100 µl PBS containing 1 µl Zombie Aqua dye (1:100, Biolegend, USA) for the live/dead cell staining. Samples were incubated at RT in the dark for 15 min. Afterwards, cells were washed and centrifuged, and the supernatant was discarded. Cells

were then incubated in Fc block solution containing an FcγIII/II receptor (CD16/CD32)-specific antibody (1:200) for 10 min at 4 °C to minimize background signals. Antibodies targeting extracellular markers (Biolegend, USA) were diluted in FACS buffer according to table 6 and added directly to the Fc block.

| Antibody | Final dilution | Clone |
|---|---|---|
| APC anti-mouse CD11b (101212) | 1:400 | M1/70 |
| PE anti-mouse CD11c (117308) | 1:200 | N418 |
| Purified anti-mouse CD16/32 (101302) | 1:400 | 93 |
| FITC anti-mouse F4/80 (123108) | 1:400 | BM8 |
| PE/Cy7 anti-mouse F4/80 (123114) | 1:400 | BM8 |
| PerCP/Cy5.5 anti-mouse Ly-6C (128012) | 1:800 | HK1.4 |
| Brilliant Violet 421™ anti-mouse Ly-6G (127628) | 1:400 | 1A8 |

**Table 6 | Flow cytometry antibodies.**

Samples were incubated an additional 20 min at 4 °C. Cells were washed and centrifuged again. The cells were then fixed using a 4% PFA solution for 10 min, washed and centrifuged. The supernatant was discarded and the samples were resuspended in 200 µl FACS buffer for flow cytometry analysis.

### 2.2.3. Flow cytometry analysis

Cell analysis was done using a BD LSRFortessa™ cell analyzer (BD Biosciences, USA). For the analysis, single color stainings of each fluorophore as well as unstained samples were prepared in order to compensate the fluorescent channels. Cellular events were acquired using BD FACSDiva™ software (BD Biosciences, USA) and subsequently analyzed using FlowJo software (Tree Star, Inc., USA). Gating strategies are shown in figure 7.

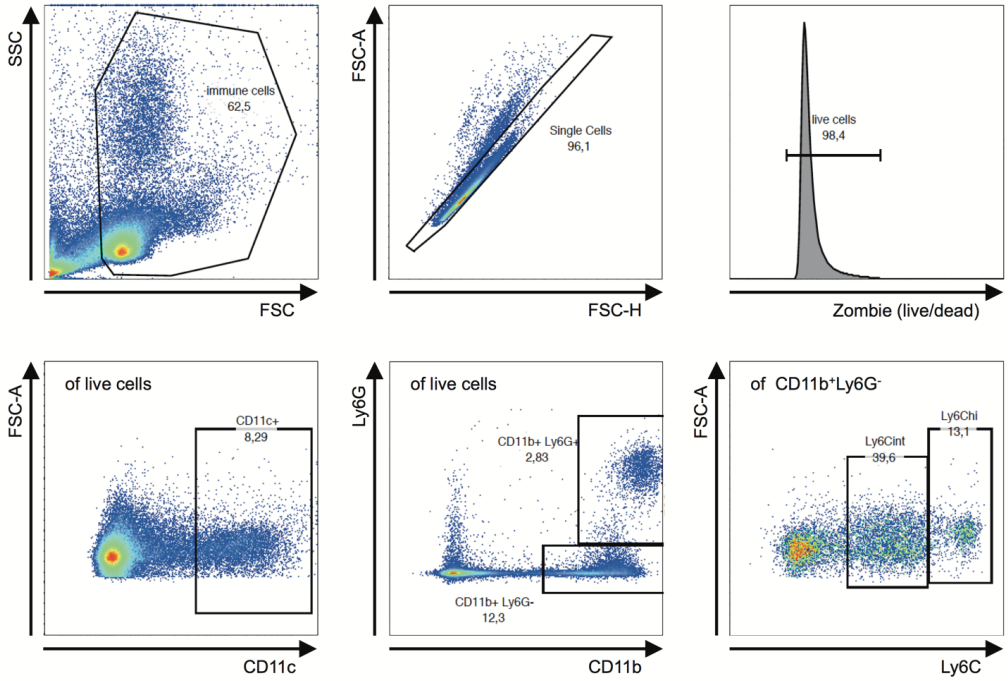


**Figure 7 | Gating strategy for flow cytometry analysis of intrahepatic immune cells.** Employing forward and sideward scatter, single immune cells are gated, followed by live cells using the live/dead cell marker Zombie. The lower panel shows the analysis of live immune cells. First, using an anti-CD11c antibody, the gate is used to separate $CD11c^+$ dendritic cells. The center scatter plot is used to differentiate $CD11b^+Ly6G^+$ neutrophils and $CD11b^+Ly6G^-$ monocytes. The latter are then further divided into $Ly6C^{low}$ and $Ly6C^{high}$ monocytes (lower right plot).

### 2.2.4 Isolation and differentiation of bone marrow-derived macrophages (BMDMs)

The bone marrow was isolated from the femurs of *Hmgb1*$^{f/f}$ and *Hmgb1*$^{\Delta LysM}$ mice and collected in a petri dish containing medium. The solution was transferred to a falcon tube and centrifuged for 10 min at 500 × g at RT. The cell pellet was resuspended in 5 ml supplemented MEM alpha medium (10 % FBS, 1 % antimicotic-antibiotic) without M-CSF, counted and diluted to a final concentration of 5 × $10^6$ cells/ml. Cells were then distributed at a concentration of 250.000 cells/well onto a 12-well tissue-culture plate in supplemented MEM alpha medium containing 10 ng/ml M-CSF and incubated at 37 °C. After two days, fresh medium was added to each well and after an additional two days, the cells were washed with PBS and fresh supplemented MEM alpha medium containing M-CSF was added. The cells were considered fully differentiated after 7 to 9 days of incubation with M-CSF.

### 2.2.5. Stimulation of BMDMs using *Listeria monocytogenes*

After 7 to 9 days of differentiation with M-CSF, bone marrow-derived macrophages were primed using IFN-γ (0.01 µg/ml) for 16 h at 37 °C. Stimulation of the cells was then done using live or heat-inactivated *Listeria monocytogenes* (MOI = 10) (see section 2.1.3.). Supernatant from the cells was collected and stored at -20 °C. RNA from cells was isolated according to section 2.3.1..

### 2.2.6. Gentamicin protection assay

In order to quantify bacterial entry, intracellular survival and replication, the gentamicin protection assay was performed as described previously [110]. Bone marrow-derived macrophages were washed three times with PBS to remove all traces of antibiotics from the cells and subsequently infected with *Listeria monocytogenes* (MOI = 10) and incubated for 1 h at 37 °C. The cells were then washed three times with PBS to remove extracellular bacteria and fully supplemented medium containing gentamicin (200 µg/ml) was added. After 30 min, cells were again washed with PBS. Cells in one part of the wells were then lysed using 0.1 % Triton X-100 in dd$H_2O$ and lysates were plated on TSB agar plates. This time point is considered 0 hours post infection. The rest of the wells containing cells were incubated for another 2 and 4 h respectively with fully-supplemented medium and then lysed and plated like the first time point. Agar plates were then incubated at 37 °C overnight and bacterial colonies subsequently quantified.

### 2.2.7. Isolation of bone marrow-derived neutrophils (PMNs)

For the isolation of bone marrow-derived polymorphonuclear neutrophils (PMNs), isolated bone marrow from femurs and tibias of *Hmgb1*$^{f/f}$ and *Hmgb1*$^{\Delta LysM}$ mice was suspended in medium (RPMI) supplemented with 2 mM EDTA and filtered through a 100 µm filter. The solution was centrifuged (500 × g, 7 min) and the supernatant subsequently discarded. Next, hypotonic lysis was performed in order to lyse the red blood cells. The pellet was resuspended in 5 ml of 0.2 % NaCl solution and after 20 s 5 ml of 1.6 % NaCl solution was added. The sample was then again centrifuged and the supernatant discarded. Afterwards, the cells were washed with medium supplemented with 1 mM EDTA, centrifuged and resuspended in 1 ml PBS. To separate the neutrophils from the rest of the cells, a gradient was performed. Histopaque 1119 (3 ml) was overlaid with Histopaque 1077 (3 ml), which in turn was overlaid with the cell suspension. The gradient was centrifuged (30 min, 2000 rpm, RT, without brake) and the

neutrophils were collected at the interface of the two Histopaque layers. The cells were washed twice with medium, counted and checked for viability.

### 2.2.8. Neutrophil killing assay

After the neutrophils were isolated, their ability to control the bacterial infection was analyzed. For this, neutrophils were seated onto 96 well plates and rested for 1 h at 37 °C. Afterwards, cells were infected with *Listeria monocytogenes* (MOI = 0.05) and incubated for 1 and 4 hours respectively at 37 °C. Neutrophils were then lysed by the addition of Triton X-100 and serial dilutions of the samples were plated on TSB agar plates. After incubating the plates overnight, bacterial colonies were counted and bacterial killing was calculated.

### 2.2.9. Annexin V staining

Isolated bone marrow-derived neutrophils were used to analyze the induction of apoptosis. Cells were again seeded onto 96 well plates and rested for 10 min at 37 °C. *Listeria monocytogenes* (MOI = 10) were added to the wells and the cells were incubated for 2 hours at 37 °C. After the infection, the cells were transferred to FACS tubes and the wells were washed twice with PBS. PMNs were stained for extracellular markers according to section 2.2.2., followed by the staining with PE Annexin V (1:20) in Binding Buffer (BD Biosciences, USA) for 15 min at RT in the dark. Afterwards, 200 µl Binding Buffer was added to each sample and the samples were analyzed according to section 2.2.3..

## 2.3. Molecular biological methods

### 2.3.1. RNA isolation, cDNA synthesis and qRT-PCR

RNA from tissue and cell culture was extracted using the NucleoSpin® RNA kit (Macherey Nagel GmbH und Co. KG, Germany) according to manufacturer's instructions. RNA concentration was determined using a ND-1000 spectrophotometer (NanoDrop Technologies, USA). cDNA was synthesized using the High-Capacity cDNA Reverse Transcription Kit (Applied Biosystems™, USA) with a starting amount of 2 µg RNA from tissue samples and 150 ng from cell culture.

To determine expression levels of pro- and anti-inflammatory genes in liver and cell lysates, qualitative real-time polymerase chain reaction (qRT-PCR) was performed. Primers and Probes

used for specific recognition of transcripts are listed in table 7 (Taqman™ Gene Expression Assays, Applied Biosystems, USA).

| **TaqMan® Gene Expression Assays** | **Identification** |
|---|---|
| *Adgre1* | Mm00802529_m1 |
| *Arg-1* | Mm00475988_m1 |
| *Ccl2* | Mm00441242_m1 |
| *Cxcl2* | Mm00436450_m1 |
| *Hmgb1* | Mm04205650_gH |
| *Ifng* | Mm01168134_m1 |
| *Il-1b* | Mm00434228_m1 |
| *Il-6* | Mm00446190_m1 |
| *Nos2* | Mm00440502_m1 |
| *Tnfa* | Mm00443258_m1 |

**Table 7 | TaqMan® Gene Expression Assays.**

qRT-PCR was performed using TaqMan™ Universal PCR Master Mix (Applied Biosystems, USA) in an ABI Viia7 (Applied Biosystems, USA) under the following conditions: UNG incubation 50 °C 2 min; polymerase activation 95 °C 10 min; 40 cycles denaturation 95 °C 15 s and anneal/extend 60 °C 1 min. Samples were normalized to 18S by comparative $C_T$ ($\Delta\Delta C_T$).

### 2.3.2. Western Blot

For the isolation of protein from liver tissue, RIPA buffer (50 mM Tris/Hcl, 150 mM NaCl, pH 7.4, 1 % Triton X-100, 50 mM NaF, 2 mM EDTA, 10 % Glycerol) was supplemented with proteinase and phosphatase inhibitors (10 mM Benzamidine, 2 mM Sodium orthovanadate, 1 µg/ml Leupeptin, 3.4 µg/ml Aprotinin, 1 mM PMSF). 1 ml supplemented RIPA Buffer per 100 mg tissue was added to the frozen samples and the tissue was then homogenized on ice using pistils. After incubation of the samples for 5 min on ice, the samples were centrifuged for 20 min with 2500 g at 4 °C. Protein concentration was determined using the BCA Protein Assay Kit (Pierce, USA) according to the provided instructions and subsequently diluted to the desired concentration and supplemented with 5× Laemmli Buffer (250 mM Tris/HCl, 10% SDS, 50% Glycerol, 0.5 M DTT).

30 - 45 µg of protein isolated from liver tissue was denatured at 95 °C for 5 min, separated on a 16 % polyacrylamide gel and blotted onto a 0.2 µm PVDF transfer membrane (Thermo Fisher, USA).

| Antibody | Dilution | Source |
|---|---|---|
| anti-HMGB1 (neutralization) | 1:200 | Masahiro Nishibori and Hidenori Wake, Okayama University, Japan |
| IgG Ctrl (neutralization) | 1:200 | Masahiro Nishibori and Hidenori Wake, Okayama University, Japan |
| HMGB1 (ab18256) | 1:1000 | Abcam, USA |
| LC3 (2775) | 1:500 | Cell Signaling Technology, Inc., USA |
| SQSTM1 / p62 (ab109012) | 1:4000 | Abcam, USA |
| α-Tubulin (3873) | 1:5000 | Cell Signaling Technology, Inc., USA |
| β-Actin (A5441) | 1:5000 | Sigma-Aldrich, Germany |
| HRP-linked anti-rabbit IgG (7074) | 1:10000 | Cell Signaling Technology, Inc., USA |
| HRP-linked anti-rat IgG (61-9520) | 1:10000 | Invitrogen™, USA |
| HRP-linked anti-mouse IgG (7076) | 1:10000 | Cell Signaling Technology, Inc., USA |

**Table 8 | Primary antibodies for western blot analyses.**

Blocking reagent used was TBS-T with 5 % non-fat dry milk and membranes were washed three times using TBS-T after primary and secondary antibodies. Primary antibodies for protein detection are listed in table 8. After incubation with HRP-linked secondary antibodies, signals were visualized using Super Signal West Dura Chemiluminescent Substrate (Pierce, USA) and Fusion FX Imager (Vilber, France). Densitometry analysis for the quantification of proteins was performed using Fusion FX Evolution Capt software (Vilber Lourmat, France). Normalization was performed with α-Tubulin or β-Actin, respectively.

### 2.3.3. ELISA

The HMGB1 ELISA (IBL International, Germany) for analysis of serum samples as well as tissue culture supernatants was performed according to the manufacturer's protocol. Signals were detected at 450 nm (wavelength correction: 620 nm) using an ELISA reader (Infinite® F50 microplate reader, Tecan Trading AG, Switzerland). Serum IFN-γ and IL-1β levels in mouse sera

were determined using R&D systems ELISAs (R&D Systems, USA) according to provided protocols. Samples and standard dilutions were detected at 450 nm with wavelength correction at 540 nm.

### 2.3.4. Nanostring

For the gene expression analysis of liver samples the nCounter® mouse myeloid innate immunity panel V2 (Nanostring Technologies, Inc., USA) was used, which comprises 754 unique gene barcodes in 19 pathways for 7 different myeloid cell types. 50 ng of RNA was prepared according to the manufacturer's protocol and subsequently analyzed on a nCounter® SPRINT Profiler. Collected data was normalized and analyzed using nSolver analysis software version 4.0 and no low-count quality control flags were observed for any of the samples. Visualization of the normalized counts of differentially expressed genes was performed using the statistical framework R (v3.5.1) and an over-representation enrichment analysis for GeneOntology-terms (Biological Process) was carried out with WebGestalt (vfcc27621) [111]. Genes with an FDR < 0.05 for the comparison within control groups/injected groups were considered significantly differentially expressed.

## 2.4. Histology

### 2.4.1. Preparation of samples

For the preparation of paraffin-embedded tissue sections, liver samples were fixed in 4 % formalin (Roti®-Histofix, Carl Roth, Germany) at 4 °C for 24 h. Subsequent dehydration and paraffin embedding of the samples were performed in the Institute of Pathology at the University Medical Center Hamburg-Eppendorf. For all immunohistochemistry stainings, 4 µm paraffin sections of mouse livers on superfrost slides were initially deparaffinized (4 × 5 min Xylene), rehydrated using a descending ethanol series (4 min each: 100 % EtOH, 90 % EtOH, 70 % EtOH, 50 % EtOH) and washed in $ddH_2O$. Dehydration after the staining, was performed using an ascending ethanol series (50 % dip twice, 70 % 30 s, 90 % 1 min, 100 % 2 min) and xylene (3 × 5 min).

For the preparation of frozen tissue sections, liver samples were fixed in 4 % PFA at 4 °C for 24 h. Afterwards, samples were incubated in 30 % sucrose at 4 °C for 24 h and finally embedded in Tissue-Tek® and stored at -20 °C. For all immunofluorescence stainings, 6 µm cryostat sections were mounted onto superfrost slides and stored at -20 °C until stained.

All antibodies for the immunohistochemical and immunofluorescent stainings are listed in table 9.

| Antibody | Dilution | Source |
|---|---|---|
| CD45 (ab10558) | IHC-P: 1:1000 | Abcam, USA |
| F4/80 (123102) | IHC-P: 1:100<br>IF: 1:100 | BioLegend, Inc., USA |
| HMGB1 (ab18256) | IHC-P: 1:1000<br>IF: 1:100 | Abcam, USA |
| *Listeria monocytogenes* (ab35132) | IHC-P: 1:400 | Abcam, USA |
| Ly6G-PE (127608) | IF: 1:100 | BioLegend, Inc., USA |
| SQSTM1 / p62 (ab109012) | IF: 1:400 | Abcam, USA |

**Table 9 | Primary antibodies for immunohistochemical and immunofluorescence stainings.**

### 2.4.2. Hematoxylin-Eosin staining

For the hematoxylin-eosin staining, rehydrated tissue sections (as described in 2.4.1.) were incubated in hematoxylin for 10 min, followed by 15 min under running tap water. Afterwards, slides were stained for 1 min in an acidified eosin solution. After being dehydrated, tissue sections were mounted using Entellan.

### 2.4.3. Immunohistochemistry

For immunohistochemical stainings, rehydrated tissue sections (as described in 2.4.1.) were cooked in plastic cuvettes in citrate buffer (10 mM tri-sodium citrate dihydrate, 0.05 % Tween20; pH 6.0) in a microwave for 20 min. Slides were then rinsed with PBS-T, followed by 10 min incubation in 3 % $H_2O_2$ in methanol to block endogenous peroxidase activity. Subsequent washing steps were always performed three times for 2 min in PBS-T. After being washed, tissue sections were covered with protein blocking solution and incubated for 30-90 min in a humid chamber at RT. Afterwards, the tissue sections were drained and rinsed with PBS-T, covered with the primary antibody and incubated overnight in a humid chamber at 4 °C. If the host species of the primary antibody is rat, the slides were then incubated with a secondary antibody (rabbit anti-rat IgG, HRP (61-9520, Invitrogen™, USA), 1:200) and incubated for 60 min in a humid chamber at RT. After being washed, the slides were covered with the serum block (2 % normal goat serum in PBS) and incubated for 10 min in a humid

chamber at RT. The sections were then rinsed and incubated with the secondary/tertiary antibody (Dako Envision labeled polymer HRP-conjugate anti-rabbit) for 30-60 min in a humid chamber at RT. Afterwards, the tissue sections were washed and incubated with DAB substrate until brown to visualize the staining. Last, the slides were counterstained with hematoxylin, dehydrated and mounted using Entellan.

### 2.4.4. Immunofluorescence

For the immunofluorescence stainings, cryostat sections were washed in PBS (2 × 5 min) and blocked using 1 % BSA in PBS for 60 min at RT. The blocking solution was then tipped from the slides and the slides were incubated with the primary antibody solution overnight in a humid chamber at 4 °C. After being washed in PBS (2 × 5 min), the sections were incubated with the secondary antibody or fluorophore-linked antibody for 60 min in a humid chamber at RT. Afterwards, the sections were washed in PBS (2 × 5 min) again and incubated in a HOECHST solution (1:10,000 in PBS) for 1 min. The sections were then washed once more in PBS (2 × 5 min), mounted using Dako Fluoromount and stored at 4 °C.

| Antibody | Dilution | Source |
|---|---|---|
| goat anti-rabbit IgG, Alexa Fluor 555 (A-21428) | IF: 1:1000 | Invitrogen™, USA |
| goat anti-rabbit IgG, Alexa Fluor 488 (A11008) | IF: 1:1000 | Invitrogen™, USA |

**Table 10 | Secondary antibodies for immunofluorescence stainings.**

### 2.4.5. TUNEL staining

TUNEL staining of cryostat sections was performed according to the protocol provided with the *In Situ* Cell Death Detection Kit (Roche, Germany). In short, tissue sections were permeabilized using Proteinase K in Tris/HCl for 20 min at 37 °C. After washing the sections with PBS, the TUNEL reaction mixture was given onto the sections and incubated for 60 min at 37 °C in a humid chamber. The slides were then washed in PBS, counterstained using HOECHST (1:10,000 in PBS) for 1 min, washed in PBS once more and mounted using Dako Fluoromount. The sections were dried at RT and subsequently stored at 4 °C. The area positive for the TUNEL staining was quantified using black/white ratio in ImageJ.

### 2.5. Statistical analysis

All results are expressed as mean ± SEM, except for bacterial titers, which are shown with their median. Data was analyzed using Graphpad Prism 8. For comparison of two groups, Mann-Whitney test was used, for multiple groups, Kruskal-Wallis test with Dunn's post-test. A p-value $< 0.05$ was considered statistically significant.

# III. Results

## 1. Efficient cell-specific depletion of HMGB1

The study of HMGB1 during sterile and infectious inflammation was long impaired due to the early postnatal lethality of mice with a global genetic HMGB1 knockout [112]. Only during the last years, several cell-specific HMGB1 knockouts using the Cre-Lox system have been developed [106,113]. The hepatocyte-specific knockout of HMGB1 was studied extensively and subsequently shown to have no defects in autophagy, regulation of gene expression or organ function. Additionally, this was also shown for mouse embryonic fibroblasts and cardiomyocytes [106].

In this study, HMGB1 was depleted using floxed mice (*Hmgb1*$^{f/f}$), in which the loxP sites span exons 2 – 4 of the *Hmgb1* gene (Fig. 8A), encoding 156 of 215 amino acids of *Hmgb1*. Mating of these mice with albumin-Cre and LysM-Cre mice resulted in the efficient depletion of HMGB1 from albumin-producing cells, which are mainly hepatocytes, (*Hmgb1*$^{\Delta hep}$) and myeloid cells (*Hmgb1*$^{\Delta LysM}$), respectively (Fig. 8B). Analysis of gene expression and protein localization of HMGB1 via histological, western blot and qRT-PCR analysis (5-fold reduction) shows efficient depletion of HMGB1 from hepatocytes in *Hmgb1*$^{\Delta hep}$ mice compared to control mice (Fig. 8C-D). Analysis of isolated bone marrow-derived macrophages (BMDMs) demonstrated comparable reduction of HMGB1 expression on RNA (5-fold reduction) and protein level in *Hmgb1*$^{\Delta LysM}$ compared to *Hmgb1*$^{f/f}$ mice (Fig. 8D). Additionally, histological analysis of HMGB1 expression in Kupffer cells clearly showed reduced numbers of HMGB1$^{+}$ and F4/80$^{+}$ Kupffer cells in the livers of *Hmgb1*$^{\Delta LysM}$ mice compared to *Hmgb1*$^{f/f}$ mice (Fig. 8F).

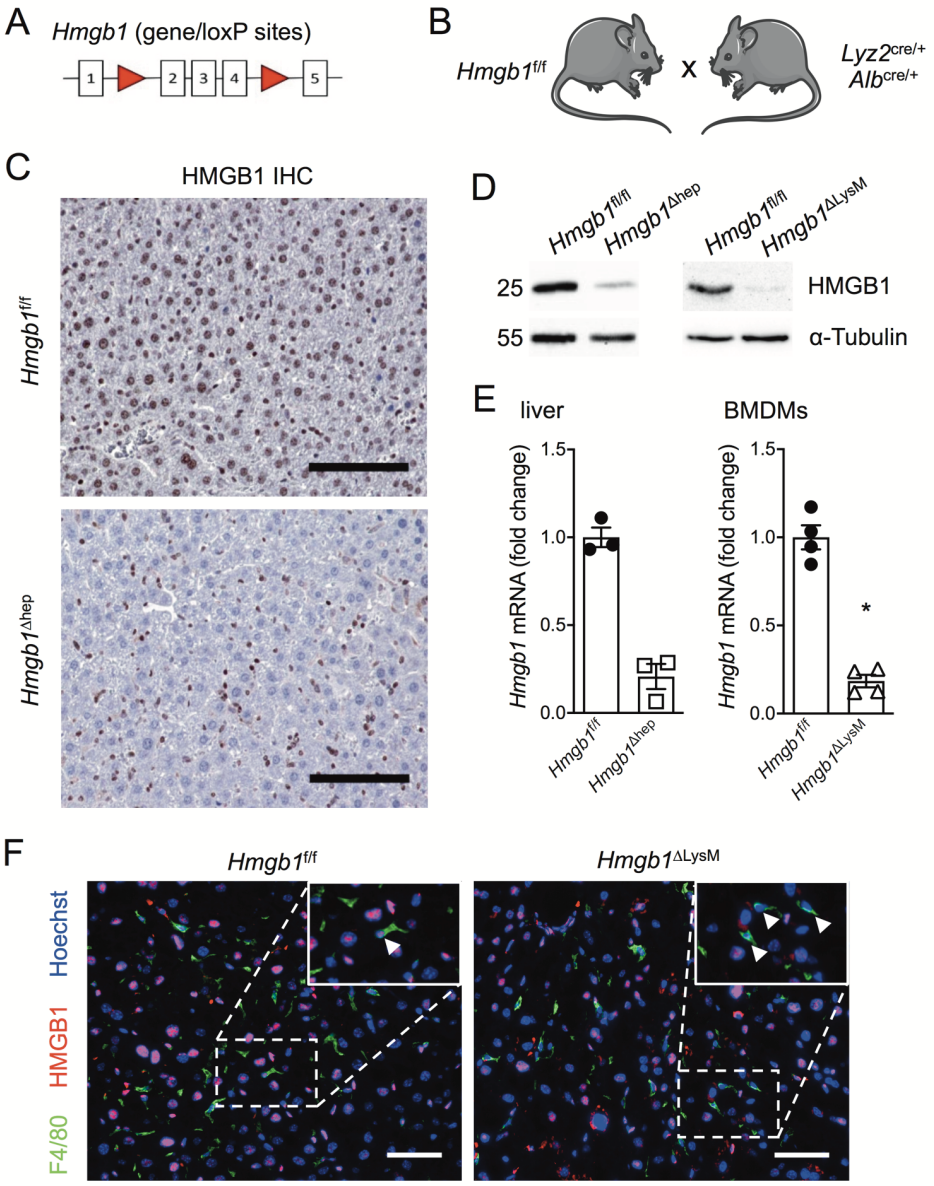


**Figure 8 | Efficient cell-specific depletion of HMGB1.** *Hmgb1* gene including loxP sites (A) as well as deletion strategy using cell-specific Cre mice (B). HMGB1 protein expression in the liver of untreated *Hmgb1*$^{f/f}$ and *Hmgb1*$^{\Delta hep}$ mice (C, immunohistochemical staining). HMGB1 protein levels (D, WB) and *Hmgb1* expression levels (E, qRT-PCR) in whole-liver lysates and isolated BMDMs of the indicated genotypes (n = 3 - 4 mice per group). All expression levels were normalized to 18S and are shown as fold induction ($\Delta\Delta C_T$). Protein expression of F4/80 and HMGB1 in the livers of untreated *Hmgb1*$^{f/f}$ and *Hmgb1*$^{\Delta LysM}$ mice (F, immunofluorescent staining; arrow heads show HMGB1-proficient F4/80$^+$ cells on the left, and HMGB1-deficient F4/80$^+$ cells on the right). Scale bars = 100 µm (C) and 50 µm (F). * $p < 0.05$.

## 2. Antibody-mediated HMGB1 neutralization impairs defense against *Listeria monocytogenes*

Previous studies employing antibody-mediated HMGB1 neutralization demonstrated beneficial effects during LPS-induced shock and polymicrobial abdominal sepsis [14,37]. Therefore, the

first aim was to ascertain whether this effect of antibody-mediated neutralization of HMGB1 on the immune reaction could also be seen towards systemic infection with *Listeria monocytogenes*.

Wild type mice were infected intravenously with *Listeria monocytogenes* and concomitantly received three consecutive intraperitoneal injections of HMGB1-neutralizing antibodies (anti-HMGB1) or control antibodies (IgG Ctrl), respectively. The antibodies used are well-established [109,114,115] and their affinity towards HMGB1 was confirmed using western blot analysis, demonstrating the absent binding of the control antibody to HMGB1 (Fig. 9A).

In contrast though to previous studies, after three days of infection, mice that received HMGB1-neutralizing antibodies displayed a 10-fold increase of bacterial burden in the liver ($p = 0.0140$), compared to mice treated with IgG Ctrl antibodies (Fig. 9B). HE stainings of liver sections showed characteristic granuloma formation in both treatment groups (Fig. 10A) and immunohistochemical staining of *Listeria monocytogenes* revealed localization of bacteria within these granulomas (Fig. 9C).

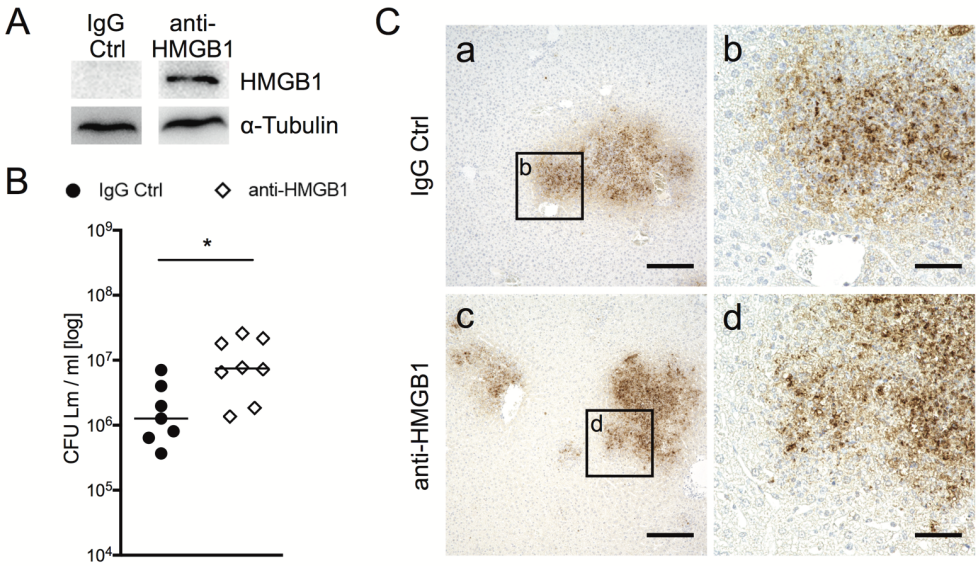


**Figure 9 | Hepatic bacterial burden following antibody-mediated HMGB1 neutralization.** WB analysis of HMGB1-neutralizing antibody (anti-HMGB1), IgG control antibody (IgG Ctrl) and a-Tubulin of wild-type whole-liver lysates (A). Hepatic bacterial burden (B, n = 7 – 8 mice per group) and localization of *Listeria monocytogenes* in the liver (C, immunohistochemical staining) of IgG control- and anti-HMGB1-treated mice (n = 7 – 8 mice per group) 72 hours after i.v.-injection of $2 \times 10^4$ *Listeria monocytogenes*. Scale bars = 200 µm (a, c) and 50 µm (b, d). * $p < 0.05$.

Gene expression analysis of both treatment groups revealed that *Listeria* infection was accompanied by induction of pro-inflammatory cytokines and chemokines like *Ccl2*, *Tnfa*, *Ifng*, *Il1b* and *Nos2* (Fig. 10B). Whereas the expression of *Tnfa*, *Ifng* and *Il1b* was comparable between both groups, expression of *Ccl2,* a chemokine which promotes the hepatic infiltration of bone marrow-derived CCR2-expressing monocytes [116,117], and *Nos2* was increased 3.8-fold in mice treated with anti-HMGB1 antibodies compared to the control group (p(*Ccl2*) = 0.0293, p(*Nos2*) = 0.0426). This demonstrates the intact induction of an immune response, accompanied by increased expression of pro-inflammatory mediators in line with the increased bacterial burden in the liver.

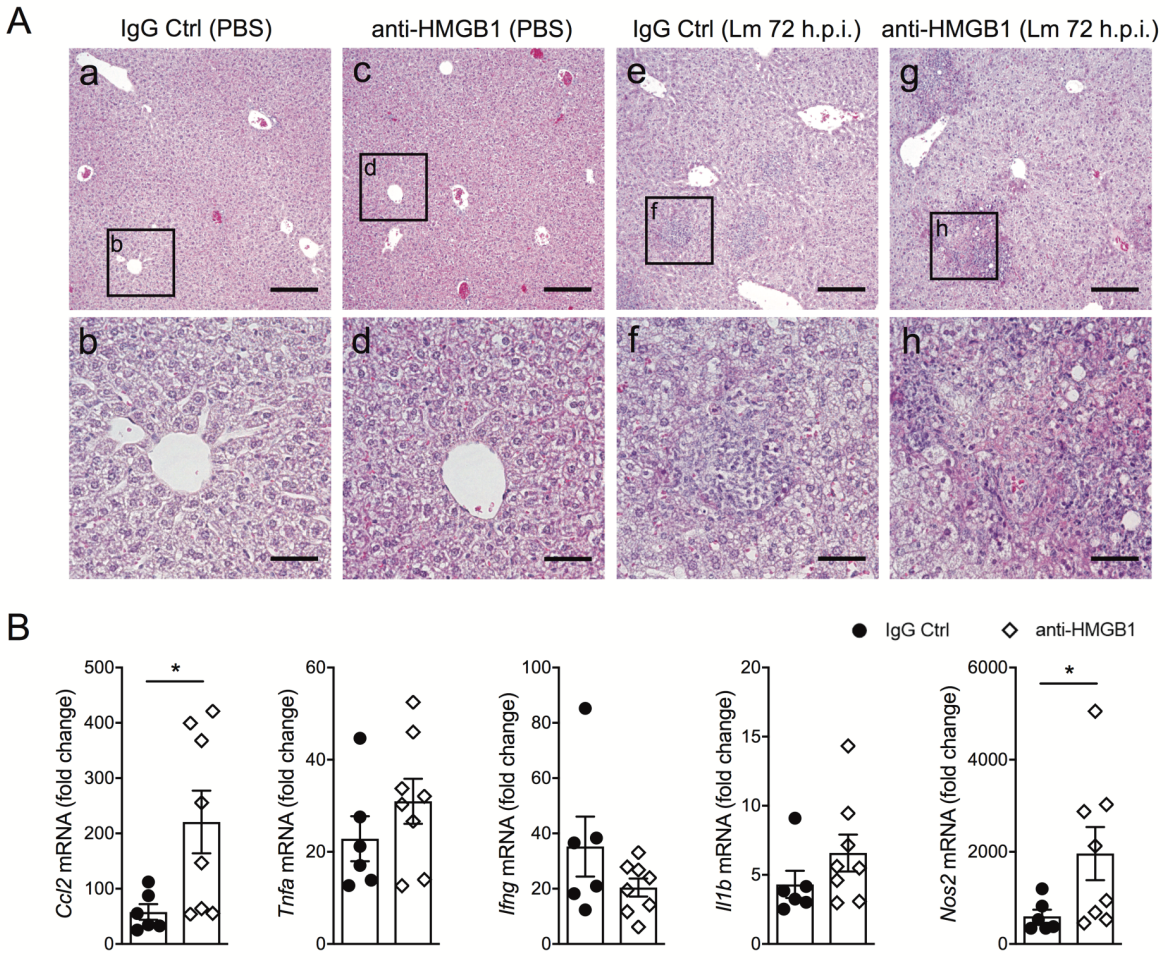


**Figure 10 | Hepatic inflammation following antibody-mediated HMGB1 neutralization.** HE staining of liver sections of mice treated with either IgG control antibodies or anti-HMGB1 antibodies, repectively, and infected with 2 × $10^4$ *Listeria monocytogenes* for 72 hours, as well as control mice treated with the respective antibodies and PBS (A). RNA expression levels of pro-inflammatory genes of IgG control- and anti-HMGB1-treated mice (n = 6 – 8 mice per group) 72 hours post infection were determined using qRT-

PCR (B). All expression levels were normalized to 18S and are shown as fold induction ($\Delta\Delta C_T$) compared to untreated mice. Scale bars = 200 μm (a, c, e, g) and 50 μm (b, d, f, h). * $p < 0.05$.

Clearance of *Listeria monocytogenes* from the liver relies on adequate infiltration of monocytes and neutrophils into the liver [57]. CD45 immunohistochemical staining depicts the infiltration of immune cells into the liver 72 hours after the infection, comparable in mice treated with anti-HMGB1 as well as IgG control antibodies (Fig. 11A). Consistent with this, flow cytometry analysis of intrahepatic immune cells revealed increased numbers of $CD11c^+$ dendritic cells, $CD11b^+Ly6G^+$ neutrophils and $CD11b^+Ly6G^-Ly6C^{hi}$ inflammatory monocytes in the liver in both groups after 72 hours (Fig. 11B). Whereas numbers of dendritic cells as well as pro-inflammatory monocytes were comparable between both treatment groups, neutrophil infiltration was only increased by trend in mice treated with anti-HMGB1 antibodies, even though the hepatic bacterial burden showed a 10-fold increase in these mice.

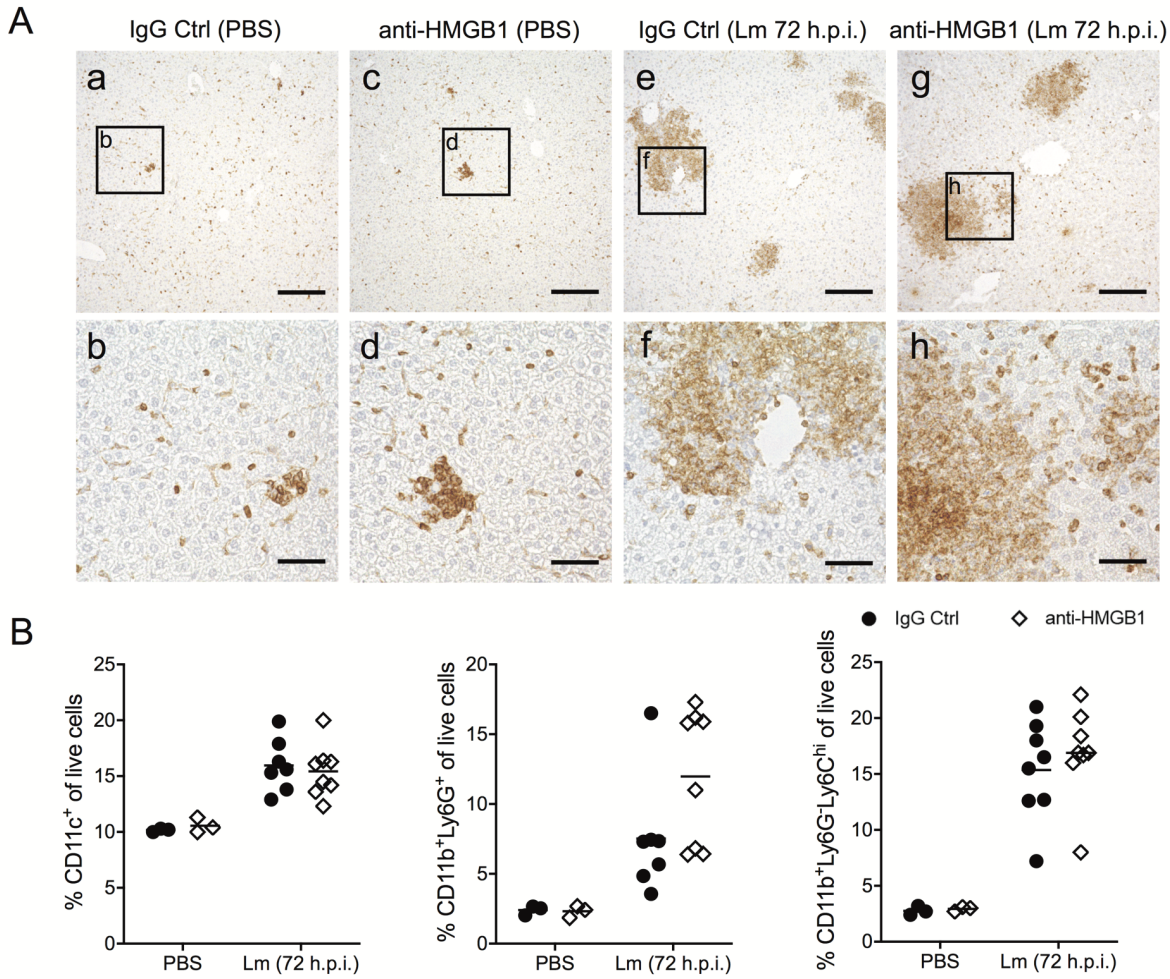


**Figure 11 | Immune cell infiltration following antibody-mediated HMGB1 neutralization.** Protein expression of CD45 (A, immunohistochemical staining) in the livers of mice treated with IgG control antibodies or anti-HMGB1 antibodies 72 hours after injection of 2 × $10^4$ *Listeria monocytogenes* or PBS, respectively. Flow cytometry analysis was used to determine infiltrating intrahepatic immune cells (B). Relative numbers of $CD11c^+$ dendritic cells, $CD11b^+Ly6G^+$ neutrophils and $CD11b^+Ly6G^-Ly6C^{hi}$ monocytes are shown for indicated treatments (n = 6 – 8 mice per group). Scale bars = 200 µm (a, c, e, g) and 50 µm (b, d, f, h).

These results indicate that antibody-mediated neutralization of extracellular HMGB1 during the systemic infection with *Listeria monocytogenes* leads to impaired control of bacterial growth in spite of a suitable induction of hepatic inflammation and that extracellular HMGB1 is necessary for an adequate control of the infection. This effect of antibody-mediated neutralization of extracellular HMGB1 also stands in contrast to the proposed intracellular role of HMGB1 during systemic Listeriosis[113].

## 3. Hepatocyte-derived HMGB1 is dispensable for the immune response to infection with *Listeria monocytogenes*

During systemic listeriosis, hepatic Kupffer cells and splenic macrophages phagocytize blood borne bacteria. In the liver, bacteria afterwards migrate from Kupffer cells directly into hepatocytes while inducing an immune reaction [50]. Hepatocyte-derived HMGB1 has previously been shown to be a key driver of post-necrotic inflammation in the liver [33,34,118], therefore, the role of hepatocyte-derived HMGB1 during the infection with *Listeria monocytogenes* was analyzed next.

To investigate whether anti-bacterial immune responses are affected by hepatocyte-derived HMGB1, hepatocyte specific knockout mice of HMGB1 were infected with *Listeria monocytogenes* and analyzed 24 and 72 hours after the infection. In contrast to its role in sterile inflammation [34], depletion of hepatocyte-derived HMGB1 did not influence the hepatic bacterial burden in *Hmgb1*$^{\Delta hep}$ compared to control *Hmgb1*$^{f/f}$ mice (Fig. 12A). The development of microabscesses in the liver 24 hours after the infection as well as the progression to granulomas 72 hours post infection was also similar in both groups (Fig. 12D). In addition, induction of pro-inflammatory cytokines and chemokines such as CCL2, IFN-γ and iNOS (Fig. 12E), as well as the amount of infiltrating immune cells like CD11c$^{+}$ dendritic cells, CD11b$^{+}$Ly6G$^{+}$ neutrophils and CD11b$^{+}$Ly6G$^{-}$Ly6C$^{hi}$ inflammatory monocytes were comparable between both groups 24 and 72 hours post infection with *Listeria monocytogenes* (Fig. 13A).

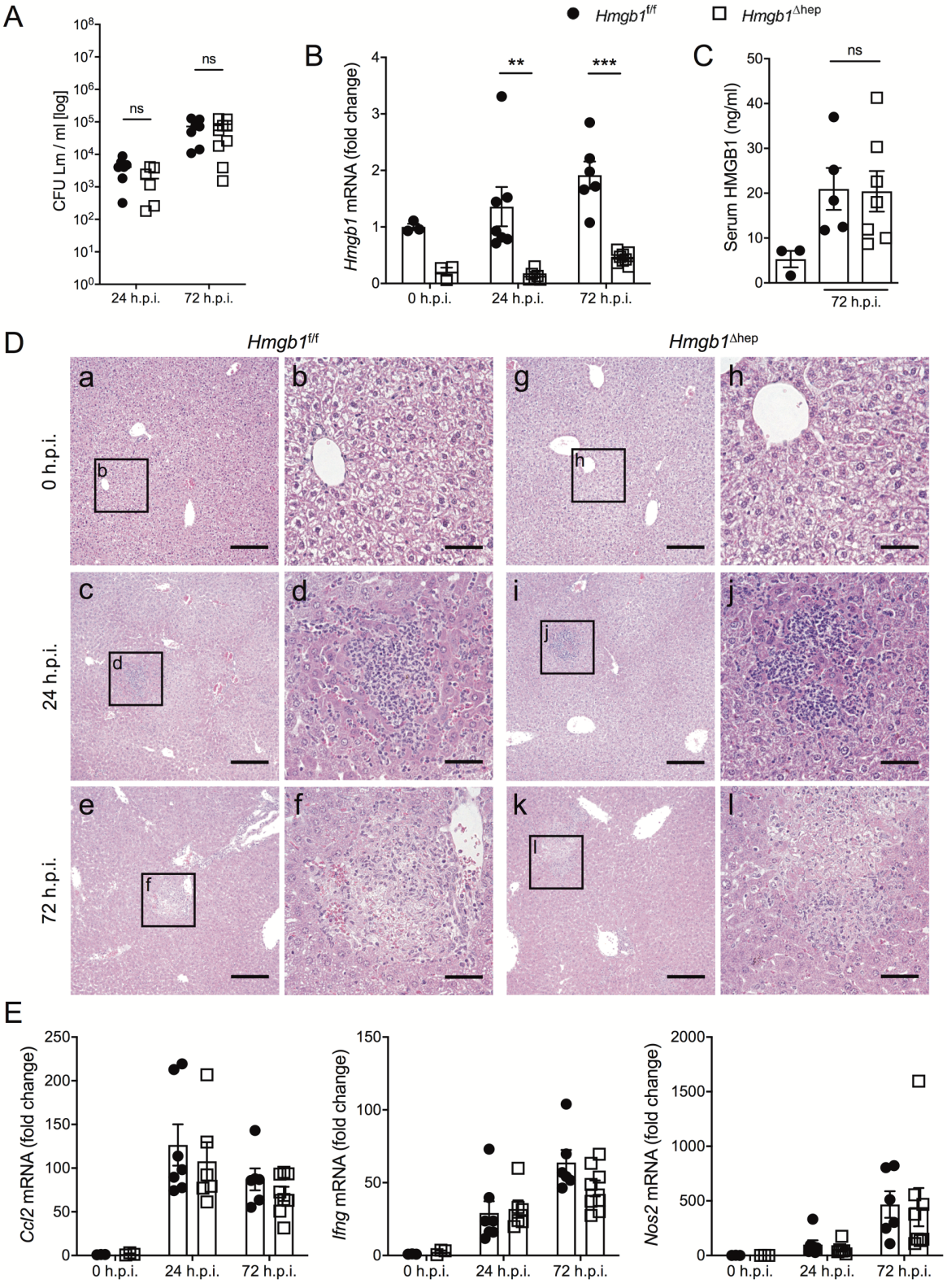


**Figure 12 | *Listeria* infection in mice with hepatocyte-specific depletion of HMGB1.** Bacterial titers in the livers of *Hmgb1*$^{f/f}$ and *Hmgb1*$^{\Delta hep}$ mice (n = 6 – 9 mice per group) 24 and 72 hours after infection with *Listeria monocytogenes* (A). Expression levels of *Hmgb1* RNA in whole-liver lysates over the course of the infection analyzed via qRT-PCR (B). Serum levels of HMGB1 0 and 72 hours after infection (C, ELISA). HE staining of liver sections of *Hmgb1*$^{f/f}$ and *Hmgb1*$^{\Delta hep}$ mice 24 and 72 hours after infection (D).

Gene expression analysis of whole-liver lysates using qRT-PCR over the course of the infection (E). All expression levels were normalized to 18S and are shown as fold induction ($\Delta\Delta C_T$). Scale bars = 200 μm (a, c, e, g, i, k) and 50 μm (b, d, f, h, j, l). ** $p < 0.01$, *** $p < 0.001$.

Despite efficient deletion of *Hmgb1* expression from hepatocytes of *Hmgb1*$^{\Delta hep}$ mice (Fig. 8C-E, Fig. 12B), circulating HMGB1 levels in the serum of *Hmgb1*$^{f/f}$ and *Hmgb1*$^{\Delta hep}$ mice were elevated after bacterial infection (Fig. 12C), but to a similar extent, indicating release of HMGB1 from other cells than hepatocytes. Additionally, immunohistochemical staining of HMGB1 in the livers 72 hours post infection showed no translocation of HMGB1 from the nuclei of hepatocytes into the cytoplasm (Fig. 13B), which is considered a step in the secretion mechanism of HMGB1 [119]. The staining also revealed strong HMGB1 localization in immune cells within granulomas, and even a few cells that seemed to have secreted HMGB1, due to their lack of staining. This suggests that tissue-resident or infiltrating innate immune cells could be responsible for the increased serum levels of HMGB1 after the infection and that myeloid cell-derived HMGB1 could be orchestrating the immune response towards *Listeria monocytogenes*.

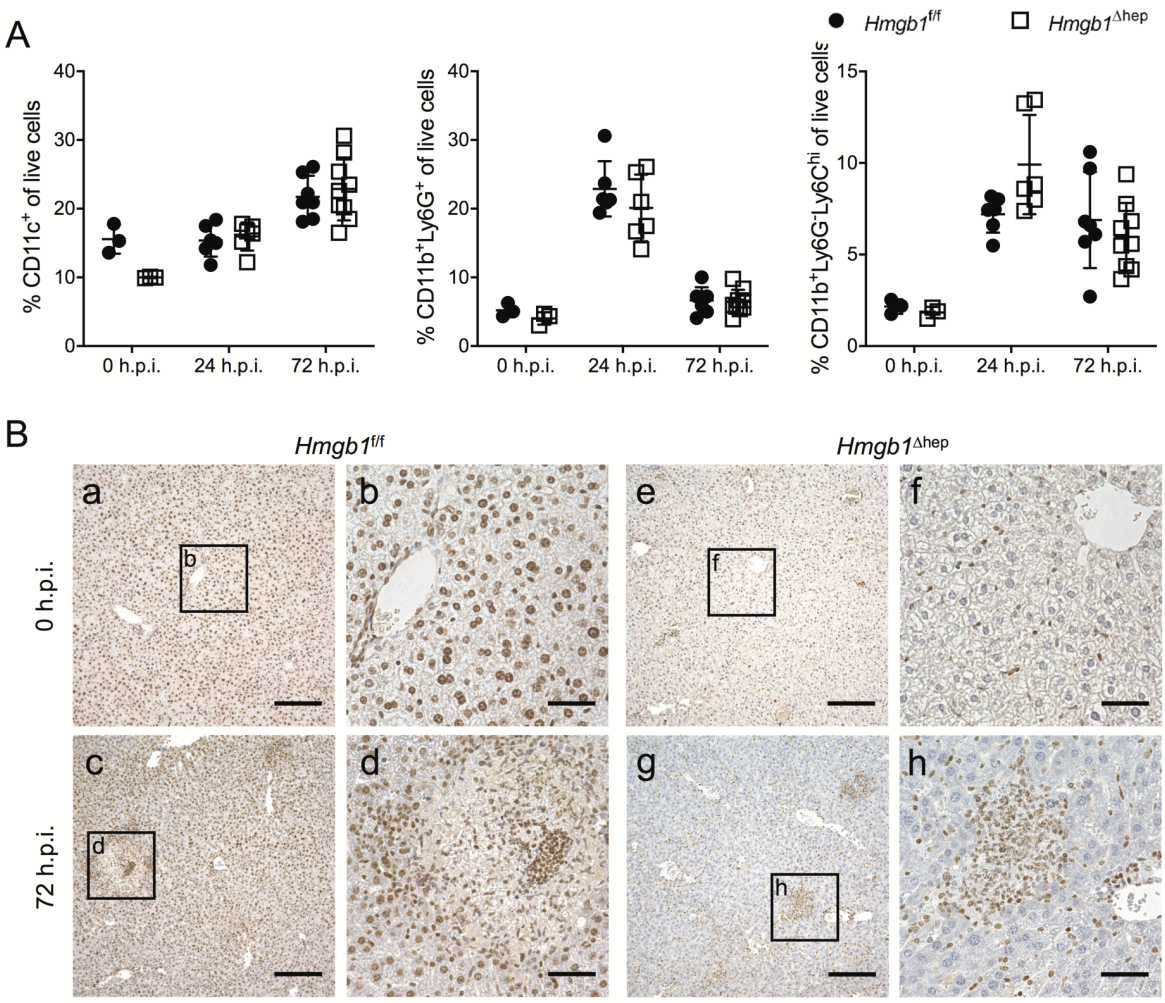


**Figure 13 | HMGB1 protein expression and immune cell infiltration following *Listeria* infection in *Hmgb1*$^{\Delta hep}$ mice.** Hepatic immune cells infiltration analyzed via flow cytometry (n = 3 – 9 mice per group). Relative numbers of CD11c$^{+}$ dendritic cells, CD11b$^{+}$Ly6G$^{+}$ neutrophils and CD11b$^{+}$Ly6G$^{-}$Ly6C$^{hi}$ monocytes are shown for indicated treatments (A). HMGB1 protein expression 0 and 72 hours post infection with *Listeria monocytogenes* in *Hmgb1*$^{f/f}$ and *Hmgb1*$^{\Delta hep}$ mice (B, immunohistochemical staining). Scale bars = 200 µm (a, c, e, g) and 50 µm (b, d, f, h).

## 4. Myeloid cell-derived HMGB1 coordinates the immune response towards *Listeria monocytogenes*

To investigate whether innate immune responses following *Listeria* infection rely on myeloid cell-specific HMGB1, *Hmgb1*$^{f/f}$ and *Hmgb1*$^{\Delta LysM}$ mice were infected with *Listeria monocytogenes* and analyzed 24 and 72 hours post infection. Using LysM-Cre mice for the myeloid deletion of HMGB1 resulted in effective ablation of HMGB1 from Kupffer cells, monocytes, neutrophils and a minority dendritic cells (Fig. 8) [108]. Already after 24 hours, *Hmgb1*$^{\Delta LysM}$ mice displayed higher hepatic bacterial burden ($p = 0.0093$), which after 72 hours was increased 100-fold compared to control mice (Fig. 14A; $p = 0.0012$). This compelling difference could also be seen

in immunohistochemical stainings of *Listeria monocytogenes* on liver sections after 72 hours of infection which showed localization of bacteria in *Hmgb1*$^{\Delta LysM}$ mice especially in the periphery of granulomas. In comparison, *Listeria* staining on liver sections of *Hmgb1*$^{f/f}$ mice showed substantially lower numbers of bacteria, which could mainly be seen within the center of the granulomas (Fig. 14B). HE stainings after 24 hours showed microabscess development in both groups, displaying accumulation of immune cells. 72 hours post infection, livers of *Hmgb1*$^{f/f}$ mice showed granuloma formation whereas livers of *Hmgb1*$^{\Delta LysM}$ mice showed larger amounts of granulomas (Fig. 15A).

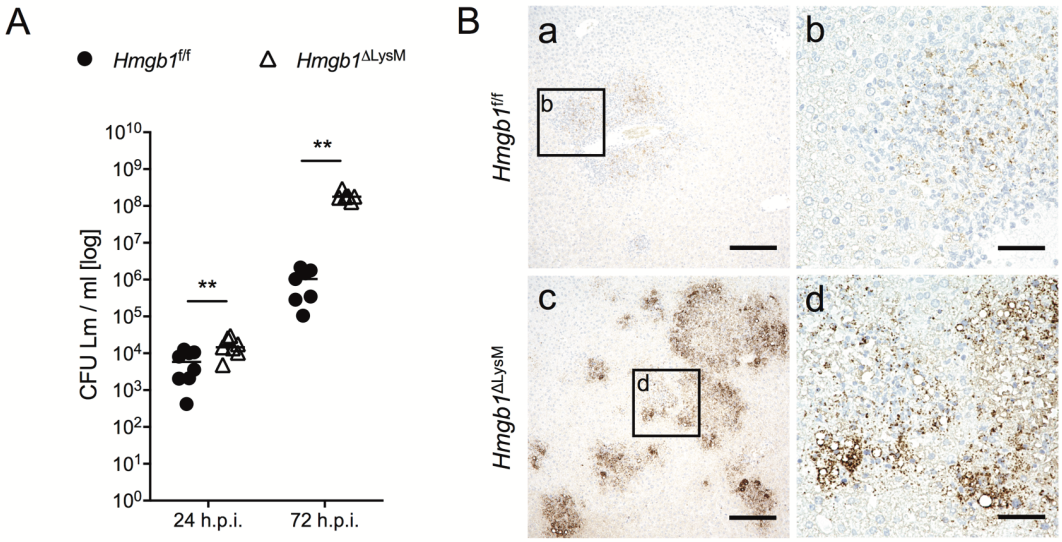


**Figure 14 | *Listeria* infection in mice with myeloid cell-specific depletion of HMGB1.** Hepatic bacterial burden of *Hmgb1*$^{f/f}$ and *Hmgb1*$^{\Delta LysM}$ mice (n = 7 – 8 mice per group) 24 and 72 hours after infection with *Listeria monocytogenes* (A). Localization of *Listeria monocytogenes* in livers of *Hmgb1*$^{f/f}$ and *Hmgb1*$^{\Delta LysM}$ mice 72 hours after infection (B, immunohistochemical staining). Scale bars = 200 µm (a, c) and 50 µm (b, d). ** $p<0.01$.

Gene expression analysis showed a continuous increase of key pro-inflammatory cytokines over the course of the *Listeria* infection in both *Hmgb1*$^{f/f}$ and *Hmgb1*$^{\Delta LysM}$ mice (Fig. 15B). In *Hmgb1*$^{\Delta LysM}$ mice gene expression of pro-inflammatory cytokines and chemokines *Ccl2*, *Tnfa*, *Cxcl2*, *Il1b* and *Il6* was already significantly increased after 24 hours of *Listeria* infection compared to control mice, and increased even further over the next 48 hours, resulting in a highly pro-inflammatory milieu 72 hours after infection. Especially *Ccl2*, *Cxcl2* and *Il6* showed a strikingly increased gene expression 72 h.p.i.. *Ccl2*, a chemokine which promotes the hepatic infiltration of bone marrow-derived CCR2-expressing monocytes [116,117], displayed a 43.4-fold increase in gene expression compared to *Hmgb1*$^{f/f}$ mice after 72 hours ($p = 0.0012$).

Comparably, *Cxcl2*, responsible for the accumulation of neutrophils in the liver, which subsequently release reactive oxygen species and proteases, allowing for pathogen control and induction of hepatocyte necrosis [120], was increased 36.63-fold ($p = 0.0012$). Gene expression of *Il6* was increased 47.35-fold 72 hours post *Listeria* infection. IL-6 is initially also important for the recruitment of neutrophils resulting in a pro-inflammatory milieu [121], but is also responsible for transitioning to mononuclear cell recruitment during inflammation [122]. Expression of *Ifng* was also significantly increased after 24 hours in *Hmgb1*$^{\Delta LysM}$ mice compared to *Hmgb1*$^{f/f}$ mice (2.4-fold increase, $p = 0.0012$), but interestingly did not increase further during the infection, resulting in comparable levels of Ifng expression in *Hmgb1*$^{\Delta LysM}$ and *Hmgb1*$^{f/f}$ mice 72 hours post infection, seemingly independent of the severely increased bacterial burden in these mice. Increased hepatic inflammatory activity is probably due to increased levels of bacteria in the liver and demonstrates the disease severity in these mice.

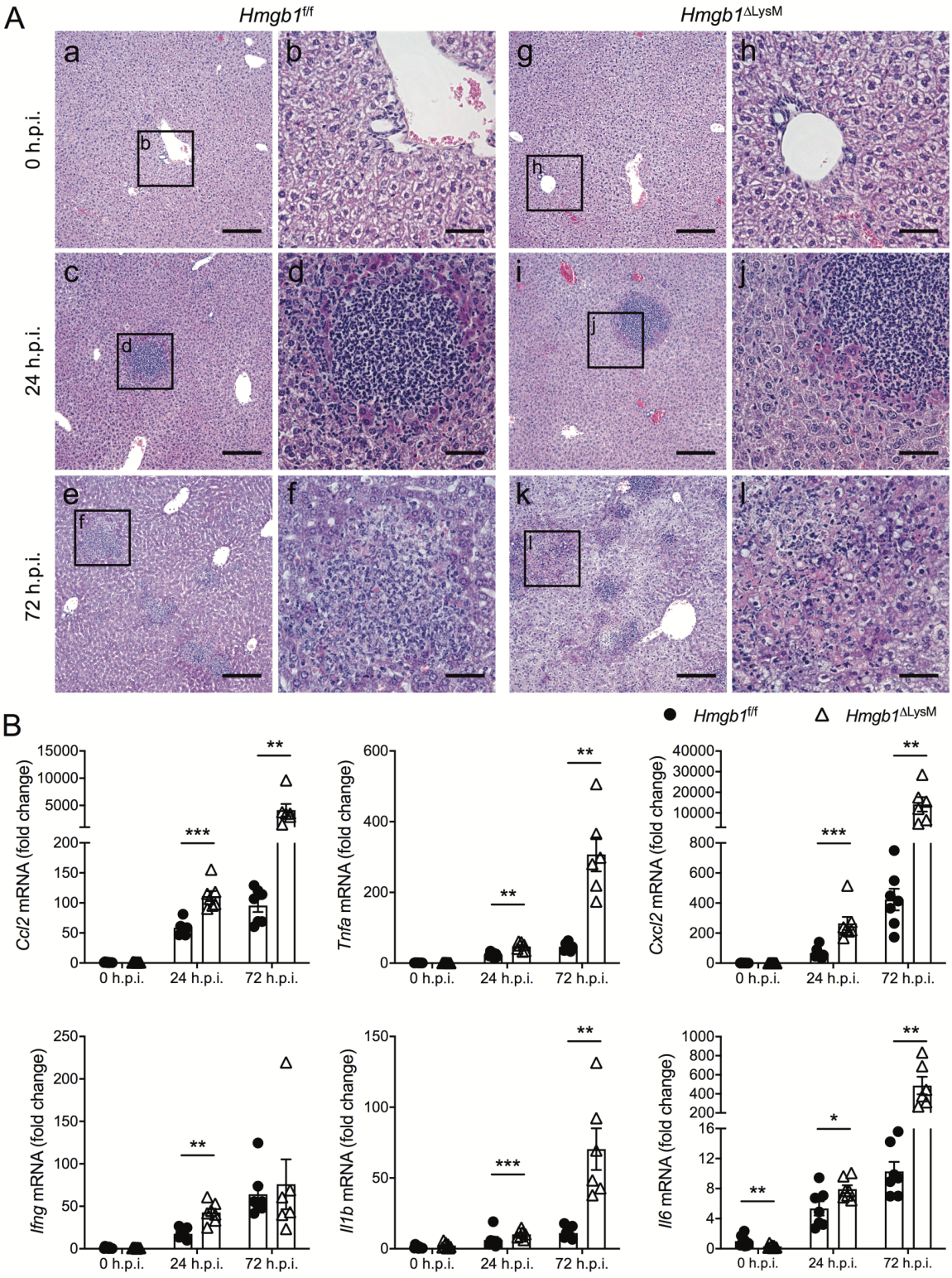


**Figure 15 | Hepatic inflammation following infection with *Listeria monocytogenes* in mice with myeloid cell-specific depletion of HMGB1.** HE staining of liver sections of *Hmgb1*$^{f/f}$ and *Hmgb1*$^{\Delta LysM}$ mice 0, 24 and 72 hours post infection, respectively (A). Expression analysis of pro-inflammatory genes in whole-liver lysates using qRT-PCR over the course of the infection (n = 6 – 9 mice per group). All expression levels were normalized to 18S and are shown as fold induction ($\Delta\Delta C_T$) compared to control

mice at 0 h.p.i.. Scale bars = 200 µm (a, c, e, g, i, k) and 50 µm (b, d, f, h, j, l). * $p < 0.05$, ** $p < 0.01$, *** $p < 0.001$.

Immune cell infiltration, analyzed by CD45 immunohistochemistry staining of liver sections, increased over the course of the infection in both groups, and was increased in *Hmgb1*$^{\Delta LysM}$ mice compared to control mice (Fig. 16A). Flow cytometry analysis revealed larger numbers of dead intrahepatic immune cells in these mice (mean 75.25 % live cells) compared to the control mice (mean 92.92 % live cells; $p = 0.0022$) 72 h.p.i. (Fig. 16B), possibly reflecting increased cellular injury and/or impeded immune cell removal by phagocytic cells. Considering only live cells for further flow cytometry analysis, both groups showed comparable numbers of dendritic cells ($CD11c^+$) over the course of the infection. Live neutrophils ($CD11b^+Ly6G^+$), on the other hand, were increased significantly after 24 hours (1.4-fold increase, $p = 0.0245$) before being significantly reduced after 72 hours of infection in *Hmgb1*$^{\Delta LysM}$ mice (1.77-fold reduction, $p = 0.0087$). Inflammatory monocytes ($CD11b^+Ly6G^-Ly6C^{hi}$) were significantly reduced 24 hours post infection in *Hmgb1*$^{\Delta LysM}$ mice (2.4-fold decreased, $p = 0.0041$) and this could still be observed as a trend 72 hours post infection (Fig. 16C).

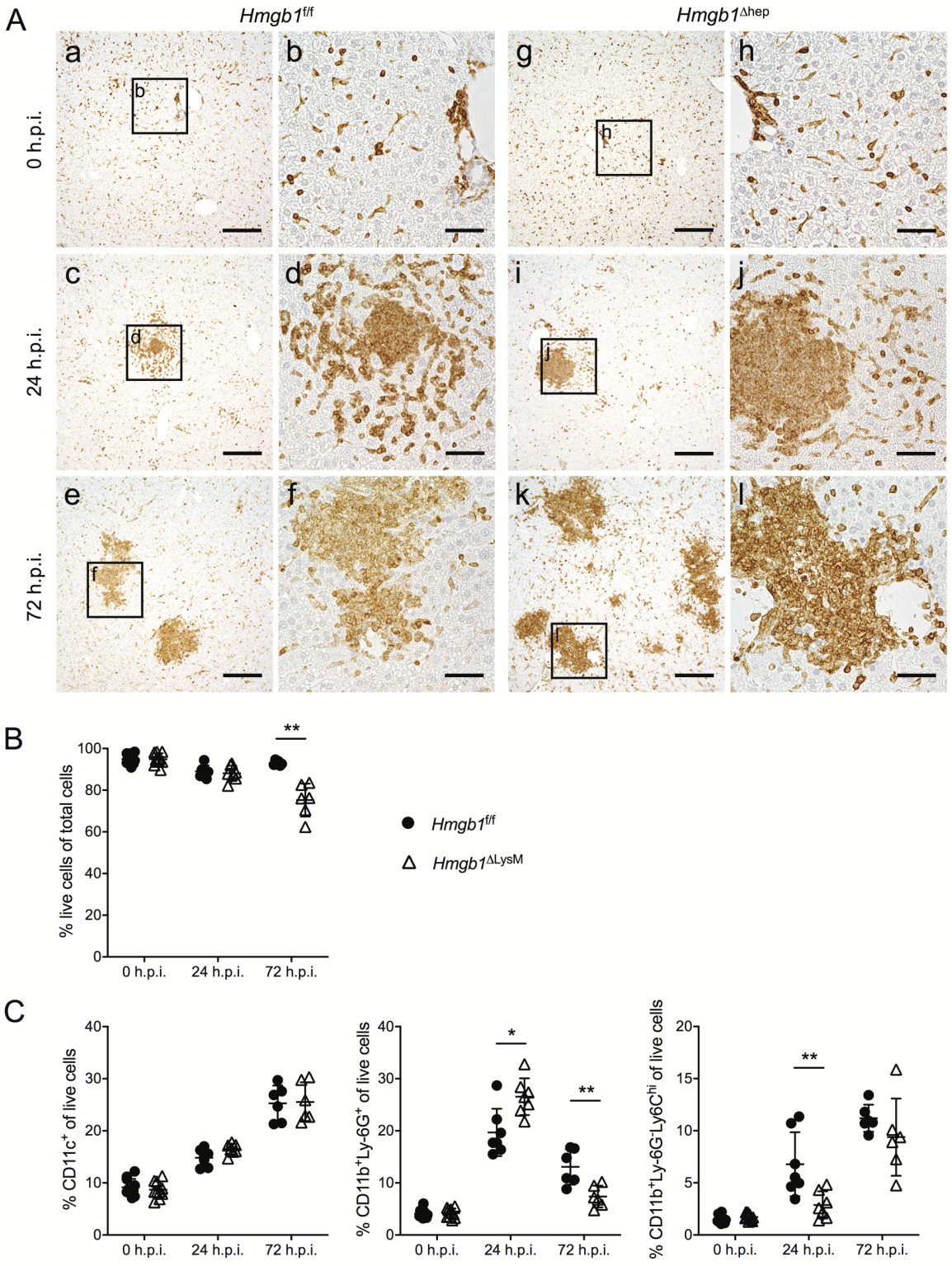


**Figure 16 | Hepatic immune cell infiltration in mice with myeloid cell-specific HMGB1 depletion.** CD45 protein expression in the livers of *Hmgb1*$^{f/f}$ and *Hmgb1*$^{\Delta LysM}$ mice 0, 24 and 72 hours post infection (A, immunohistochemical staining). Flow cytometry analysis of liver infiltrating immune cells over the course of infection of the indicated genotypes (n = 6 – 11 mice per group) using a live/dead marker (B). Relative numbers of CD11c$^+$ dendritic cells, CD11b$^+$Ly6G$^+$ neutrophils and CD11b$^+$Ly6G$^-$Ly6C$^{hi}$ monocytes

at specified time points in both genotypes (C, flow cytometry). Scale bars = 200 μm (a, c, e, g, i, k) and 50 μm (b, d, f, h, j, l). * $p < 0.05$, ** $p < 0.01$.

Using histology analysis, localization of F4/80-expressing Kupffer cells could be determined, demonstrating a severe reduction of F4/80$^+$ cells 24 and 72 h.p.i., indicating Kupffer cell death due to *Listeria* infection (Fig. 17A). Monocyte-derived macrophages only express low levels of F4/80 [123], therefore, these cells were probably not detected here. The reduction of F4/80-expressing cells was also confirmed by RNA expression of *Adgre1*, the gene encoding for F4/80, which showed a significant reduction 72 h.p.i. in *Hmgb1*$^{\Delta LysM}$ mice (2.8-fold reduction, $p = 0.0012$). Polarization of macrophages is also important during anti-bacterial inflammation. Whereas pro-inflammatory M1-polarization is important for the clearance of pathogens, anti-inflammatory M2-polarization of macrophages leads to regeneration of the tissue and a return to homeostasis. Whereas expression of *Nos2*, encoding for iNOS, an important effector of M1 polarized macrophages, was progressively increased in *Hmgb1*$^{f/f}$ mice, this expression was significantly increased in *Hmgb1*$^{\Delta LysM}$ mice 24 (5.9-fold increase, $p = 0.0006$) and 72 h.p.i. (21.7-fold increase, $p = 0.0012$), correlating with the increased bacterial burden in these mice (Fig. 17B). Expression of arginase, the main effector of M2a macrophages, was stably expressed in control animals, but significantly reduced in *Hmgb1*$^{\Delta LysM}$ mice after 72 hours (5-fold reduction, $p = 0.0012$), indicating an impaired differentiation to tissue-regenerating M2 macrophages (Fig. 17B). This could be part of the explanation for the increased tissue damage evident in these mice 72 hours after infection (HE).

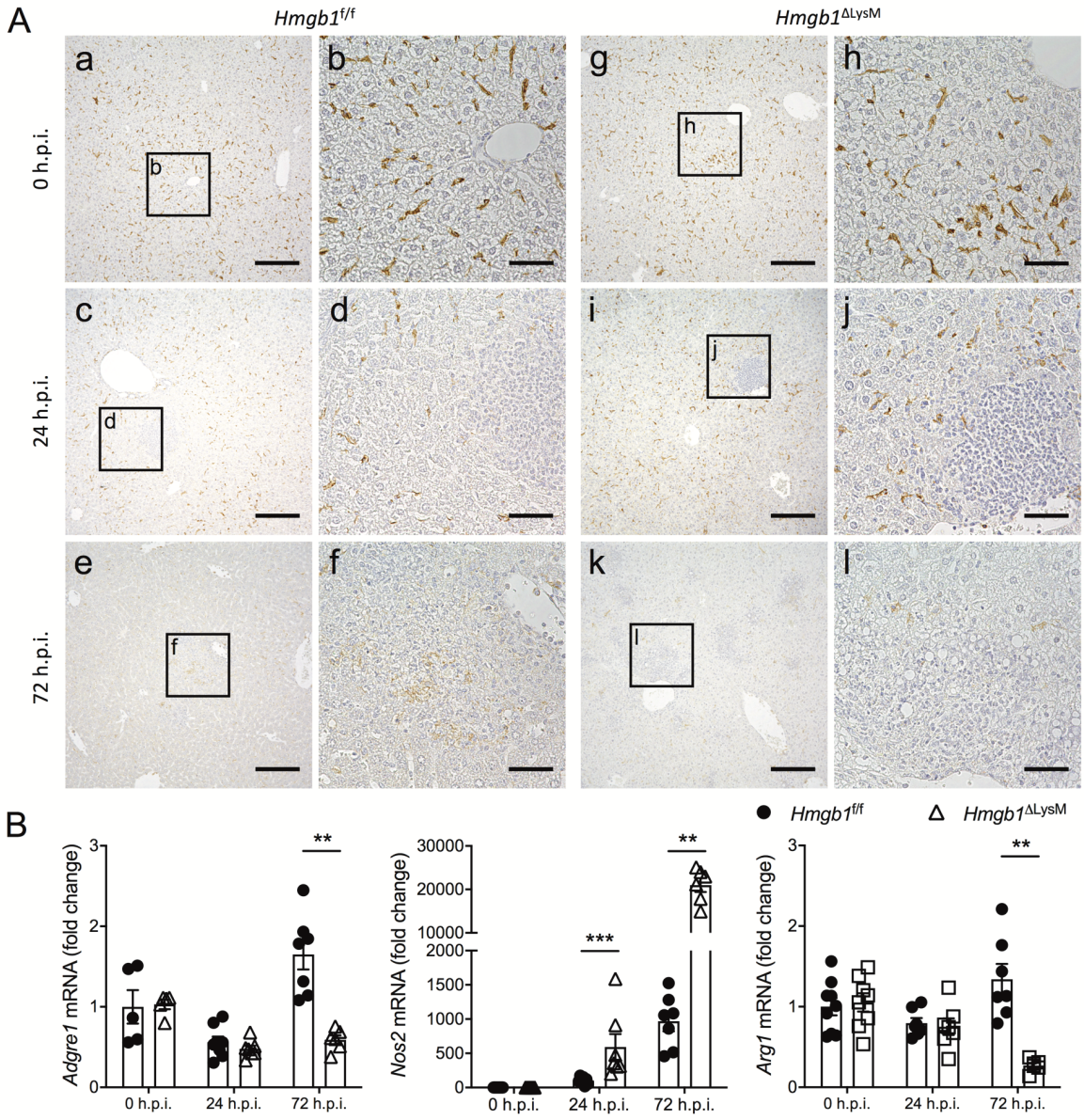


**Figure 17 | Kupffer cell localization and macrophage polarization during *Listeria* infection.** F4/80 expression in the livers of *Hmgb1*$^{f/f}$ and *Hmgb1*$^{\Delta LysM}$ mice 0, 24 and 72 hours post infection (A, immunohistochemical staining). Expression analysis of *Adgre1*, *Nos2* and *Arg1* in whole-liver lysates using qRT-PCR over the course of the infection (n = 6 – 9 mice per group). All expression levels were normalized to 18S and are shown as fold induction ($\Delta\Delta C_T$) compared to control mice at 0 h.p.i.. Scale bars = 200 µm (a, c, e, g, i, k) and 50 µm (b, d, f, h, j, l). ** $p < 0.01$, *** $p < 0.001$.

Using immunohistochemical staining of liver tissue, localization of Ly6G$^+$ neutrophils during the infection of *Hmgb1*$^{f/f}$ and *Hmgb1*$^{\Delta LysM}$ mice was determined. After 24 hours of infection, forming microabscesses largely consisted of infiltrating Ly6G$^+$ neutrophils (Fig. 18). This could be seen in both groups. After 72 hours, neutrophils were not clustered together anymore, but scattered

within the granulomas. In contrast to the flow cytometry analysis, where only live cells were considered for Ly6G$^+$ cells, immunohistochemistry stains live and dead cells within the tissue.

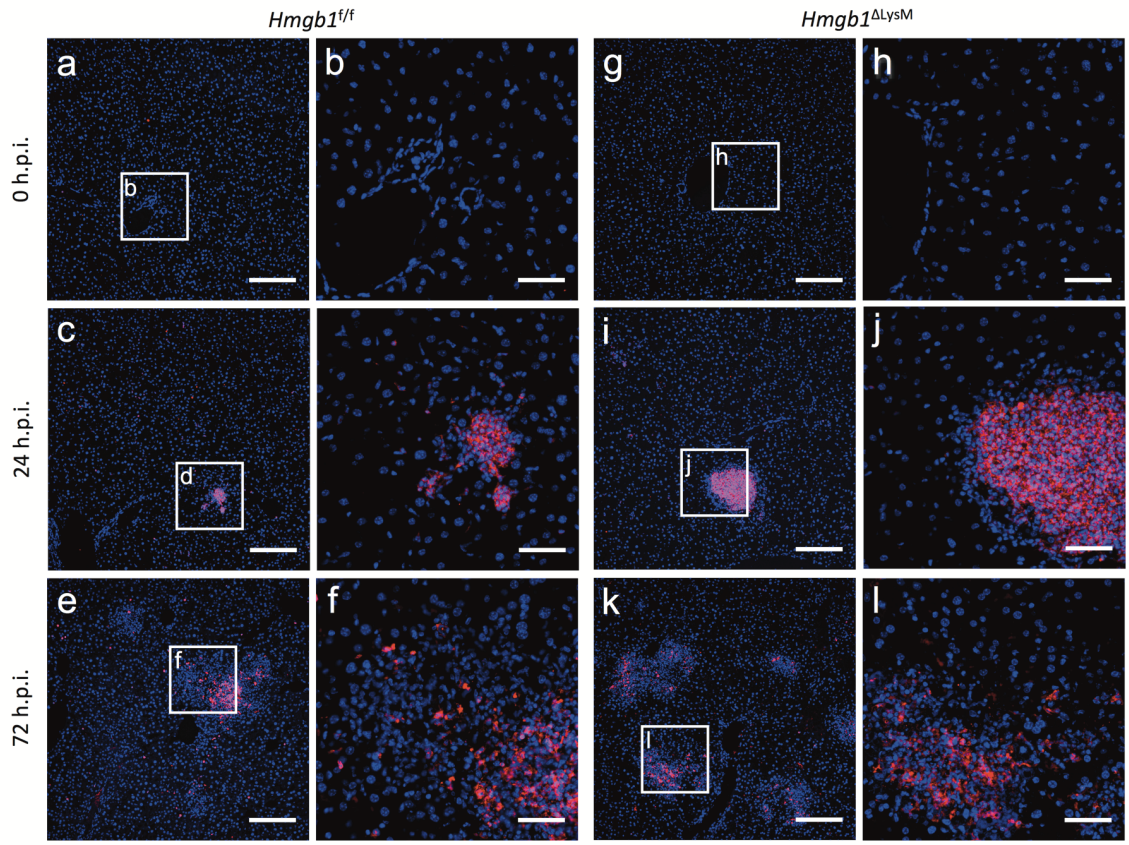


**Figure 18 | Neutrophil infiltration and localization during *Listeria* infection.** Immunofluorescent staining of Ly6G on liver sections of *Hmgb1*$^{f/f}$ and *Hmgb1*$^{\Delta LysM}$ mice 0, 24 and 72 hours, respectively, following infection with *Listeria*. Scale bars = 200 µm (a, c, e, g, i, k) and 50 µm (b, d, f, h, j, l).

During homeostasis, HMGB1 is localized within the nuclei of cells, which can be observed in the livers of untreated mice. Secretion of HMGB1 is characterized by preceding translocation of HMGB1 from the nucleus into the cytoplasm [119]. 72 h.p.i. hepatocytes surrounding granulomas in *Hmgb1*$^{\Delta LysM}$ mice translocated HMGB1 from the nuclei into the cytoplasm (Fig. 19A). This effect could not be observed in *Hmgb1*$^{f/f}$ mice, suggesting that this effect is due to the increased bacterial burden in the liver, which possibly induces stress mechanisms in hepatocytes or early apoptosis. Serum levels of HMGB1 were also increased 2.3-fold in *Hmgb1*$^{\Delta LysM}$ mice compared to control mice 72 h.p.i. ($p = 0.0087$), presumably due to the release from hepatocytes (Fig. 19B).

Serum IL-1β levels over the course of the infection were comparable between both groups, initially being greatly increased after 12 hours of infection, due to the immediate availability of the cytokine. Subsequently, serum levels decreased almost to base line 24 h.p.i. and were then increased again after 72 hours of infection in *Hmgb1*$^{f/f}$ and *Hmgb1*$^{\Delta LysM}$ mice (Fig. 19C). Serum IFN-γ on the other hand increased in both groups after 24 hours of infection. In *Hmgb1*$^{\Delta LysM}$ mice, the serum IFN-γ level remained high after 72 hours of infection, whereas, in *Hmgb1*$^{f/f}$ mice the amount of IFN-γ in the serum was reduced 2.4-fold compared to the level of *Hmgb1*$^{f/f}$ mice 24 h.p.i. (Fig. 19C).

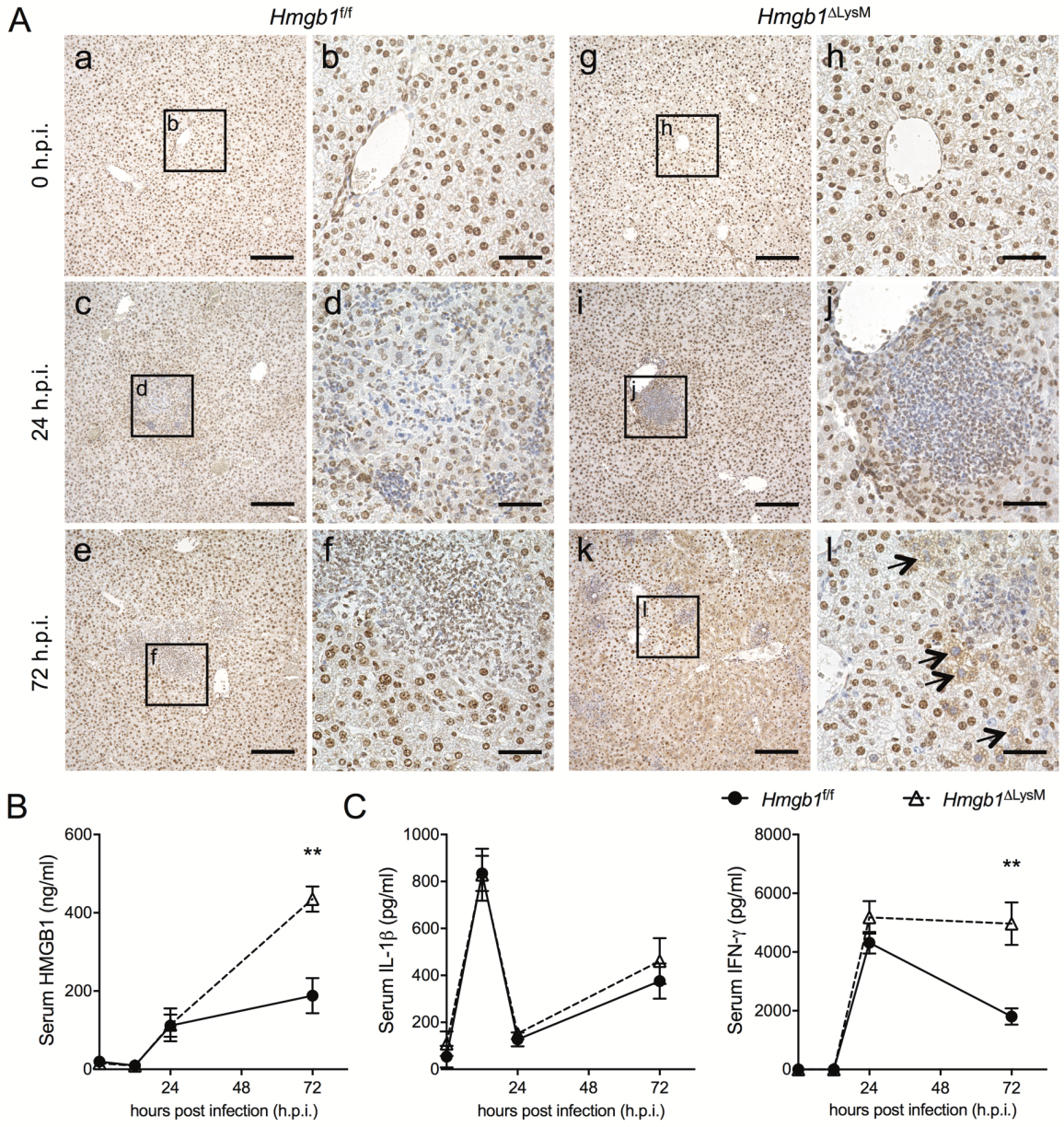


**Figure 19 | Hepatic HMGB1 localization and pro-inflammatory factors during *Listeria* infection.** HMGB1 protein expression in the livers of *Hmgb1*$^{f/f}$ and *Hmgb1*$^{\Delta LysM}$ mice 0, 24 and 72 hours post infection (A, immunohistochemical staining). Arrows indicate hepatocytes with translocation of HMGB1 into the cytoplasm. Serum HMGB1 levels (A, ELISA) as well as serum IL-1β and IFN-γ levels (B, ELISA) over the course of the *Listeria* infection for the indicated genotypes (n = 6 – 8 mice per group). Scale bars = 200 µm (a, c, e, g, i, k) and 50 µm (b, d, f, h, j, l). ** $p < 0.01$.

Taken together, cell-specific depletion of HMGB1 from myeloid cells led to an impaired early immune response resulting in strikingly increased bacterial titers and tissue damage as well as vastly elevated inflammation. Overall, this data suggest that myeloid cell-derived HMGB1 is critically involved in the early immune response towards *Listeria monocytogenes*.

# 5. Induction of autophagy and bactericidal activity of macrophages and neutrophils is preserved following *Listeria* infection despite HMGB1 depletion

## 5.1. Induction of autophagy and apoptosis following *Listeria* infection

During the process of autophagy, the cytosolic form of light chain 3 (LC3-I) is initially cleaved, followed by the conjugation to phosphatidylethanolamine (LC3-II), which is then associated with the membrane of autophagosomes. Autophagy and autophagy-related processes can be detected by western blot or histological analysis of LC3 [124], where the progression of autophagy is marked by an increase of LC3-II. Another marker protein for autophagy analysis is p62 (or also SQSTM1). P62 expression is increased following oxygen radical stress [125] and its accumulation is indicative of impaired autophagy within the cell [126].

Previous studies have proposed HMGB1 as a regulator of apoptosis and autophagy under cellular stress, indicating HMGB1 as a pro-autophagic protein. Following cellular stress, HMGB1 is translocated into the cytoplasm where it binds Beclin1, disrupting the bond with Bcl-2 and thereby progressing autophagy [127,128]. Although the mice used in this project had previously not shown any defects in the regulation of autophagy at baseline or under metabolic stress despite HMGB1 ablation [106], autophagy induction in the specific context of *Listeria* infection was analyzed.

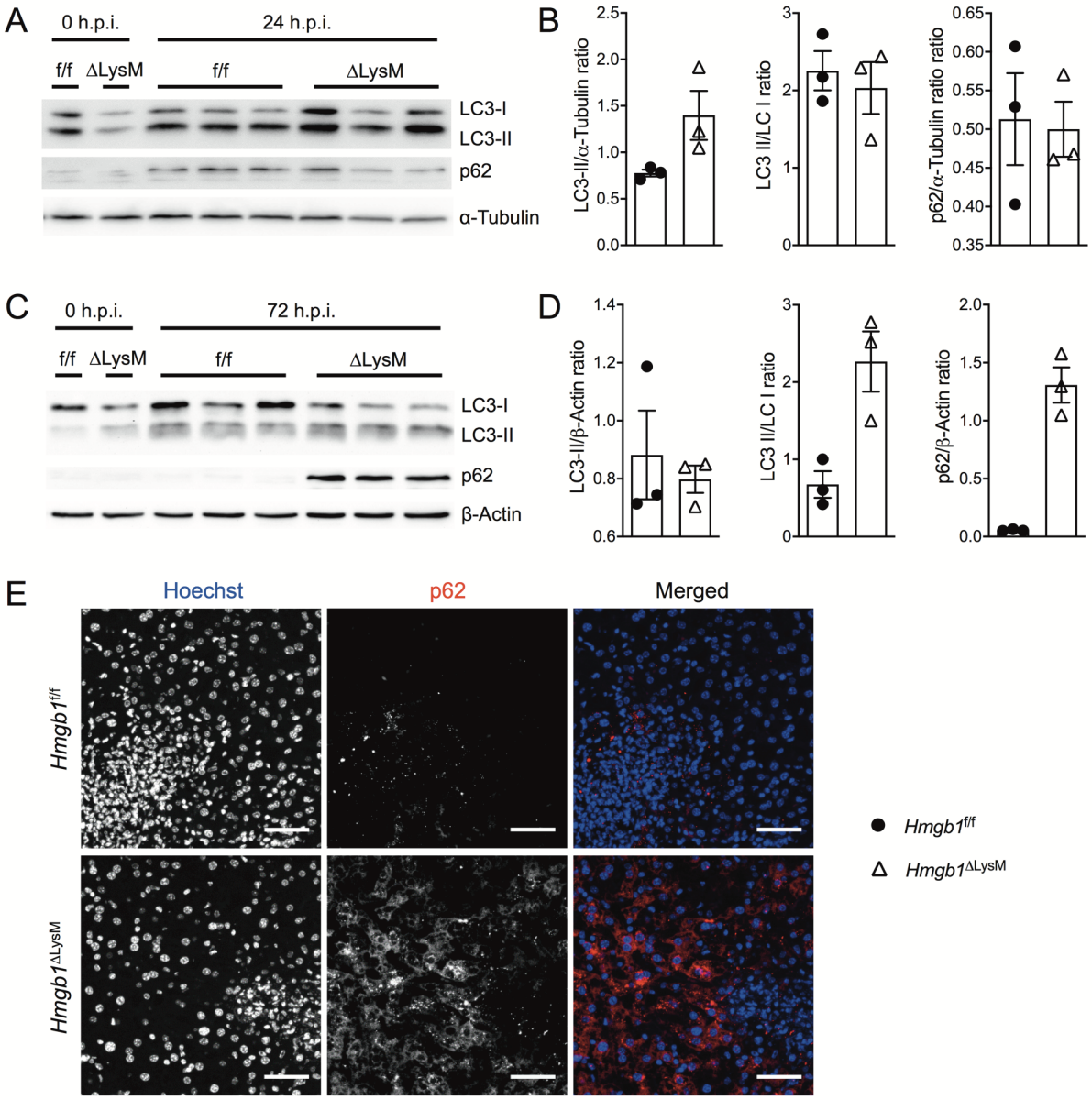


**Figure 20 | Autophagy induction during *Listeria monocytogenes* infection.** Western blot analysis of autophagy factors LC3-I, LC3-II and p62 and α-Tubulin as housekeeper in whole liver extracts of *Hmgb1*$^{f/f}$ and *Hmgb1*$^{\Delta LysM}$ mice (n = 1 – 3 mice per group) at 0, 24 (A) and 72 (C) hours post *Listeria* infection and corresponding densitometry analysis (B, D). p62 protein expression in the livers of *Hmgb1*$^{f/f}$ and *Hmgb1*$^{\Delta LysM}$ mice 72 hours post *Listeria* infection (E, immunofluorescent staining). Scale bars = 50 µm.

As in previous analyses, comparable levels of LC3 protein expression were observed in whole liver extracts of mice infected with 2 × $10^4$ *Listeria monocytogenes* over the course of the infection (Fig. 20A-D). The ratio of LC3-II/LC3-I was increased about 3-fold in *Hmgb1*$^{\Delta LysM}$ mice 72 h after infection, which could possibly be attributed to the increased amount of stressed cells due to copious amounts of tissue damage in the liver at this point of the infection. This increase in the LC3-ratio was also accompanied by increased accumulation of p62 in the liver, which was

not observed at the earlier time point (Fig. 20C-D). However, immunofluorescence analysis revealed accumulation of p62 in cells outside of myeloid cell-containing hepatic granulomas (Fig. 20E). This suggests that the accumulation of p62 is not due to a defect in autophagy in HMGB1-depleted myeloid cells, but more likely a result of stressed hepatocytes due to high bacterial burden and inflammation in the liver. To further support this hypothesis, autophagy induction in bone marrow-derived macrophages (BMDMs) infected with *Listeria* (multiplicity of infection (MOI) = 10) *in vitro* was investigated. After 4 hours, analysis of cell lysates by western blot showed an increase of LC3-II as well as accumulation of p62, but at similar levels in *Hmgb1*$^{f/f}$ and *Hmgb1*$^{\Delta LysM}$–derived BMDMs (Fig. 21A-B). This effectively rules out defects in autophagy due to the depletion of HMGB1 as an explanation of the amplified *Listeria* infection in *Hmgb1*$^{\Delta LysM}$ mice.

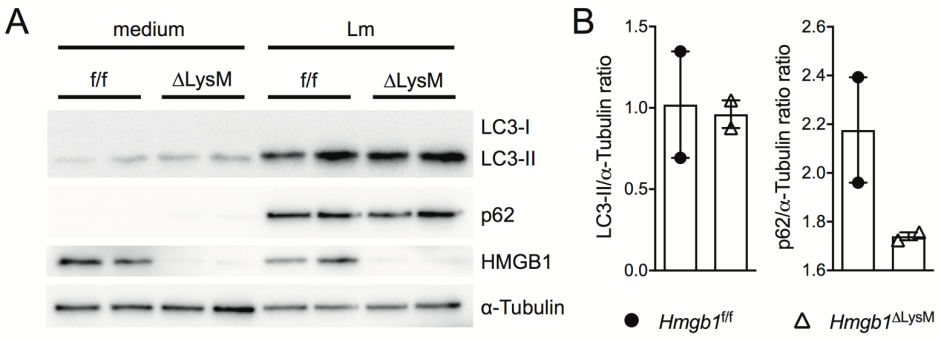


**Figure 21 | Autophagy induction in BMDMs during *in vitro Listeria* infection.** Western blot analysis of LC3-I, LC3-II, p62, HMGB1 and α-Tubulin in lysates of bone marrow-derived macrophages (n = 2 mice per group, A) and corresponding densitometry analysis (B).

As previously described, the processes of autophagy and apoptosis within the cell are closely linked. Increased levels of dead intrahepatic immune cells had already been observed using flow cytometry analysis. Therefore, following infection with *Listeria monocytogenes*, livers of *Hmgb1*$^{f/f}$ and *Hmgb1*$^{\Delta LysM}$ mice were analyzed using TUNEL staining. TUNEL assays are used to visualize apoptotic cells by detecting DNA fragmentation, a hallmark of late-stage apoptosis [129]. Immunofluorescence analysis showed significantly increased levels of TUNEL$^{+}$ cells in the livers of *Hmgb1*$^{\Delta LysM}$ mice 24 (1.6-fold increase, p = 0.0175) and 72 hours (19.5-fold increase, p = 0.0043) after infection (Fig. 22A-B). These late-apoptotic cells were in both groups located within the *Listeria*-containing granulomas, consisting mostly of neutrophils and monocytes. The amount of apoptotic cells, especially in *Hmgb1*$^{\Delta LysM}$ mice, increased over the last 48 hours from mean 0.2 % to 3.9 % TUNEL$^{+}$ cells of the area, filling almost entire granulomas at 72 hours post

infection. This striking amount of late-apoptotic cells within the livers of *Listeria*-infected *Hmgb1*$^{\Delta LysM}$ mice indicates increased cellular injury and death and/or defective cellular turnover and removal of dead cells from the liver.

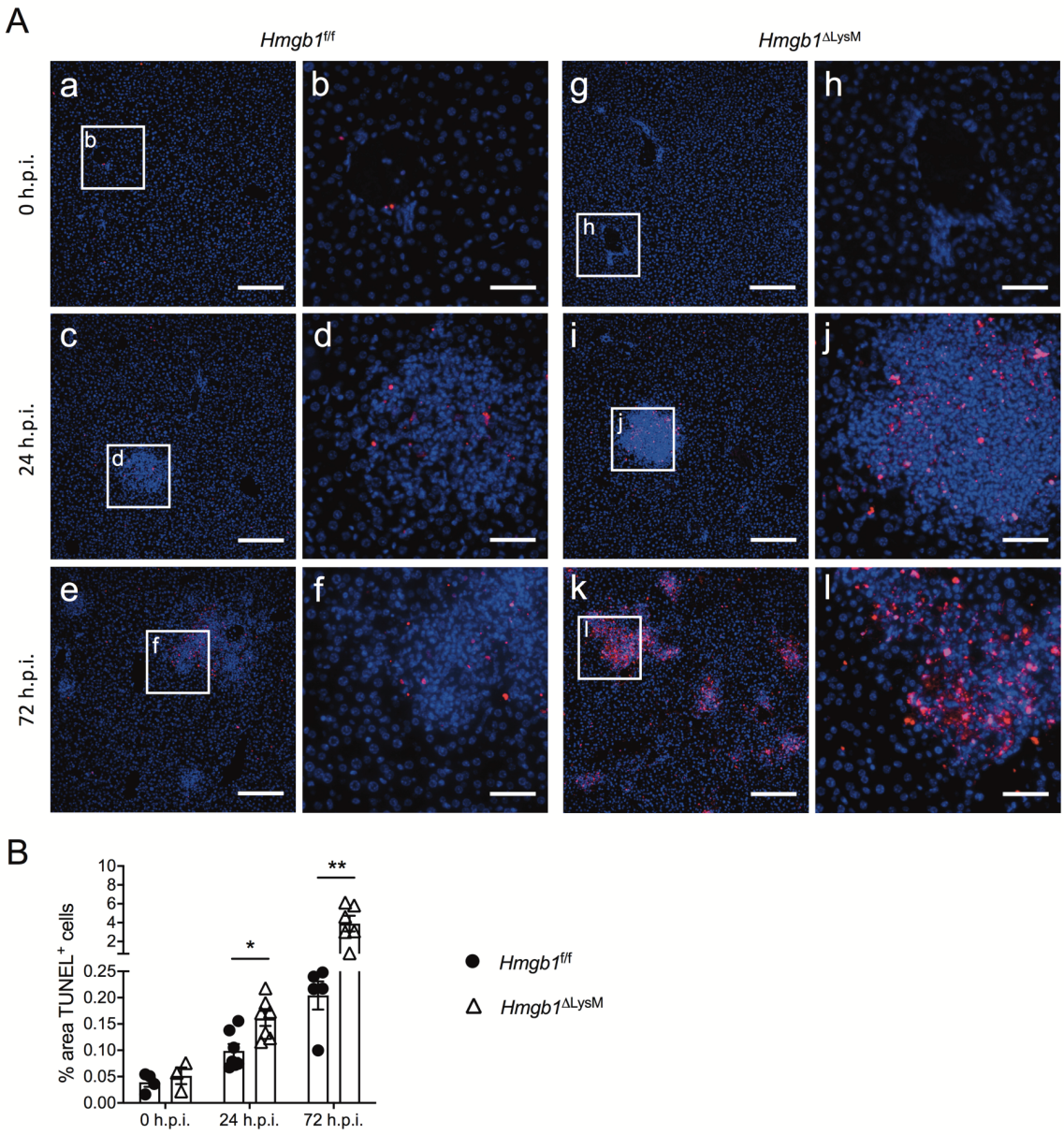


**Figure 22 | Apoptotic cells in the liver of mice infected with *Listeria monocytogenes*.** TUNEL$^+$ cells in the livers of *Hmgb1*$^{f/f}$ and *Hmgb1*$^{\Delta LysM}$ mice 0, 24 and 72 hours post *Listeria* infection (A, immunohistochemical staining) and their quantification (n = 3 – 7 mice per group, B). Scale bars = 200 µm (a, c, e, g, i, k) and 50 µm (b, d, f, h, j, l). * $p < 0.05$, ** $p < 0.01$.

## 5.2. Antibacterial activity of macrophages *in vitro*

Considering the profound defects in anti-bacterial defense mechanisms in *Hmgb1*$^{\Delta LysM}$ mice following infection with *Listeria monocytogenes*, the next step was to analyze the bactericidal activity of macrophages and neutrophils, two effector cells during *Listeria* infection, which in *Hmgb1*$^{\Delta LysM}$ mice are depleted of HMGB1 (Fig. 8D-F)[108].

As stated before, following systemic infection, *Listeria* target Kupffer cells within the liver and induce necroptotic cell death, which leads to the release of intracellular components [84]. Therefore, infected Kupffer cells could release HMGB1 as a DAMP following *Listeria*-induced necroptosis. *In vitro* infection of bone-marrow derived macrophages (BMDMs) derived from *Hmgb1*$^{f/f}$ mice with *Listeria monocytogenes* (MOI = 10) led to the release of HMGB1 into the cell culture supernatant (mean = 51.5 ng/ml) compared to cells treated only with medium (mean = 20.46 ng/ml). BMDMs from *Hmgb1*$^{\Delta LysM}$ mice expectedly did not show an increase of HMGB1 in the supernatant (mean = 16.34 ng/ml) (Fig. 23A). Differentiated macrophages within the liver are also responsible for the phagocytosis and subsequent clearance of bacteria in the liver. To analyze the bactericidal activity of isolated BMDMs, cells were infected with *Listeria monocytogenes* (MOI = 10) and after 1 hour extracellular bacteria were removed using gentamicin treatment. This allowed for the analysis of phagocytosis activity (0 h.p.i.) and subsequent incubation of intracellular bacteria and macrophages demonstrated the bactericidal activity of the BMDMs. This test showed a slightly increased phagocytosis activity of HMGB1-depleted cells, but the progression of bacterial clearance was comparable in both groups, resulting in more than 80 % degraded bacteria 8 hours after phagocytosis of *Listeria* in both *Hmgb1*$^{f/f}$ and *Hmgb1*$^{\Delta LysM}$ BMDMs (Fig. 23B).

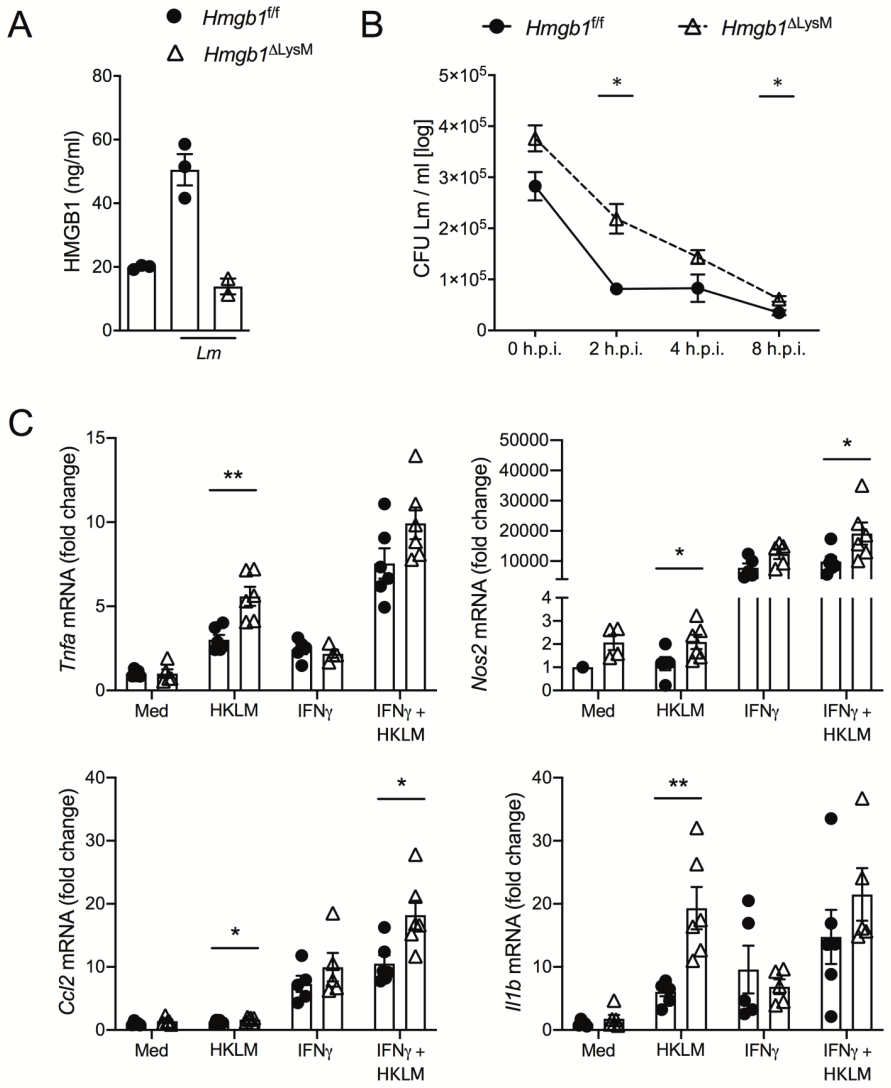


**Figure 23 | Bactericidal function and inflammatory capacity of BMDMs *in vitro*.** HMGB1 levels in the supernatants of *Hmgb1*$^{f/f}$ and *Hmgb1*$^{\Delta LysM}$ BMDMs, (n = 2 – 3 samples per group) untreated or infected with *Listeria monocytogenes* (MOI = 10) for 12 hours (A, ELISA). Analysis of phagocytosis and intracellular bacterial degradation of *Hmgb1*$^{f/f}$ and *Hmgb1*$^{\Delta LysM}$ BMDMs (n = 4 samples per group, B, gentamicin assay). Expression levels of *Tnfa, Nos2, Ccl2* and *Il1b* in BMDM lysates using qRT-PCR after stimulation with HKLM (MOI = 10) and IFN-γ for 1 hour (n = 5 – 6 samples per group). All expression levels were normalized to 18S and are shown as fold induction ($\Delta\Delta C_T$) compared to untreated BMDMs. * $p < 0.05$, ** $p < 0.01$.

Additionally, the responsiveness of *Hmgb1*$^{f/f}$ and *Hmgb1*$^{\Delta LysM}$ BMDMs to heat-inactivated *Listeria monocytogenes* (HKLM) as well as IFN-γ was tested by analyzing the gene expression of pro-inflammatory mediators (Fig. 23C). IFN-γ in combination with a secondary signal via PRR recognition induces the differentiation of M1 macrophages, enabling phagocytosis of pathogens and bactericidal activity [79,130,131]. Therefore, this analysis enabled the investigation of the capability of *Hmgb1*$^{f/f}$ and *Hmgb1*$^{\Delta LysM}$ BMDMs to differentiate into M1 macrophages in order to

clear the bacterial infection. In control BMDMs, stimulation with HKLM and IFN-γ respectively led to a slight increase in *Tnfa* expression, which was increased further with the combination treatment of HKLM and IFN-γ. Expression of *Tnfa* was comparable in *Hmgb1*$^{f/f}$ and *Hmgb1*$^{\Delta LysM}$ BMDMs and only after treatment with HKLM alone significantly increased in *Hmgb1*$^{\Delta LysM}$ BMDMs compared to *Hmgb1*$^{f/f}$ BMDMs (1.85-fold increase, p = 0.0022). Treatment of BMDMs of both groups with HKLM did not change the expression of *Nos2* compared to non-treated cells, but treatment with IFN-γ alone and the combination of IFN-γ and HKLM led to a striking increase. Comparing *Hmgb1*$^{f/f}$ and *Hmgb1*$^{\Delta LysM}$ BMDMs, *Nos2* showed a higher expression in *Hmgb1*$^{\Delta LysM}$ BMDMs, untreated and HKLM-stimulated (1.8-fold increase, p = 0.0303). This slight difference was also maintained after treatment with IFN-γ alone as well as IFN-γ and HKLM (1.9-fold increase, p = 0.0260). Expression of *Ccl2* was comparably increased in both groups after treatment with IFN-γ, but increased even further after addition of HKLM in *Hmgb1*$^{\Delta LysM}$ BMDMs compared to *Hmgb1*$^{f/f}$ BMDMs (1.7-fold increase, p = 0.0152). *Il1b* expression was already significantly increased in *Hmgb1*$^{\Delta LysM}$ BMDMs compared to *Hmgb1*$^{f/f}$ BMDMs after treatment with HKLM alone (3.2-fold increase, p = 0.0022), a level that was only reached in *Hmgb1*$^{f/f}$ BMDMs after treatment with both IFN-γ and HKLM. Addition of IFN-γ to the treatment with HKLM did not affect the expression of Il1b in *Hmgb1*$^{\Delta LysM}$ BMDMs.

Taken together, HMGB1-depleted macrophages displayed a slightly higher phagocytic activity, but this did not affect their ability to eliminate intracellular bacteria. Interestingly, *Hmgb1*$^{\Delta LysM}$–derived macrophages demonstrated a slight hyper-responsiveness to HKLM treatment *in vitro*, on the one hand ruling out a lack of inflammatory mediators after infection as the reason for reduced anti-bacterial activity and suggesting this increased production of pro-inflammatory mediators as a reason for increased hepatic inflammation observed in *Hmgb1*$^{\Delta LysM}$ mice after *Listeria* infection.

### 5.3. Antibacterial activity of neutrophils *in vitro*

Since neutrophils have also been repeatedly discussed as potent effector cells during the immune response following infection with *Listeria monocytogenes* [74,75], isolated primary polymorphonuclear granulocytes (PMNs) were analyzed next. First, isolated PMNs from *Hmgb1*$^{f/f}$ and *Hmgb1*$^{\Delta LysM}$ mice were analyzed in respect to their ability to control the proliferation of *Listeria monocytogenes in vitro* (Fig. 24A). PMNs were infected with live *Listeria monocytogenes* at a MOI of 0.05. After 1 and 4 hours, PMNs were lysed, the culture was plated on Agar plates and colony-forming units (CFU) were counted the next day. This analysis showed that after one hour, incubation of *Listeria monocytogenes* with PMNs from either group did not

affect the bacterial proliferation. In contrast, after 4 hours, PMNs from both *Hmgb1*$^{f/f}$ and *Hmgb1*$^{\Delta LysM}$ mice were able to reduce bacterial proliferation by about 40 – 50 % compared to bacterial proliferation in the absence of cells (p(*Hmgb1*$^{f/f}$) = 0.0327; p(*Hmgb1*$^{\Delta LysM}$) = 0.0066), suggesting that PMNs derived from *Hmgb1*$^{f/f}$ and *Hmgb1*$^{\Delta LysM}$ mice have a comparable cytotoxic activity.

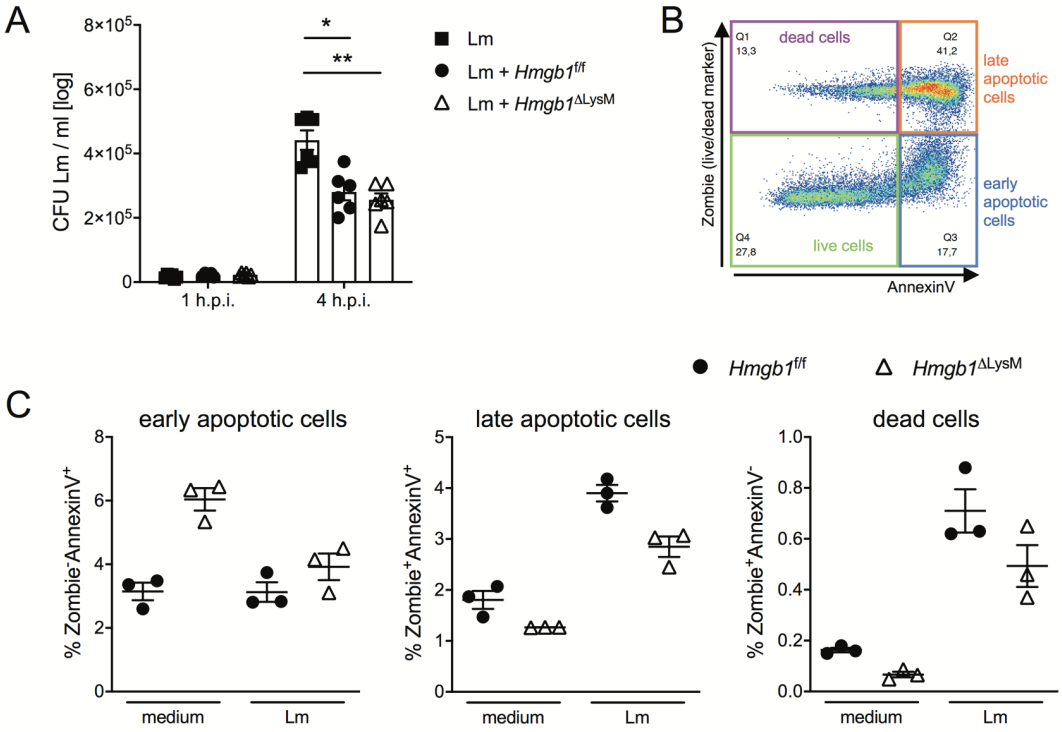


**Figure 24 | Anti-bacterial function and induction of apoptosis of neutrophils *in vitro*.** Analysis of bactericidal activity of neutrophils isolated from *Hmgb1*$^{f/f}$ and *Hmgb1*$^{\Delta LysM}$ mice (n = 5 – 6 samples per group) 1 and 4 hours after infection with *Listeria monocytogenes* (MOI = 0.05) (A). Flow cytometry analysis of live/dead marker (Zombie) and AnnexinV of neutrophils isolated from *Hmgb1*$^{f/f}$ and *Hmgb1*$^{\Delta LysM}$ mice (n = 3 samples per group) 2 hour post infection in order to differentiate live, apoptotic and dead cells of CD11b$^+$Ly6G$^+$ neutrophils(B, C). * $p < 0.05$, ** $p < 0.01$.

After 24 and 72 hours of infection, granulomas in the livers of *Hmgb1*$^{\Delta LysM}$ mice, which mainly consisted of neutrophils at 24 h.p.i., showed increased numbers of late apoptotic cells. A possible explanation could be, that neutrophils depleted of HMGB1 increasingly died due to apoptosis compared to control cells. In order to investigate this theory, staining of Annexin V and a live/dead marker (Zombie) was used to analyze the induction of apoptosis in PMNs following infection with *Listeria monocytogenes in vitro*. Annexin V is used to stain phosphatidylserine, which is usually located in the intracellular leaflet of the membrane, but

externalized continuously during the progression of apoptosis [132]. Co-staining using a live/dead marker allows for the distinction of live (AnnexinV$^-$Zombie$^-$) and dead (AnnexinV$^-$Zombie$^+$) cells, as well as early (AnnexinV$^+$Zombie$^-$) and late (AnnexinV$^+$Zombie$^+$) apoptotic cells (Fig. 24B). Incubation of PMNs and *Listeria monocytogenes* resulted in similar induction of cell membrane disintegration and apoptosis in *Hmgb1*$^{f/f}$ and *Hmgb1*$^{\Delta LysM}$ PMNs, demonstrated by the 2- to 3-fold increase of late apoptotic and dead cells following infection *in vitro* (Fig. 24C). Interestingly though, the amount of early apoptotic cells was already twice as high in the cell culture of *Hmgb1*$^{\Delta LysM}$ PMNs compared to *Hmgb1*$^{f/f}$ PMNs, an effect that was reduced after addition of *Listeria* to the culture. This suggests that HMGB1 at baseline could be involved in intracellular anti-apoptotic effects, that leads to early induction of apoptosis when HMGB1 is removed from these cells.

Overall, this data suggests that HMGB1 is not involved in the induction of anti-bacterial activity of macrophages or neutrophils *in vitro*, but might play a role in anti-apoptotic signaling. This could, at least partially, be the reason for the striking accumulation of dying cells in the liver of *Hmgb1*$^{\Delta LysM}$ mice 3 days post infection with *Listeria monocytogenes* witnessed in flow cytometry and TUNEL analysis.

## 6. HMGB1 from liver-resident and circulating immune cells contributes to anti-bacterial immune response

During the systemic infection with *Listeria monocytogenes*, Kupffer cells are targeted by bacteria and subsequently die due to necroptosis, followed by the infiltration of monocytes and neutrophils to the sites of infection and induction of a Type 1 inflammatory immune response [84]. To further investigate the role of tissue-resident macrophages and infiltrating monocytes and neutrophils, bone-marrow chimeric mice were generated and infected with *Listeria monocytogenes*. While microglia (tissue-resident macrophages in the brain) [133] and Langerhans cells (tissue-resident macrophages in the epidermis) [134] are able to survive lethal doses of irradiation, Kupffer cells are comparably less radioresistant and only a subset survives lethal irradiation [135,136]. The survival of this subset allows for the distinction of the importance of HMGB1 in liver-resident cells and infiltrating immune cells in respect to the induction of an immune response following infection. Irradiated wild-type and *Hmgb1*$^{\Delta LysM}$ mice were each reconstituted with wild-type bone marrow and ΔLysM bone marrow cells, respectively, and analyzed 72 hours post infection with *Listeria monocytogenes*.

*Hmgb1*$^{\Delta LysM}$ mice replenished with ΔLysM bone marrow (ΔLysM > ΔLysM) displayed increased bacterial burden in the liver, heightened expression of pro-inflammatory mediators as well as exacerbated hepatic granuloma formation and tissue injury, compared to wild-type mice reconstituted with wild-type bone marrow (wt > wt) (Fig. 25A). This was comparable to the effect previously observed in the genetic model of myeloid cell-specific ablation of HMGB1 (section 4). Wild-type mice that received bone marrow from *Hmgb1*$^{\Delta LysM}$ mice (ΔLysM > wt) showed a slightly increased bacterial burden (4.6-fold increase) compared to *Hmgb1*$^{\Delta LysM}$ mice reconstituted with wild-type bone marrow (wt > ΔLysM) (Fig. 25A). Gene expression of inflammatory markers *Ccl2*, *Tnfa* and *Nos2* in ΔLysM > wt and wt > ΔLysM mice though was comparably increased in comparison to wt > wt mice, but to a lesser extent than ΔLysM > ΔLysM mice (Fig. 25B). Analyzing live intrahepatic immune cells via flow cytometry revealed significantly decreased levels of dendritic cells in ΔLysM > ΔLysM and ΔLysM > wt mice compared to wt > wt mice, suggesting a role of HMGB1 in circulating immune cells for the infiltration of dendritic cells, although this could not be seen in mice with myeloid-cell specific ablation of HMGB1 (section 4). Infiltration of neutrophils and inflammatory monocytes 72 hours post infection was comparable between the four groups, possibly with a slight trend towards reduced numbers in ΔLysM > ΔLysM mice, although this is not completely clear due to the small numbers of mice (n = 3 mice per group) and scattering of samples within the groups (Fig. 25D).

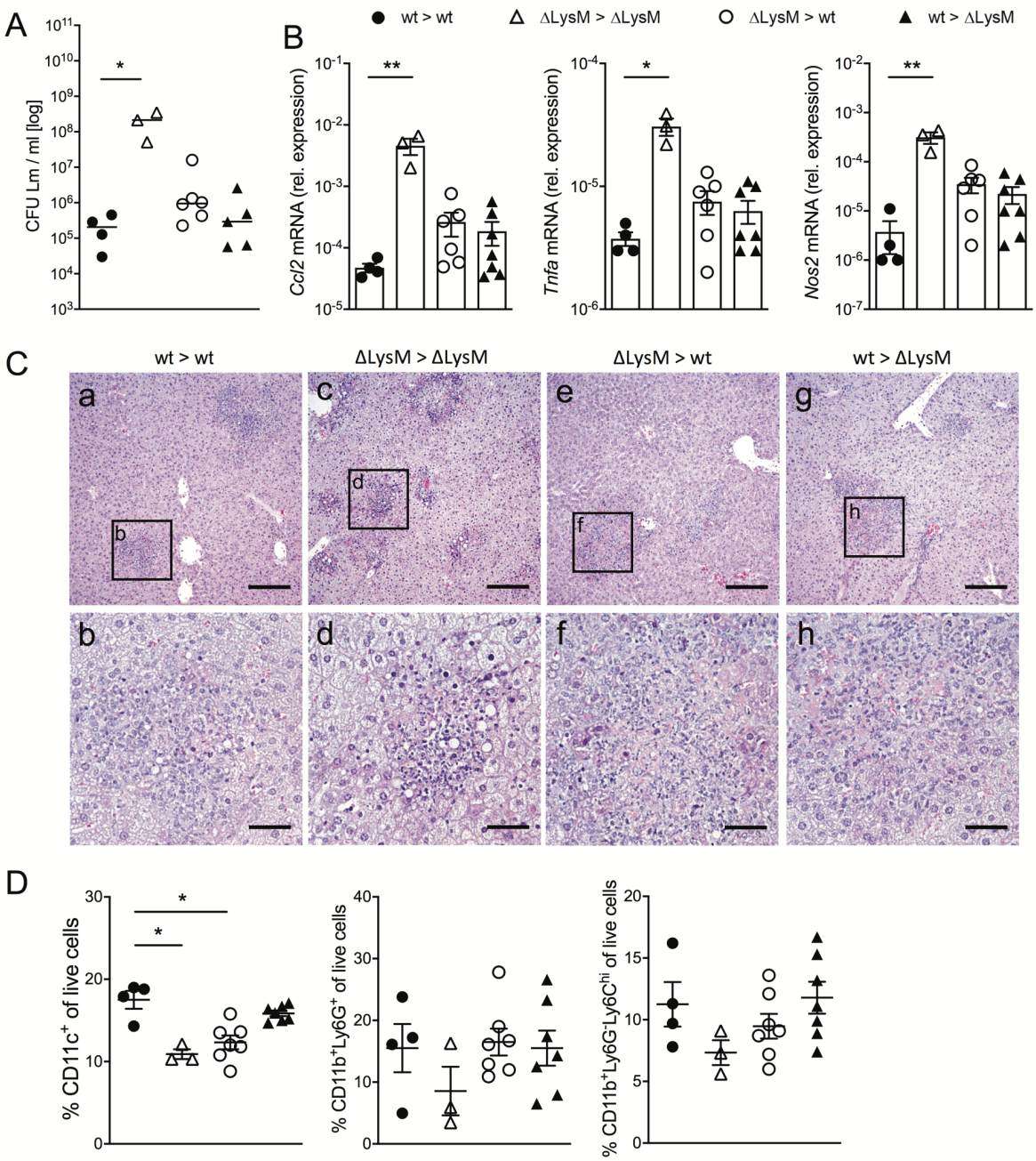


**Figure 25 | Hepatic inflammation in bone marrow chimera following *Listeria* infection.** Hepatic bacterial burden in bone marrow chimera of wild-type and *Hmgb1*$^{\Delta LysM}$ mice (n = 3 – 7 mice per group) after infection with 2 × $10^4$ *Listeria monocytogenes* (A). Expression analysis of *Ccl2*, *Tnfa* and *Nos2* in whole-liver lysates using qRT-PCR 72 hours after infection (n = 3 – 7 mice per group, B). All expression levels were normalized to 18S and are shown as relative expression levels. HE staining of liver sections of the indicated chimeric mice 72 hours post infection (C). Flow cytometry analysis of intrahepatic immune cells 72 hours after infection, showing relative numbers of $CD11c^+$ dendritic cells, $CD11b^+Ly6G^+$ neutrophils and $CD11b^+Ly6G^-Ly6C^{hi}$ monocytes (n = 3 – 7 mice per group, D). Scale bars = 200 µm (a, c, e, g) and 50 µm (b, d, f, h). * $p < 0.05$, ** $p < 0.01$.

Taken together, it seems that HMGB1 in both tissue-resident and infiltrating immune cells plays a critical role in the activation of anti-bacterial immune responses. Immune cell and tissue crosstalk needs to be analyzed further for a more decisive conclusion on the role of HMGB1 in different cell types during bacterial infection.

## 7. HMGB1 deficiency in myeloid cells is associated with differential hepatic inflammatory gene expression early after infection with *Listeria monocytogenes*

Since HMGB1 from myeloid cells plays a crucial role in anti-bacterial activity following infection with *Listeria monocytogenes*, and *in vitro* analyses of macrophages and neutrophils did not show inherent cellular deficiencies, NanoString analysis was used to analyze expression profiles of 734 myeloid cell-related genes. NanoString technology uses probes carrying specific barcodes to identify and quantify single mRNA molecules. For this analysis, samples from *Hmgb1*$^{f/f}$ and *Hmgb1*$^{\Delta LysM}$ mice with similar hepatic bacterial titers after 24 hours of infection were used to ensure comparable amounts of bacteria in the liver as well as comparable exposure of immune cells to PAMPs, highlighting only differences as a result of HMGB1 (Fig. 26A).

Heatmap analysis showed clear clustering of mice according to their treatment as well as their genotype, illustrating transcriptional differences due to the presence or absence of HMGB1 in myeloid cells (Fig. 26B). In general, infection with *Listeria monocytogenes* led to the upregulation of pro-inflammatory mediators in both groups. For example, transcription of *Tlr2* as well as *Cxcl9*, *Cxcl10* and *Cxcl11*, chemokines that regulate migration, differentiation and activation of immune cells [137], were clearly upregulated after infection with *Listeria*, indicating an induction of an immune response in both *Hmgb1*$^{f/f}$ and *Hmgb1*$^{\Delta LysM}$ animals. In contrast, some pro-inflammatory mediators were differentially expressed. As an example, $Ca2^{+}$ sensors *S100a8* and *S100a9* as well as *Cd14* were upregulated in *Hmgb1*$^{\Delta LysM}$ mice. S100A8 and S100A9 are constitutively expressed in neutrophils and monocytes. During inflammation, the heterodimer S100A8/9 is actively released and subsequently induces leukocyte infiltration and cytokine secretion [138]. CD14 acts as a co-receptor for PAMPs such as LPS and lipoteichoic acid and is therefore directly involved in the recognition of pathogens [139,140].

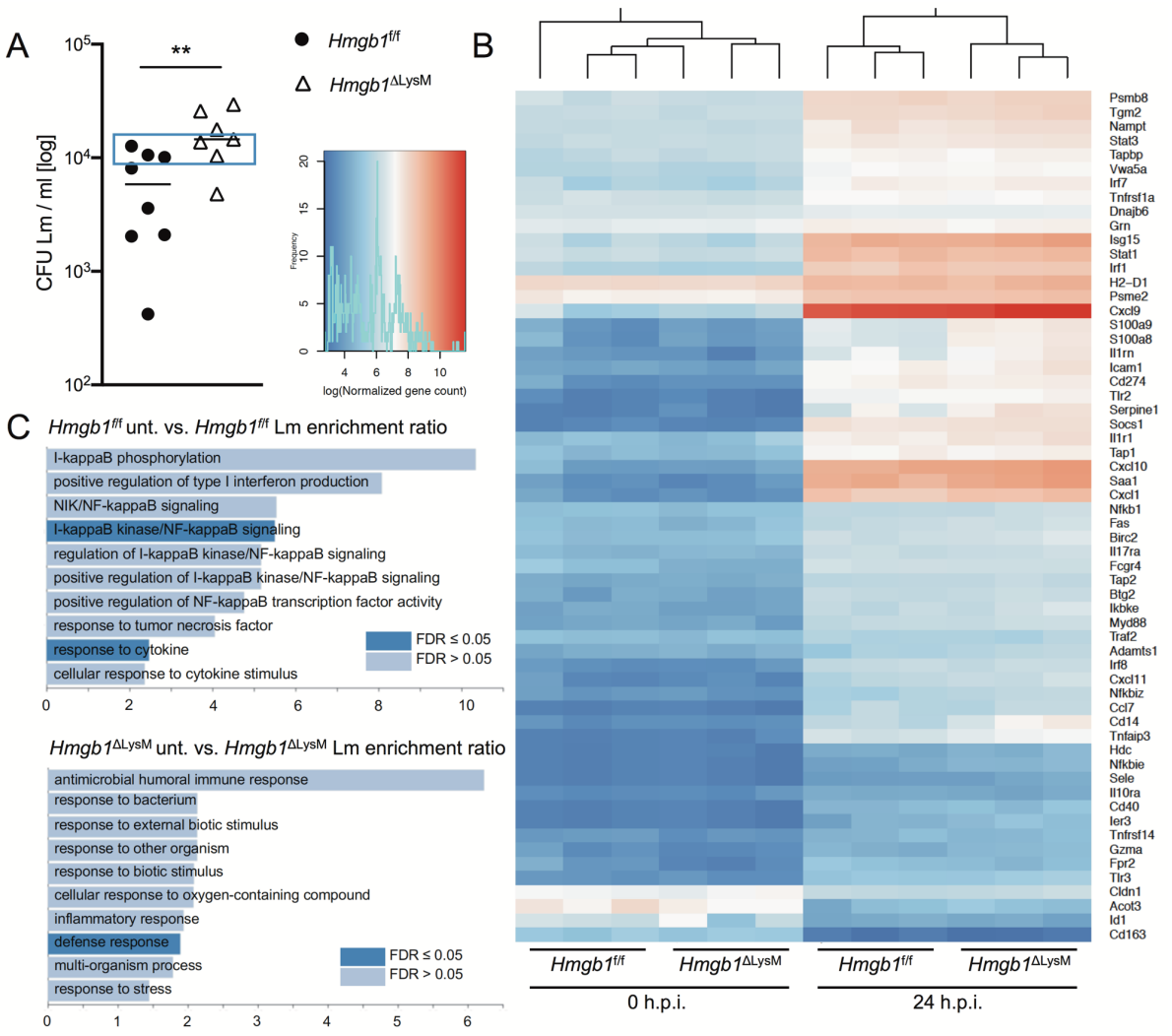


**Figure 26 | Nanostring analysis of myeloid genes 24 hours after infection with *Listeria monocytogenes*.** Hepatic bacterial burden of *Hmgb1*$^{f/f}$ and *Hmgb1*$^{\Delta LysM}$ mice (n = 7 – 8 mice per group) 24 hours after infection with *Listeria monocytogenes* (A). Whole liver lysates of titer-matched samples (blue box) were used for Nanostring analysis. Heatmap analysis of hepatic gene expression of indicated samples at baseline and 24 hours after infection(B). Overrepresentation enrichment analysis of *Hmgb1*$^{f/f}$ and *Hmgb1*$^{\Delta LysM}$ samples (C).

When analyzing the activation of signaling pathways rather than single mediators, overrepresentation enrichment analysis revealed differentially activated immune pathways in *Hmgb1*$^{f/f}$ and *Hmgb1*$^{\Delta LysM}$ mice despite comparable hepatic bacterial burden (Fig. 26C). *Listeria* infection in *Hmgb1*$^{f/f}$ mice led to a strong activation of NF-κB -mediated signaling pathways, leading to the transcription of a vast array of inflammatory mediators. Also, myeloid cells from *Hmgb1*$^{f/f}$ mice displayed increased responses to cytokines, especially TNF-α following infection. In striking contrast, infected *Hmgb1*$^{\Delta LysM}$ mice upregulated anti-bacterial defense mechanisms and antimicrobial humoral immune responses.

This data indicates that, even though only a small number of genes are significantly differentially expressed due to the ablation of HMGB1 from myeloid cells, it results in a strikingly different activation of immune pathways in response to infection with *Listeria monocytogenes*. The absence of NF-κB signaling pathways in *Hmgb1*$^{\Delta LysM}$ mice also suggests that HMGB1 might be directly involved in the activation of NF-κB -mediated immune pathways and the subsequent responses towards bacterial pathogens.

# IV. Discussion

Comparable to the properties of PAMPs in the initiation of immune responses, DAMPs, released from stressed or decaying cells, induce inflammation following tissue damage, as well as subsequent wound healing [141]. Elevated levels of circulating DAMPs can be detected during viral [38,142] and bacterial [40,143] infections, most likely due to tissue damage caused by infections and activated immune and parenchymal cells. Since the prototypical DAMP HMGB1 has been shown to be highly conserved across species and is greatly expressed in nearly all cells, it is believed to have important functions, not only during homeostasis, but also during inflammation, since it has been suggested to facilitate inflammation by acting as an adjuvant for the immune response [144-146]. Until recently, the limited availability of genetic models hindered the discoveries concerning HMGB1. This study, using genetic models of cell-specific depletion of HMGB1, analyzed the role of HMGB1 in inducing an immune response towards *Listeria monocytogenes*. While HMGB1 from hepatocytes was shown to be dispensable during the controlled infection, myeloid cell-derived HMGB1 seems to be a critical co-activator of immune responses towards *Listeria monocytogenes*, by inducing gene expression of an array of pro-inflammatory mediators as well as early monocyte infiltration following infection. Additionally, this work raises concerns about antibody-mediated neutralization of HMGB1 as a general therapeutic strategy for sepsis, due to its negative impact during systemic Listeriosis.

## 1. Antibody-mediated HMGB1 neutralization impairs defense against *Listeria monocytogenes*

The positive effect of antibody-mediated HMGB1 neutralization has previously been shown for LPS-induced septic shock [37] and polymicrobial abdominal sepsis [14]. The lethality of established sepsis could be reversed by inhibiting endogenous HMGB1, suggesting HMGB1 inhibition as a relevant clinical therapeutic option for sepsis [14]. In striking contrast to these findings, HMGB1 neutralization in the context of systemic *Listeria monocytogenes* infection resulted in increased bacterial titer and aggravated tissue damage and inflammation in the liver 72 hours after infection. Infiltration of neutrophils into the liver following infection seemed to be slightly increased in HMGB1-neutralized mice, which was also accompanied by increased expression levels of the monocyte-attracting chemokine CCL2 and effector molecule iNOS. This confirms previous results showing no survival benefit following LPS-induced shock even though HMGB1 release was suppressed [34]. Possible explanations for these differing results are adverse effects of antibody injections, subtle differences in mouse models due to genetics or

housing (e.g. intestinal microbiome), or context-dependent differences in the function of HMGB1. For example, differing roles of HMGB1 could be due to varying release mechanisms from different cell subsets (active release from immunocompetent cells or passive release from dying or decaying cells) or due to varying infection and inflammation mechanisms (e.g. viral and bacterial infections).

## 2. Aggravated bacterial infection in mice with myeloid cell-specific ablation of HMGB1 is not caused by defects in autophagy

In contrast to its role during sterile inflammation [34], hepatocyte-derived HMGB1 was dispensable for the anti-bacterial immune response during the systemic infection with *Listeria monocytogenes*. However, specific HMGB1 ablation in myeloid cells demonstrated a comparable phenotype to mice with antibody-mediated HMGB1 neutralization. The notion, that HMGB1 from myeloid cells plays a critical role during the immune response towards *Listeria monocytogenes*, is supported by the fact, that the initial target of *Listeria* in the liver and spleen are phagocytes [147], which die due to necroptosis releasing DAMPs into their surrounding. This indicates a potential DAMP role of HMGB1 during systemic Listeriosis.

The phenotype that was observed in *Hmgb1*$^{\Delta LysM}$ mice is also in accordance with a previous study of the consequences of HMGB1 depletion from myeloid cells during systemic Listeriosis, which concluded that the impaired anti-bacterial immune response was a result of autophagy defects in phagocytes due to the absence of HMGB1 [148]. In this current study, analysis of LC3, a marker for the induction of autophagy, was not differentially induced following infection with *Listeria monocytogenes* in either HMGB1-proficient or –deficient mice. Additionally, macrophages of both mice *in vitro* showed a comparable upregulation of LC3 following infection with *Listeria monocytogenes*. However, *in vivo*, an upregulation of p62 could be observed in *Hmgb1*$^{\Delta LysM}$ mice, which could be shown to localize mainly in hepatocytes surrounding granulomas in the liver. Inhibition of p62 degradation within cells has usually been suggested to indicate defects in autophagy [126]. In contrast to this, heightened p62 expression and subsequent accumulation has also been suggested to aid in autophagy and therefore restriction of intracellular replication of bacteria [149]. Activation of p62 has also been shown to have beneficial effects in prion diseases [150], as well as activation of NLRP3 inflammasome during mycobacterium infection [151], indicating various important roles of p62 during innate immunity. In addition to the *in vivo* analysis, protein levels of p62 in extracts of BMDMs stimulated with heat-inactivated *Listeria monocytogenes* were comparable in *Hmgb1*$^{f/f}$ and

*Hmgb1*$^{\Delta LysM}$ cells, confirming the absence of autophagy defects in myeloid cells due to HMGB1 ablation.

*Listeria monocytogenes* has been shown to evade autophagy using actin-based motility via ActA-mediated protection from ubiquitylation [105,152]. Targeting for autophagy is increased when *Listeria* lack ActA, since they then undergo ubiquitylation, followed by p62 and LC3 recruitment and finally degradation by autophagy [105], implying that *Listeria* have found a functioning mode of autophagy escape. P62 accumulation in hepatocytes surrounding granulomas containing *Listeria* can therefore be the result of stress responses and antibacterial activation of hepatocytes due to overwhelming amounts of bacteria and defects in containment within granulomas in the liver, demonstrating an important role for p62-mediated autophagy as an innate immune defense mechanism. Defects in autophagy due to ablation of HMGB1 could, in this model, be largely ruled out as the cause of impaired bacterial control.

Following infection with *Listeria*, no apparent defects in inflammatory gene induction or cytokine release could be observed in *Hmgb1*$^{\Delta LysM}$ mice. Increased induction of pro-inflammatory cytokines correlated with the increased hepatic bacterial burden in HMGB1-ablated animals. This indicates that these essential inflammatory pathways are not affected by missing HMGB1, therefore, more likely induced by released PAMPs or DAMPs other than HMGB1, because of the infection.

During the overwhelming infection with *Listeria* in *Hmgb1*$^{\Delta LysM}$ mice, HMGB1 is shuttled from the nuclei of hepatocytes into their cytoplasm, which is likely followed by active secretion of HMGB1 [119], since increased levels of circulating HMGB1 in the serum could be detected in these animals. This release is most likely due to hepatocyte stress because of the high bacterial titer and inflammation in the liver and can serve as a reinforcement of immune activation following bacterial infection. This conclusion in connection with our previous observations in hepatocyte-specific knockouts of HMGB1 urges the differentiation of controlled and uncontrolled infection with *Listeria monocytogenes*. Hepatocyte-derived HMGB1 seems dispensable during a controlled bacterial infection, but may also be the cause of excessive inflammation during an uncontrolled bacterial infection, which is accompanied by aggravated tissue damage. These processes still need further analysis in order to elucidate the role of HMGB1 during different magnitudes of infection.

## 3. Reduced monocyte infiltration possibly contributes to impaired antibacterial immune response in *Hmgb1*$^{\Delta LysM}$ mice

After 24 hours of infection, significantly lower numbers of Ly6C$^{hi}$ inflammatory monocytes could be detected in the liver of *Hmgb1*$^{\Delta LysM}$ mice, an effect that could still be observed at 72 hours post infection, but to a lesser extent. Since the differentiation of inflammatory monocytes into Tip-DCs and M1 monocyte-derived macrophages is required for an adequate immune response towards *Listeria monocytogenes*, this decreased infiltration could possibly lead to the observed increase in bacterial burden in the liver of *Hmgb1*$^{\Delta LysM}$ mice. HMGB1 has previously been shown to be responsible for monocyte recruitment via the RAGE/NF-κB signaling pathway by inducing the production of CCL2 as well as inhibiting apoptotic cell death of monocytes by impeding the degradation of the pro-apoptotic protein myeloid cell leukemia 1 (MCL-1) via the MAPK/ERK signaling pathway [153,154].

Inflammatory monocytes express high levels of CCR2, the receptor for the chemoattractant CCL2, and Ly6C [155]. CCR2 on monocytes is necessary for the extravasation from the bone marrow and subsequent recruitment to sites of infection, where monocytes differentiate into Tip-DCs in order to support bacterial clearance [156]. CCR2-deficient mice (CCR2$^{-/-}$) are highly susceptible to *Listeria* infection [65,157] with increased severity of the infection also in the liver [72]. Infection of CCR2$^{-/-}$ mice with *Listeria monocytogenes* infection resulted in a phenotype comparable to the one observed in *Hmgb1*$^{\Delta LysM}$ mice in this study, including decreased infiltration of inflammatory monocytes into the liver and increased bacterial burden already 24 hours, resulting in 100-fold increase 72 hours post infection. Immunofluorescent staining showed that on day 3 of the infection, monocytes localized to the periphery of granuloma in the liver [63]. Interestingly, immunohistochemical analysis of *Listeria* in the liver of *Hmgb1*$^{\Delta LysM}$ mice showed localization of bacteria also in the periphery of the granuloma in the liver 72 hours post infection. This was in contrast to *Hmgb1*$^{f/f}$ mice, where *Listeria* could mainly be seen in the center of the granulomas. On the one hand, this supports the notion of an uncontrolled infection, since the cells in the granulomas are not able to contain the bacteria within this cellular cluster. On the other hand, this raises the question whether the decreased infiltration of monocytes leads to lower numbers of monocytes in the periphery of the granuloma and therefore increased spread of bacteria or if the monocytes are even infected by *Listeria*, which is normally not observed during *Listeria* infection [63]. Additionally, the fact that RNA expression of *Ccl2*, the chemokine responsible for monocyte infiltration following infection[116,117], is already significantly increased 24 hours after *Listeria* infection in mice with myeloid cell-specific depletion of HMGB1, suggests a direct effect of HMGB1 on the infiltration of monocytes. The characterization of monocytes depleted of HMGB1 during the infection with *Listeria*

*monocytogenes* as well as the effect of HMGB1 on the extravasation and migration of monocytes following infection still needs further analysis.

In contrast to decreased levels of monocytes, increased levels of neutrophils could be observed in the livers of *Hmgb1*$^{\Delta LysM}$ mice 24 hours post infection, which is most likely in response to increased hepatic bacterial burden and inflammation. Histological analysis of neutrophils showed granuloma formation with large amounts of neutrophils in the center. The decrease in living neutrophils in the liver 72 hours post infection, compared to the previous time point, in both groups can possibly be explained with increased levels of cell death, especially in the HMGB1-depleted animals due to high bacterial burden and high levels of inflammation in the liver, which correlates with the large amounts of TUNEL$^{+}$ cells within the granulomas of *Hmgb1*$^{\Delta LysM}$ mice.

## 4. Increased accumulation of dead immune cells possibly contributes to exacerbated inflammation and infection

Histological and flow cytometry analysis revealed exacerbated apoptosis and accumulation of dead cells within disseminating hepatic granulomas in the livers of *Hmgb1*$^{\Delta LysM}$ mice. Since granulomas were shown to largely contain neutrophils 24 hours post infection, it can be speculated that these accumulated dead cells are mainly consist of neutrophils, which is also supported by the decreased levels of living neutrophils observed in flow cytometry analysis 72 hours post infection in *Hmgb1*$^{\Delta LysM}$ mice. Neutrophils *in vitro* did not display increased apoptosis following *Listeria* infection, indicating that the accumulation of dead cells could more likely be due to decreased clearance of dead cells from the tissue. The mechanism of efferocytosis, phagocytosis of apoptotic cells, is a critical step towards the resolution of inflammation [96] since it leads to the removal of potentially pro-inflammatory and tissue-damaging intracellular contents of dying cells, and also induces the release of anti-inflammatory factors like IL-10 and TGF-β and suppresses the production of pro-inflammatory cytokines by macrophages [158]. *In vitro*, M2 macrophages show an increased ability to ingest apoptotic cells in comparison to M1-polarized macrophages [159,160]. Since the livers of *Hmgb1*$^{\Delta LysM}$ mice were still clearly M1-polarized 72 hours after infection with *Listeria monocytogenes*, in comparison to control mice, which displayed signs of regenerative M2 polarization, this could support the notion of reduced efferocytosis in these livers. Impairment of efferocytosis can lead to prolonged inflammation due to the progression of apoptotic cells to necrosis and the concomitant release of proinflammatory cellular components. Additionally, reduction in efferocytosis may also impede

phagocytosis of bacteria and other microorganisms, leading to prolonged proliferation and inflammation.

It has been shown that both intra- and extracellular HMGB1 are able to decrease phagocytic activities of macrophages. Since hepatocytes in *Hmgb1*$^{\Delta LysM}$ mice were shown to translocate and subsequently release large amounts of HMGB1 after *Listeria* infection, extracellular HMGB1 could diminish the abilities of macrophages to phagocytose apoptotic neutrophils in *Hmgb1*$^{\Delta LysM}$ mice. A previous study showed, that released HMGB1 can prevent macrophage efferocytosis by binding to exposed phosphatidylserine (PS) on apoptotic neutrophils [161] as well as obstructing the activation of $\alpha_v\beta_3$ and the ensuing phosphorylation of ERK and activation of Rac-1 [162], which is required for efficient efferocytosis [163-166]. The reduction in efferocytosis due to the large amounts of extracellular HMGB1 does not only impede phagocytosis of *Listeria*, leading to prolonged proliferation and inflammation, but apoptotic cells have also been shown to enhance the pathogenesis of *Listeria monocytogenes* [93], possibly adding to the overwhelming bacterial burden in *Hmgb1*$^{\Delta LysM}$ mice 72 hours after infection.

## 5. HMGB1 from both tissue-resident and circulating immune cells contributes to the immune response towards *Listeria monocytogenes*

To further distinguish the role of HMGB1 from tissue-resident and infiltrating immune cells, *Listeria monocytogenes* infection was analyzed in chimeric mice. Irradiation of mice led to a depletion of immune cells, with the exception of tissue-resident Kupffer cells, and allowed for reconstitution of the immune system with bone marrow cells from mice with a different genetic background. Therefore, mice with HMGB1-proficient Kupffer cells and –deficient circulating immune cells as well as mice with HMGB1-deficient Kupffer cells and –proficient circulating immune cells could be analyzed. The only very slight increase in hepatic bacterial burden and inflammatory markers in both groups compared to wild type mice infected with *Listeria monocytogenes* could be because only a subset of Kupffer cells resists lethal irradiation and the rest is subsequently replaced by bone marrow monocyte-derived Kupffer cells [135,136]. This might lead to an attenuated effect, since only a part of the Kupffer cells would be HMGB1-deficient or –proficient, respectively.

The minor effect of HMGB1 from either tissue-resident or circulating immune cells though, could also suggest a compensatory effect of HMGB1 when it is missing from only one population, and that therefore the depletion of HMGB1 from all myeloid cells is detrimental for the antibacterial immune response. This would indicate that HMGB1 acts both as a DAMP,

released from dying infected tissue-resident phagocytes, as well as a cytokine and chemokine actively secreted from infiltrating activated immune and parenchymal cells.

## 6. HMGB1 deficiency in myeloid cells is associated with differential hepatic inflammatory gene expression early after infection with *Listeria monocytogenes*

Nanostring analysis of liver samples 24 hours after infection with *Listeria monocytogenes* was performed in order to gain more insight into the gene expression profile of myeloid cells proficient and deficient of HMGB1, respectively. According to this analysis, *Hmgb1*$^{f/f}$ liver samples displayed over-representation of NF-κB-related pathways, which was not detectable in *Hmgb1*$^{\Delta LysM}$ animals. In contrast, livers of *Hmgb1*$^{\Delta LysM}$ mice showed increased responses to pathogens, which was absent in *Hmgb1*$^{f/f}$ livers. Therefore one possibility would be, that HMGB1 during Listeriosis acts as a co-activator of NF-κB signaling. Although the over-representation analysis points towards differing activation of immune pathways, the increased expression of DAMPs like S100A8 and S100A9, the TLR4-coreceptor CD14 and chemokines CXCL2 and CXCL3 could also be due to varying amounts of infiltrating immune cells in the livers of *Hmgb1*$^{f/f}$ and *Hmgb1*$^{\Delta LysM}$ mice. RNA sequencing analysis showed high expression levels of Cd14, S100a8, S100a9 and Cxcl2 in bone marrow and peritoneal neutrophils, but only very low levels in inflammatory monocytes [167]. Therefore the increased expression seen in the Nanostring analysis correlates with the larger number of infiltrating neutrophils into the livers of *Hmgb1*$^{\Delta LysM}$ mice 24 hours post infection in comparison to *Hmgb1*$^{f/f}$ mice.

Increased expression of the $Ca^{2+}$ binding proteins S100A8 and S100A9 has been associated with exacerbation of inflammation for example during HIV-1 infection [168], Influenza A Virus infection [142] or septic shock [169]. S100A8 and S100A9 usually form heterodimers in order to aid in cytoskeleton rearrangement and arachidonic acid metabolism. Excessive expression und secretion by neutrophils, monocytes and macrophages following bacterial infection exacerbate innate immune responses by stimulating increased cytokine release by neutrophils and macrophages, aggravating inflammation [138]. CD14, combined with TLR4 and MD2, is crucial for the recognition of LPS and/or endotoxin from Gram-negative bacteria, which results in the activation of an immune response.

In order to really determine the role of these differentially regulated genes during *Listeria* infection in *Hmgb1*$^{f/f}$ and *Hmgb1*$^{\Delta LysM}$ mice, further analysis of immune pathways and verification of these results using qRT-PCR is needed.

## 7. Final conclusion

Elevated levels of serum HMGB1 have been detected in patients with surgical sepsis [37] and hemorrhagic shock [170] and has additionally been shown to increase in mice after LPS administration, where it remains elevated for more than 36 hours after injection [37], indicating a function for HMGB1 during inflammation. Therefore, HMGB1 has repeatedly been proposed as a potent therapeutic target in sterile and infectious inflammation. Especially antibody-mediated neutralization has been shown in various settings like endotoxemia [37,171], sepsis [14,172,173] or gastrointestinal disorders [174,175] to have beneficial effects on the disease outcome. In this study, antibody-mediated neutralization and myeloid cell-specific depletion of HMGB1 were shown to lead to exacerbated systemic listeriosis and concomitant inflammation. The properties of released HMGB1 seem to be highly context-dependent and therefore it requires closer analysis in order to function as a therapeutic target.

The limitation of this study lies in the myeloid cell-specific knockout, which affects multiple cell types (neutrophils, monocytes, macrophages, dendritic cells), which complicates the differentiation of effects according to cell type, especially in an infection that involves all these different cell types. Isolating these cell populations and analyzing their effects *in vitro* on the other hand, eliminates interactions with other cell populations, also limiting the investigation. In order to more accurately determine the role of HMGB1 from each cell type, cell-specific depletion models of HMGB1 in monocytes, neutrophils and dendritic cells would have to be analyzed.

Overall, the performed analyses in this study propose a time course of HMGB1 influence on the innate immune response during Listeriosis. Initially, depletion of HMGB1 from myeloid cells leads to decreased infiltration of inflammatory monocytes resulting in reduced anti-bacterial defenses and subsequent increased hepatic bacterial burden and heightened inflammation. This is accompanied by increased infiltration of neutrophils, further exacerbating inflammation. At the same time, it is possible, that differential activation of anti-bacterial gene regulatory pathways leads to a decreased activation of immune cells in HMGB1-depleted cells. This aggravated infection and increased inflammation in the liver leads to the secretion of HMGB1 from hepatocytes, accumulation of dead cells in the liver due to reduced efferocytosis and subsequently further increase in bacterial burden. Finally, this study shows the context-dependent nature of HMGB1 activity, cautioning a universal application of HMGB1 as a therapeutic target in sterile and infectious inflammation.

# V. References


1. Burnet FM. The Clonal Selection Theory of Acquired Immunity. Nashville, TN: Vanderbilt Univ. Press; 1959.

2. Bretscher P, Cohn M. A theory of self-nonself discrimination. Science. 1970;169:1042–9.

3. Lafferty KJ, Cunningham AJ. A new analysis of allogeneic interactions. Aust J Exp Biol Med Sci. 1975;53:27–42.

4. Janeway CA. Approaching the asymptote? Evolution and revolution in immunology. Cold Spring Harb. Symp. Quant. Biol. 1989;54 Pt 1:1–13.

5. Matzinger P. The danger model: a renewed sense of self. Science. American Association for the Advancement of Science; 2002;296:301–5.

6. Chen GY, Nuñez G. Sterile inflammation: sensing and reacting to damage. Nat. Rev. Immunol. 2010;10:826–37.

7. Agresti A, Bianchi ME. HMGB proteins and gene expression. Curr. Opin. Genet. Dev. 2003;13:170–8.

8. Andersson U, Tracey KJ. HMGB1 Is a Therapeutic Target for Sterile Inflammation and Infection. Annu. Rev. Immunol. 2011;29:139–62.

9. Rovere-Querini P, Capobianco A, Scaffidi P, Valentinis B, Catalanotti F, Giazzon M, et al. HMGB1 is an endogenous immune adjuvant released by necrotic cells. EMBO Rep. 2004;5:825–30.

10. Su Z, Zhang P, Yu Y, Lu H, Liu Y, Ni P, et al. HMGB1 Facilitated Macrophage Reprogramming towards a Proinflammatory M1-like Phenotype in Experimental Autoimmune Myocarditis Development. Scientific Reports. Nature Publishing Group; 2016;6:21884.

11. Lotze MT, Tracey KJ. High-mobility group box 1 protein (HMGB1): nuclear weapon in the immune arsenal. Nat. Rev. Immunol. 2005;5:331–42.

12. Stros M. HMGB proteins: interactions with DNA and chromatin. Biochim. Biophys. Acta. 2010;1799:101–13.

13. Li J, Kokkola R, Tabibzadeh S, Yang R, Ochani M, Qiang X, et al. Structural basis for the proinflammatory cytokine activity of high mobility group box 1. Mol. Med. 2003;9:37–45.

14. Yang H, Ochani M, Li J, Qiang X, Tanovic M, Harris HE, et al. Reversing established sepsis with antagonists of endogenous high-mobility group box 1. Proceedings of the National Academy of Sciences. 2004;101:296–301.

15. Bonaldi T, Talamo F, Scaffidi P, Ferrera D, Porto A, Bachi A, et al. Monocytic cells hyperacetylate chromatin protein HMGB1 to redirect it towards secretion. EMBO J. John Wiley & Sons, Ltd; 2003;22:5551–60.

16. Gardella S, Andrei C, Ferrera D, Lotti LV, Torrisi MR, Bianchi ME, et al. The nuclear protein HMGB1 is secreted by monocytes via a non-classical, vesicle-mediated secretory pathway.

EMBO Rep. 2002;3:995–1001.

17. Lu B, Antoine DJ, Kwan K, Lundbäck P, Wähämaa H, Schierbeck H, et al. JAK/STAT1 signaling promotes HMGB1 hyperacetylation and nuclear translocation. Proc. Natl. Acad. Sci. U.S.A. 2014;111:3068–73.

18. Lamkanfi M, Sarkar A, Vande Walle L, Vitari AC, Amer AO, Wewers MD, et al. Inflammasome-dependent release of the alarmin HMGB1 in endotoxemia. J. Immunol. 2010;185:4385–92.

19. Lu B, Nakamura T, Inouye K, Li J, Tang Y, Lundbäck P, et al. Novel role of PKR in inflammasome activation and HMGB1 release. Nature. 2012;488:670–4.

20. Antoine DJ, Harris HE, Andersson U, Tracey KJ, Bianchi ME. A Systematic Nomenclature for the Redox States of High Mobility Group Box (HMGB) Proteins. Mol. Med. 2014;20:135–7.

21. Hoppe G, Talcott KE, Bhattacharya SK, Crabb JW, Sears JE. Molecular basis for the redox control of nuclear transport of the structural chromatin protein Hmgb1. Exp. Cell Res. 2006;312:3526–38.

22. Venereau E, Casalgrandi M, Schiraldi M, Antoine DJ, Cattaneo A, De Marchis F, et al. Mutually exclusive redox forms of HMGB1 promote cell recruitment or proinflammatory cytokine release. J. Exp. Med. 2012;209:1519–28.

23. Schiraldi M, Raucci A, Muñoz LM, Livoti E, Celona B, Vénéreau E, et al. HMGB1 promotes recruitment of inflammatory cells to damaged tissues by forming a complex with CXCL12 and signaling via CXCR4. J. Exp. Med. 2012;209:551–63.

24. Yang H, Hreggvidsdottir HS, Palmblad K, Wang H, Ochani M, Li J, et al. A critical cysteine is required for HMGB1 binding to Toll-like receptor 4 and activation of macrophage cytokine release. Proc. Natl. Acad. Sci. U.S.A. 2010;107:11942–7.

25. Yang H, Lundbäck P, Ottosson L, Erlandsson-Harris H, Venereau E, Bianchi ME, et al. Redox modification of cysteine residues regulates the cytokine activity of high mobility group box-1 (HMGB1). Mol. Med. 2012;18:250–9.

26. Yang H, Wang H, Ju Z, Ragab AA, Lundbäck P, Long W, et al. MD-2 is required for disulfide HMGB1-dependent TLR4 signaling. J. Exp. Med. 2015;212:5–14.

27. Parkkinen J, Raulo E, Merenmies J, Nolo R, Kajander EO, Baumann M, et al. Amphoterin, the 30-kDa protein in a family of HMG1-type polypeptides. Enhanced expression in transformed cells, leading edge localization, and interactions with plasminogen activation. J. Biol. Chem. 1993;268:19726–38.

28. Kokkola R, Andersson A, Mullins G, Ostberg T, Treutiger C-J, Arnold B, et al. RAGE is the major receptor for the proinflammatory activity of HMGB1 in rodent macrophages. Scand. J. Immunol. John Wiley & Sons, Ltd (10.1111); 2005;61:1–9.

29. Huttunen HJ, Fages C, Rauvala H. Receptor for advanced glycation end products (RAGE)-mediated neurite outgrowth and activation of NF-kappaB require the cytoplasmic domain of the receptor but different downstream signaling pathways. J. Biol. Chem. 1999;274:19919–24.

30. Xu J, Jiang Y, Wang J, Shi X, Liu Q, Liu Z, et al. Macrophage endocytosis of high-mobility group box 1 triggers pyroptosis. Nature Publishing Group; 2014;21:1229–39.

31. Kew RR, Penzo M, Habiel DM, Marcu KB. The IKKα-dependent NF-κB p52/RelB noncanonical pathway is essential to sustain a CXCL12 autocrine loop in cells migrating in response to HMGB1. J. Immunol. 2012;188:2380–6.

32. Zhang W, Guo S, Li B, Liu L, Ge R, Cao T, et al. Proinflammatory effect of high-mobility group protein B1 on keratinocytes: an autocrine mechanism underlying psoriasis development. J. Pathol. John Wiley & Sons, Ltd; 2017;241:392–404.

33. Tsung A, Sahai R, Tanaka H, Nakao A, Fink MP, Lotze MT, et al. The nuclear factor HMGB1 mediates hepatic injury after murine liver ischemia-reperfusion. Journal of Experimental Medicine. 2005;201:1135–43.

34. Huebener P, Pradere J-P, Hernandez C, Gwak G-Y, Caviglia JM, Mu X, et al. The HMGB1/RAGE axis triggers neutrophil-mediated injury amplification following necrosis. J. Clin. Invest. 2015;125:539–50.

35. Yuan H, Jin X, Sun J, Li F, Feng Q, Zhang C, et al. Protective effect of HMGB1 a box on organ injury of acute pancreatitis in mice. Pancreas. 2009;38:143–8.

36. Sawa H, Ueda T, Takeyama Y, Yasuda T, Shinzeki M, Nakajima T, et al. Blockade of high mobility group box-1 protein attenuates experimental severe acute pancreatitis. World J. Gastroenterol. Baishideng Publishing Group Inc; 2006;12:7666–70.

37. Wang H, Bloom O, Zhang M, Vishnubhakat JM, Ombrellino M, Che J, et al. HMG-1 as a late mediator of endotoxin lethality in mice. Science. American Association for the Advancement of Science; 1999;285:248–51.

38. Alleva LM, Budd AC, Clark IA. Systemic release of high mobility group box 1 protein during severe murine influenza. J. Immunol. American Association of Immunologists; 2008;181:1454–9.

39. Jung JH, Park JH, Jee MH, Keum SJ, Cho M-S, Yoon SK, et al. Hepatitis C virus infection is blocked by HMGB1 released from virus-infected cells. J. Virol. American Society for Microbiology Journals; 2011;85:9359–68.

40. Achouiti A, van der Meer AJ, Florquin S, Yang H, Tracey KJ, van 't Veer C, et al. High-mobility group box 1 and the receptor for advanced glycation end products contribute to lung injury during Staphylococcus aureus pneumonia. Crit Care. BioMed Central; 2013;17:R296.

41. Kitahara T, Takeishi Y, Harada M, Niizeki T, Suzuki S, Sasaki T, et al. High-mobility group box 1 restores cardiac function after myocardial infarction in transgenic mice. Cardiovasc. Res. 2008;80:40–6.

42. Limana F, Germani A, Zacheo A, Kajstura J, Di Carlo A, Borsellino G, et al. Exogenous high-mobility group box 1 protein induces myocardial regeneration after infarction via enhanced cardiac C-kit+ cell proliferation and differentiation. Circ. Res. Lippincott Williams & Wilkins; 2005;97:e73–83.

43. Yanai H, Matsuda A, An J, Koshiba R, Nishio J, Negishi H, et al. Conditional ablation of HMGB1 in mice reveals its protective function against endotoxemia and bacterial infection. Proc. Natl. Acad. Sci. U.S.A. 2013;110:20699–704.

44. Bianchi ME, Crippa MP, Manfredi AA, Mezzapelle R, Rovere-Querini P, Vénéreau E. High-mobility group box 1 protein orchestrates responses to tissue damage via inflammation,

innate and adaptive immunity, and tissue repair. Immunol. Rev. John Wiley & Sons, Ltd (10.1111); 2017;280:74–82.

45. Murray EGD, Webb RA, Swann MBR. A disease of rabbits characterised by a large mononuclear leucocytosis, caused by a hitherto undescribed bacillus Bacterium monocytogenes (n.sp.). The Journal of Pathology and Bacteriology. 1926;29:407–39.

46. Schlech WF, Lavigne PM, Bortolussi RA, Allen AC, Haldane EV, Wort AJ, et al. Epidemic listeriosis--evidence for transmission by food. N. Engl. J. Med. 1983;308:203–6.

47. de Noordhout CM, Devleesschauwer B, Angulo FJ, Verbeke G, Haagsma J, Kirk M, et al. The global burden of listeriosis: a systematic review and meta-analysis. Lancet Infect Dis. 2014;14:1073–82.

48. Vázquez-Boland JA, Kuhn M, Berche P, Chakraborty T, Domínguez-Bernal G, Goebel W, et al. Listeria pathogenesis and molecular virulence determinants. Clin. Microbiol. Rev. 2001;14:584–640.

49. Agaisse H, Burrack LS, Philips JA, Rubin EJ, Perrimon N, Higgins DE. Genome-wide RNAi screen for host factors required for intracellular bacterial infection. Science. 2005;309:1248–51.

50. Pamer EG. Immune responses to Listeria monocytogenes. Nat. Rev. Immunol. 2004;4:812–23.

51. Mengaud J, Ohayon H, Gounon P, Mege R-M, Cossart P. E-cadherin is the receptor for internalin, a surface protein required for entry of L. monocytogenes into epithelial cells. Cell. 1996;84:923–32.

52. Lecuit M, Dramsi S, Gottardi C, Fedor-Chaiken M, Gumbiner B, Cossart P. A single amino acid in E-cadherin responsible for host specificity towards the human pathogen Listeria monocytogenes. EMBO J. 1999;18:3956–63.

53. Shen Y, Naujokas M, Park M, Ireton K. InIB-dependent internalization of Listeria is mediated by the Met receptor tyrosine kinase. Cell. 2000;103:501–10.

54. Bielecki J, Youngman P, Connelly P, Portnoy DA. Bacillus subtilis expressing a haemolysin gene from Listeria monocytogenes can grow in mammalian cells. Nature. 1990;345:175–6.

55. Domann E, Wehland J, Rohde M, Pistor S, Hartl M, Goebel W, et al. A novel bacterial virulence gene in Listeria monocytogenes required for host cell microfilament interaction with homology to the proline-rich region of vinculin. EMBO J. European Molecular Biology Organization; 1992;11:1981–90.

56. Kocks C, Gouin E, Tabouret M, Berche P, Ohayon H, Cossart P. L. monocytogenes-induced actin assembly requires the actA gene product, a surface protein. Cell. 1992;68:521–31.

57. Tripp CS, Wolf SF, Unanue ER. Interleukin 12 and tumor necrosis factor alpha are costimulators of interferon gamma production by natural killer cells in severe combined immunodeficiency mice with listeriosis, and interleukin 10 is a physiologic antagonist. Proceedings of the National Academy of Sciences. National Academy of Sciences; 1993;90:3725–9.

58. Murphy KP. Janeway's Immunobiology. 8 ed. New York: Garland Science, Taylor & Francis

Group, LLC; 2012.

59. Rogers HW, Callery MP, Deck B, Unanue ER. Listeria monocytogenes induces apoptosis of infected hepatocytes. The Journal of Immunology. 1996;156:679–84.

60. Heymer B, Wirsing von König CH, Finger H, Hof H, Emmerling P. Histomorphology of experimental listeriosis. Infection. Springer-Verlag; 1988;16 Suppl 2:S106–11.

61. Mandel TE, Cheers C. Resistance and susceptibility of mice to bacterial infection: histopathology of listeriosis in resistant and susceptible strains. Infect. Immun. American Society for Microbiology (ASM); 1980;30:851–61.

62. Portnoy DA. Innate immunity to a facultative intracellular bacterial pathogen. Curr. Opin. Immunol. 1992;4:20–4.

63. Shi C, Velázquez P, Hohl TM, Leiner I, Dustin ML, Pamer EG. Monocyte trafficking to hepatic sites of bacterial infection is chemokine independent and directed by focal intercellular adhesion molecule-1 expression. J. Immunol. American Association of Immunologists; 2010;184:6266–74.

64. Serbina NV, Salazar-Mather TP, Biron CA, Kuziel WA, Pamer EG. TNF/iNOS-producing dendritic cells mediate innate immune defense against bacterial infection. Immunity. 2003;19:59–70.

65. Serbina NV, Pamer EG. Monocyte emigration from bone marrow during bacterial infection requires signals mediated by chemokine receptor CCR2. Nat. Immunol. Nature Publishing Group; 2006;7:311–7.

66. Havell EA. Evidence that tumor necrosis factor has an important role in antibacterial resistance. The Journal of Immunology. 1989;143:2894–9.

67. Buchmeier NA, Schreiber RD. Requirement of endogenous interferon-gamma production for resolution of Listeria monocytogenes infection. Proceedings of the National Academy of Sciences. 1985;82:7404–8.

68. Pfeffer K, Matsuyama T, Kündig TM, Wakeham A, Kishihara K, Shahinian A, et al. Mice deficient for the 55 kd tumor necrosis factor receptor are resistant to endotoxic shock, yet succumb to L. monocytogenes infection. Cell. 1993;73:457–67.

69. Rothe J, Lesslauer W, Lötscher H, Lang Y, Koebel P, Köntgen F, et al. Mice lacking the tumour necrosis factor receptor 1 are resistant to TNF-mediated toxicity but highly susceptible to infection by Listeria monocytogenes. Nature. Nature Publishing Group; 1993;364:798–802.

70. Harty JT, Bevan MJ. Specific immunity to Listeria monocytogenes in the absence of IFN gamma. Immunity. 1995;3:109–17.

71. Rosen H, Gordon S, North RJ. Exacerbation of murine listeriosis by a monoclonal antibody specific for the type 3 complement receptor of myelomonocytic cells. Absence of monocytes at infective foci allows Listeria to multiply in nonphagocytic cells. Journal of Experimental Medicine. 1989;170:27–37.

72. Kurihara T, Warr G, Loy J, Bravo R. Defects in macrophage recruitment and host defense in mice lacking the CCR2 chemokine receptor. Journal of Experimental Medicine. 1997;186:1757–62.

73. Shi C, Hohl TM, Leiner I, Equinda MJ, Fan X, Pamer EG. Ly6G+ neutrophils are dispensable for defense against systemic Listeria monocytogenes infection. J. Immunol. 2011;187:5293–8.

74. Carr KD, Sieve AN, Indramohan M, Break TJ, Lee S, Berg RE. Specific depletion reveals a novel role for neutrophil-mediated protection in the liver during Listeria monocytogenes infection. Eur. J. Immunol. 2011;41:2666–76.

75. Okunnu BM, Berg RE. Neutrophils Are More Effective than Monocytes at Phagosomal Containment and Killing of Listeria monocytogenes. Immunohorizons. ImmunoHorizons; 2019;3:573–84.

76. Gregory SH, Sagnimeni AJ, Wing EJ. Bacteria in the bloodstream are trapped in the liver and killed by immigrating neutrophils. J. Immunol. 1996;157:2514–20.

77. Gregory SH, Cousens LP, van Rooijen N, Döpp EA, Carlos TM, Wing EJ. Complementary adhesion molecules promote neutrophil-Kupffer cell interaction and the elimination of bacteria taken up by the liver. The Journal of Immunology. American Association of Immunologists; 2002;168:308–15.

78. Nathan CF, Murray HW, Wiebe ME, Rubin BY. Identification of interferon-gamma as the lymphokine that activates human macrophage oxidative metabolism and antimicrobial activity. Journal of Experimental Medicine. 1983;158:670–89.

79. Martinez FO, Gordon S, Locati M, Mantovani A. Transcriptional profiling of the human monocyte-to-macrophage differentiation and polarization: new molecules and patterns of gene expression. The Journal of Immunology. American Association of Immunologists; 2006;177:7303–11.

80. MacMicking J, Xie QW, Nathan C. Nitric oxide and macrophage function. Annu. Rev. Immunol. Annual Reviews 4139 El Camino Way, P.O. Box 10139, Palo Alto, CA 94303-0139, USA; 1997;15:323–50.

81. Stein M, Keshav S, Harris N, Gordon S. Interleukin 4 potently enhances murine macrophage mannose receptor activity: a marker of alternative immunologic macrophage activation. Journal of Experimental Medicine. 1992;176:287–92.

82. Doherty TM, Kastelein R, Menon S, Andrade S, Coffman RL. Modulation of murine macrophage function by IL-13. The Journal of Immunology. 1993;151:7151–60.

83. Pesce JT, Ramalingam TR, Mentink-Kane MM, Wilson MS, Kasmi El KC, Smith AM, et al. Arginase-1-expressing macrophages suppress Th2 cytokine-driven inflammation and fibrosis. Kazura JW, editor. PLoS Pathog. 2009;5:e1000371.

84. Blériot C, Dupuis T, Jouvion G, Eberl G, Disson O, Lecuit M. Liver-Resident Macrophage Necroptosis Orchestrates Type 1 Microbicidal Inflammation and Type-2-Mediated Tissue Repair during Bacterial Infection. Immunity. Elsevier Inc; 2015;42:145–58.

85. Baker LA, Campbell PA, Hollister JR. Chemotaxigenesis and complement fixation by Listeria monocytogenes cell wall fractions. The Journal of Immunology. 1977;119:1723–6.

86. Shaughnessy LM, Swanson JA. The role of the activated macrophage in clearing Listeria monocytogenes infection. Front. Biosci. 2007;12:2683–92.

87. Blériot C, Lecuit M. The interplay between regulated necrosis and bacterial infection. Cell.

Mol. Life Sci. 2016;73:2369–78.

88. Kerr JF, Wyllie AH, Currie AR. Apoptosis: a basic biological phenomenon with wide-ranging implications in tissue kinetics. Br. J. Cancer. Nature Publishing Group; 1972;26:239–57.

89. Merrick JC, Edelson BT, Bhardwaj V, Swanson PE, Unanue ER. Lymphocyte apoptosis during early phase of Listeria infection in mice. Am. J. Pathol. American Society for Investigative Pathology; 1997;151:785–92.

90. Santos SAD, Andrade DR de, Andrade Júnior DR de. Rat hepatocyte invasion by Listeria monocytogenes and analysis of TNF-alpha role in apoptosis. Rev. Inst. Med. Trop. Sao Paulo. 2nd ed. Instituto de Medicina Tropical de São Paulo; 2005;47:73–80.

91. Santos dos SA, de Andrade Júnior DR, de Andrade DR. TNF-α production and apoptosis in hepatocytes after Listeria monocytogenes and Salmonella Typhimurium invasion. Rev. Inst. Med. Trop. Sao Paulo. 2nd ed. Instituto de Medicina Tropical de São Paulo; 2011;53:107–12.

92. Hansen K, Prabakaran T, Laustsen A, Jørgensen SE, Rahbæk SH, Jensen SB, et al. Listeria monocytogenes induces IFNβ expression through an IFI16-, cGAS- and STING-dependent pathway. EMBO J. 2014;33:1654–66.

93. Pattabiraman G, Palasiewicz K, Visvabharathy L, Freitag NE, Ucker DS. Apoptotic cells enhance pathogenesis of Listeria monocytogenes. Microbial Pathogenesis. Elsevier Ltd; 2017;105:218–25.

94. Margaroli C, Oberle S, Lavanchy C, Scherer S, Rosa M, Strasser A, et al. Role of proapoptotic BH3-only proteins in Listeria monocytogenes infection. Eur. J. Immunol. John Wiley & Sons, Ltd; 2016;46:1427–37.

95. Zheng S-J, Jiang J, Shen H, Chen YH. Reduced apoptosis and ameliorated listeriosis in TRAIL-null mice. The Journal of Immunology. American Association of Immunologists; 2004;173:5652–8.

96. Haslett C. Granulocyte apoptosis and its role in the resolution and control of lung inflammation. Am. J. Respir. Crit. Care Med. American Thoracic SocietyNew York, NY; 1999;160:S5–11.

97. Levine B, Kroemer G. Autophagy in the pathogenesis of disease. Cell. 2008;132:27–42.

98. Messer JS. The cellular autophagy/apoptosis checkpoint during inflammation. Cell. Mol. Life Sci. 2017;74:1281–96.

99. Kroemer G, Mariño G, Levine B. Autophagy and the integrated stress response. Mol. Cell. 2010;40:280–93.

100. Galluzzi L, Baehrecke EH, Ballabio A, Boya P, Bravo-San Pedro JM, Cecconi F, et al. Molecular definitions of autophagy and related processes. EMBO J. 2017;36:1811–36.

101. Yang Z, Klionsky DJ. Mammalian autophagy: core molecular machinery and signaling regulation. Curr. Opin. Cell Biol. 2010;22:124–31.

102. Huang J, Brumell JH. Bacteria-autophagy interplay: a battle for survival. Nat. Rev. Microbiol. Nature Publishing Group; 2014;12:101–14.

103. Randow F, Youle RJ. Self and nonself: how autophagy targets mitochondria and bacteria. Cell Host and Microbe. 2014;15:403–11.

104. Deretic V, Saitoh T, Akira S. Autophagy in infection, inflammation and immunity. Nature Publishing Group. Nature Publishing Group; 2013;13:722–37.

105. Yoshikawa Y, Ogawa M, Hain T, Yoshida M, Fukumatsu M, Kim M, et al. Listeria monocytogenes ActA-mediated escape from autophagic recognition. Nat. Cell Biol. Nature Publishing Group; 2009;11:1233–40.

106. Huebener P, Gwak G-Y, Pradere J-P, Quinzii CM, Friedman R, Lin C-S, et al. High-Mobility Group Box 1 Is Dispensable for Autophagy, Mitochondrial Quality Control, and Organ Function In Vivo. Cell Metab. Elsevier Inc; 2014;19:539–47.

107. Postic C, Shiota M, Niswender KD, Jetton TL, Chen Y, Moates JM, et al. Dual roles for glucokinase in glucose homeostasis as determined by liver and pancreatic beta cell-specific gene knock-outs using Cre recombinase. J. Biol. Chem. American Society for Biochemistry and Molecular Biology; 1999;274:305–15.

108. Clausen BE, Burkhardt C, Reith W, Renkawitz R, Förster I. Conditional gene targeting in macrophages and granulocytes using LysMcre mice. Transgenic Res. 1999;8:265–77.

109. Liu K, Mori S, Takahashi HK, Tomono Y, Wake H, Kanke T, et al. Anti-high mobility group box 1 monoclonal antibody ameliorates brain infarction induced by transient ischemia in rats. The FASEB Journal. 2007;21:3904–16.

110. Vaudaux P, Waldvogel FA. Gentamicin antibacterial activity in the presence of human polymorphonuclear leukocytes. Antimicrob. Agents Chemother. American Society for Microbiology (ASM); 1979;16:743–9.

111. Wang J, Vasaikar S, Shi Z, Greer M, Zhang B. WebGestalt 2017: a more comprehensive, powerful, flexible and interactive gene set enrichment analysis toolkit. Nucleic Acids Res. 2017;45:W130–7.

112. Calogero S, Grassi F, Aguzzi A, Voigtländer T, Ferrier P, Ferrari S, et al. The lack of chromosomal protein Hmg1 does not disrupt cell growth but causes lethal hypoglycaemia in newborn mice. Nat. Genet. Nature Publishing Group; 1999;22:276–80.

113. Yanai H, Matsuda A, An J, Koshiba R, Nishio J, Negishi H, et al. Conditional ablation of HMGB1 in mice reveals its protective function against endotoxemia and bacterial infection. Proceedings of the National Academy of Sciences. 2013;110:20699–704.

114. Wang D, Liu K, Wake H, Teshigawara K, Mori S, Nishibori M. Anti-high mobility group box-1 (HMGB1) antibody inhibits hemorrhage-induced brain injury and improved neurological deficits in rats. Scientific Reports. Nature Publishing Group; 2017;7:46243.

115. Fu L, Liu K, Wake H, Teshigawara K, Yoshino T, Takahashi H, et al. Therapeutic effects of anti-HMGB1 monoclonal antibody on pilocarpine-induced status epilepticus in mice. Scientific Reports. Nature Publishing Group; 2017;7:1179–13.

116. Dambach DM, Watson LM, Gray KR, Durham SK, Laskin DL. Role of CCR2 in macrophage migration into the liver during acetaminophen-induced hepatotoxicity in the mouse. Hepatology. 2002;35:1093–103.

117. Karlmark KR, Weiskirchen R, Zimmermann HW, Gassler N, Ginhoux F, Weber C, et al.

Hepatic recruitment of the inflammatory Gr1+ monocyte subset upon liver injury promotes hepatic fibrosis. Hepatology. 2009;50:261–74.

118. Deng M, Tang Y, Li W, Wang X, Zhang R, Zhang X, et al. The Endotoxin Delivery Protein HMGB1 Mediates Caspase-11-Dependent Lethality in Sepsis. Immunity. Elsevier; 2018;49:740–7.

119. Evankovich J, Cho SW, Zhang R, Cardinal J, Dhupar R, Zhang L, et al. High mobility group box 1 release from hepatocytes during ischemia and reperfusion injury is mediated by decreased histone deacetylase activity. J. Biol. Chem. 2010;285:39888–97.

120. Zimmermann HW, Tacke F. Modification of chemokine pathways and immune cell infiltration as a novel therapeutic approach in liver inflammation and fibrosis. Inflamm Allergy Drug Targets. 2011;10:509–36.

121. Liu F, Poursine-Laurent J, Wu HY, Link DC. Interleukin-6 and the granulocyte colony-stimulating factor receptor are major independent regulators of granulopoiesis in vivo but are not required for lineage commitment or terminal differentiation. Blood. 1997;90:2583–90.

122. Kaplanski G, Marin V, Montero-Julian F, Mantovani A, Farnarier C. IL-6: a regulator of the transition from neutrophil to monocyte recruitment during inflammation. Trends in Immunology. 2003;24:25–9.

123. Italiani P, Boraschi D. From Monocytes to M1/M2 Macrophages: Phenotypical vs. Functional Differentiation. Front. Immunol. Frontiers; 2014;5:514.

124. Mizushima N, Yoshimori T. How to interpret LC3 immunoblotting. Autophagy. Taylor & Francis; 2007;3:542–5.

125. Ishii T, Yanagawa T, Yuki K, Kawane T, Yoshida H, Bannai S. Low micromolar levels of hydrogen peroxide and proteasome inhibitors induce the 60-kDa A170 stress protein in murine peritoneal macrophages. Biochem. Biophys. Res. Commun. 1997;232:33–7.

126. Bjørkøy G, Lamark T, Brech A, Outzen H, Perander M, Overvatn A, et al. p62/SQSTM1 forms protein aggregates degraded by autophagy and has a protective effect on huntingtin-induced cell death. J Cell Biol. Rockefeller University Press; 2005;171:603–14.

127. Tang D, Kang R, Livesey KM, Cheh C-W, Farkas A, Loughran P, et al. Endogenous HMGB1 regulates autophagy. J Cell Biol. 2010;190:881–92.

128. Tang D, Kang R, Livesey KM, Kroemer G, Billiar TR, Van Houten B, et al. High-Mobility Group Box 1 Is Essential for Mitochondrial Quality Control. Cell Metab. Elsevier Inc; 2011;13:701–11.

129. Nagata S. Apoptotic DNA fragmentation. Exp. Cell Res. 2000;256:12–8.

130. Maródi L, Schreiber S, Anderson DC, MacDermott RP, Korchak HM, Johnston RB. Enhancement of macrophage candidacidal activity by interferon-gamma. Increased phagocytosis, killing, and calcium signal mediated by a decreased number of mannose receptors. J. Clin. Invest. American Society for Clinical Investigation; 1993;91:2596–601.

131. Thomas GR, McCrossan M, Selkirk ME. Cytostatic and cytotoxic effects of activated macrophages and nitric oxide donors on Brugia malayi. Infect. Immun. American Society for Microbiology (ASM); 1997;65:2732–9.

132. Martin SJ, Reutelingsperger CP, McGahon AJ, Rader JA, van Schie RC, LaFace DM, et al. Early redistribution of plasma membrane phosphatidylserine is a general feature of apoptosis regardless of the initiating stimulus: inhibition by overexpression of Bcl-2 and Abl. Journal of Experimental Medicine. 1995;182:1545–56.

133. Ginhoux F, Lim S, Hoeffel G, Low D, Huber T. Origin and differentiation of microglia. Front Cell Neurosci. Frontiers; 2013;7:45.

134. Bogunovic M, Ginhoux F, Wagers A, Loubeau M, Isola LM, Lubrano L, et al. Identification of a radio-resistant and cycling dermal dendritic cell population in mice and men. Journal of Experimental Medicine. 2006;203:2627–38.

135. Klein I, Cornejo JC, Polakos NK, John B, Wuensch SA, Topham DJ, et al. Kupffer cell heterogeneity: functional properties of bone marrow derived and sessile hepatic macrophages. Blood. 2007;110:4077–85.

136. Beattie L, Sawtell A, Mann J, Frame TCM, Teal B, de Labastida Rivera F, et al. Bone marrow-derived and resident liver macrophages display unique transcriptomic signatures but similar biological functions. Journal of Hepatology. 2016;65:758–68.

137. Tokunaga R, Zhang W, Naseem M, Puccini A, Berger MD, Soni S, et al. CXCL9, CXCL10, CXCL11/CXCR3 axis for immune activation - A target for novel cancer therapy. Cancer Treat. Rev. 2018;63:40–7.

138. Wang S, Song R, Wang Z, Jing Z, Wang S, Ma J. S100A8/A9 in Inflammation. Front. Immunol. 2018;9:1–14.

139. Kitchens RL. Role of CD14 in cellular recognition of bacterial lipopolysaccharides. Chem. Immunol. 2000;74:61–82.

140. Ranoa DRE, Kelley SL, Tapping RI. Human lipopolysaccharide-binding protein (LBP) and CD14 independently deliver triacylated lipoproteins to Toll-like receptor 1 (TLR1) and TLR2 and enhance formation of the ternary signaling complex. J. Biol. Chem. 2013;288:9729–41.

141. Rock KL, Latz E, Ontiveros F, Kono H. The sterile inflammatory response. Annu. Rev. Immunol. 2010;28:321–42.

142. Tsai S-Y, Segovia JA, Chang T-H, Morris IR, Berton MT, Tessier PA, et al. DAMP molecule S100A9 acts as a molecular pattern to enhance inflammation during influenza A virus infection: role of DDX21-TRIF-TLR4-MyD88 pathway. Gack MU, editor. PLoS Pathog. Public Library of Science; 2014;10:e1003848.

143. Jonsson N, Nilsen T, Gille-Johnson P, Bell M, Martling C-R, Larsson A, et al. Calprotectin as an early biomarker of bacterial infections in critically ill patients: an exploratory cohort assessment. Crit Care Resusc. 2017;19:205–13.

144. Bianchi ME. HMGB1 loves company. J. Leukoc. Biol. 2009;86:573–6.

145. Hreggvidsdottir HS, Ostberg T, Wähämaa H, Schierbeck H, Aveberger A-C, Klevenvall L, et al. The alarmin HMGB1 acts in synergy with endogenous and exogenous danger signals to promote inflammation. J. Leukoc. Biol. John Wiley & Sons, Ltd; 2009;86:655–62.

146. Tsan M-F. Heat shock proteins and high mobility group box 1 protein lack cytokine function. J. Leukoc. Biol. John Wiley & Sons, Ltd; 2011;89:847–53.

147. Pamer EG. Immune responses to Listeria monocytogenes. Nat. Rev. Immunol. 2004;4:812–23.

148. Yanai H, Matsuda A, An J, Koshiba R, Nishio J, Negishi H, et al. Conditional ablation of HMGB1 in mice reveals its protective function against endotoxemia and bacterial infection. Proc. Natl. Acad. Sci. U.S.A. National Academy of Sciences; 2013;110:20699–704.

149. Zheng YT, Shahnazari S, Brech A, Lamark T, Johansen T, Brumell JH. The adaptor protein p62/SQSTM1 targets invading bacteria to the autophagy pathway. J. Immunol. 2009;183:5909–16.

150. Homma T, Ishibashi D, Nakagaki T, Satoh K, Sano K, Atarashi R, et al. Increased expression of p62/SQSTM1 in prion diseases and its association with pathogenic prion protein. Scientific Reports. Nature Publishing Group; 2014;4:4504–7.

151. Lee H-M, Yuk J-M, Kim K-H, Jang J, Kang G, Park JB, et al. Mycobacterium abscessus activates the NLRP3 inflammasome via Dectin-1-Syk and p62/SQSTM1. Immunol. Cell Biol. John Wiley & Sons, Ltd; 2012;90:601–10.

152. Ogawa M, Yoshikawa Y, Mimuro H, Hain T, Chakraborty T, Sasakawa C. Autophagy targeting of Listeria monocytogenes and the bacterial countermeasure. Autophagy. Taylor & Francis; 2011;7:310–4.

153. Vogel S, Rath D, Borst O, Mack A, Loughran P, Lotze MT, et al. Platelet-derived high-mobility group box 1 promotes recruitment and suppresses apoptosis of monocytes. Biochem. Biophys. Res. Commun. 2016;478:143–8.

154. Tan J-Y, Zhao F, Deng S-X, Zhu H-C, Gong Y, Wang W. Glycyrrhizin affects monocyte migration and apoptosis by blocking HMGB1 signaling. Mol Med Rep. 2018;17:5970–5.

155. Geissmann F, Jung S, Littman DR. Blood monocytes consist of two principal subsets with distinct migratory properties. Immunity. 2003;19:71–82.

156. Serbina NV, Kuziel W, Flavell R, Akira S, Rollins B, Pamer EG. Sequential MyD88-independent and -dependent activation of innate immune responses to intracellular bacterial infection. Immunity. 2003;19:891–901.

157. Jia T, Serbina NV, Brandl K, Zhong MX, Leiner IM, Charo IF, et al. Additive roles for MCP-1 and MCP-3 in CCR2-mediated recruitment of inflammatory monocytes during Listeria monocytogenes infection. The Journal of Immunology. American Association of Immunologists; 2008;180:6846–53.

158. Fadok VA, Bratton DL, Konowal A, Freed PW, Westcott JY, Henson PM. Macrophages that have ingested apoptotic cells in vitro inhibit proinflammatory cytokine production through autocrine/paracrine mechanisms involving TGF-beta, PGE2, and PAF. J. Clin. Invest. American Society for Clinical Investigation; 1998;101:890–8.

159. Chinetti-Gbaguidi G, Baron M, Bouhlel MA, Vanhoutte J, Copin C, Sebti Y, et al. Human atherosclerotic plaque alternative macrophages display low cholesterol handling but high phagocytosis because of distinct activities of the PPARγ and LXRα pathways. Circ. Res. Lippincott Williams & Wilkins Hagerstown, MD; 2011;108:985–95.

160. Leidi M, Gotti E, Bologna L, Miranda E, Rimoldi M, Sica A, et al. M2 macrophages phagocytose rituximab-opsonized leukemic targets more efficiently than m1 cells in vitro. J. Immunol. 2009;182:4415–22.

161. Liu G, Wang J, Park YJ, Tsuruta Y, Lorne EF, Zhao X, et al. High Mobility Group Protein-1 Inhibits Phagocytosis of Apoptotic Neutrophils through Binding to Phosphatidylserine. The Journal of Immunology. 2008;181:4240–6.

162. Friggeri A, Yang Y, Banerjee S, Park Y-J, Liu G, Abraham E. HMGB1 inhibits macrophage activity in efferocytosis through binding to the α vβ 3-integrin. American Journal of Physiology-Cell Physiology. 2010;299:C1267–76.

163. Henson PM, Tuder RM. Apoptosis in the lung: induction, clearance and detection. Am. J. Physiol. Lung Cell Mol. Physiol. American Physiological Society; 2008;294:L601–11.

164. Kinchen JM, Ravichandran KS. Journey to the grave: signaling events regulating removal of apoptotic cells. J. Cell. Sci. 2007;120:2143–9.

165. Ravichandran KS, Lorenz U. Engulfment of apoptotic cells: signals for a good meal. Nature Publishing Group. Nature Publishing Group; 2007;7:964–74.

166. Wu Y, Tibrewal N, Birge RB. Phosphatidylserine recognition by phagocytes: a view to a kill. Trends Cell Biol. 2006;16:189–97.

167. Heng TSP, Painter MW, Immunological Genome Project Consortium. The Immunological Genome Project: networks of gene expression in immune cells. Nat. Immunol. Nature Publishing Group; 2008;9:1091–4.

168. Ryckman C, Robichaud GA, Roy J, Cantin R, Tremblay MJ, Tessier PA. HIV-1 transcription and virus production are both accentuated by the proinflammatory myeloid-related proteins in human CD4+ T lymphocytes. The Journal of Immunology. 2002;169:3307–13.

169. Lorey MB, Rossi K, Eklund KK, Nyman TA, Matikainen S. Global Characterization of Protein Secretion from Human Macrophages Following Non-canonical Caspase-4/5 Inflammasome Activation. Mol. Cell Proteomics. American Society for Biochemistry and Molecular Biology; 2017;16:S187–99.

170. Ombrellino M, Wang H, Ajemian MS, Talhouk A, Scher LA, Friedman SG, et al. Increased serum concentrations of high-mobility-group protein 1 in haemorrhagic shock. Lancet. 1999;354:1446–7.

171. Abeyama K, Stern DM, Ito Y, Kawahara K-I, Yoshimoto Y, Tanaka M, et al. The N-terminal domain of thrombomodulin sequesters high-mobility group-B1 protein, a novel antiinflammatory mechanism. J. Clin. Invest. American Society for Clinical Investigation; 2005;115:1267–74.

172. Qin S, Wang H, Yuan R, Li H, Ochani M, Ochani K, et al. Role of HMGB1 in apoptosis-mediated sepsis lethality. Journal of Experimental Medicine. Rockefeller University Press; 2006;203:1637–42.

173. Levy RM, Mollen KP, Prince JM, Kaczorowski DJ, Vallabhaneni R, Liu S, et al. Systemic inflammation and remote organ injury following trauma require HMGB1. Am. J. Physiol. Regul. Integr. Comp. Physiol. American Physiological Society; 2007;293:R1538–44.

174. Maeda S, Hikiba Y, Shibata W, Ohmae T, Yanai A, Ogura K, et al. Essential roles of high-mobility group box 1 in the development of murine colitis and colitis-associated cancer. Biochem. Biophys. Res. Commun. 2007;360:394–400.

175. Yang R, Miki K, Oksala N, Nakao A, Lindgren L, Killeen ME, et al. Bile high-mobility group

box 1 contributes to gut barrier dysfunction in experimental endotoxemia. Am. J. Physiol. Regul. Integr. Comp. Physiol. American Physiological Society; 2009;297:R362–9.

# VI. Publication List

## Publications

**Leukocyte-derived High-mobility group box 1 governs hepatic immune responses to Listeria monocytogenes**
Volmari A, Foelsch K, Zierz E, Yan K, Qi M, Bartels K, Kondratowicz S, Boettcher M, Reimers D, Nishibori M, Liu K, Schwabe R, Lohse A, Huber S, Mittruecker HW, Huebener P
Hepatol Commun. 2021 Dec;5(12):2104-2120. doi: 10.1002/hep4.1777.

**Control of Listeria monocytogenes infection requires classical IL-6 signaling in myeloid cells**
Lücke K, Yan I, Krohn S, Volmari A, Klinge S, Schmid J, Schumacher V, Steinmetz OM, Rose-John S, Mittrücker HW
PLoS One. 2018 Aug 31;13(8):e0203395. doi: 10.1371/journal.pone.0203395.

## Congress presentations

| | |
|---|---|
| 26.-27.01.2018<br>Hamburg, Germany | **Jahrestagung der Deutschen Arbeitsgemeinschaft zum Studium der Leber** [poster]<br>**The nucleoprotein High-mobility group box 1 critically regulates the immune response to bacterial infection**<br>Volmari A, Luecke K, Mittruecker HW, Schwabe RF, Wake H, Nishibori M, Lohse AW, Huebener P |
| 12.-15.09.2017<br>Erlangen, Germany | **Jahrestagung der Deutschen Gesellschaft für Immunologie** [oral presentation]<br>**HMGB1 regulates the immune response to bacterial infection**<br>Volmari A, Luecke K, Mittruecker HW, Schwabe RF, Arnold B, Lohse AW, Huebener P |
| 19.-23.04.2017<br>Amsterdam, Netherlands | **2017 EASL The International Liver Congress**<br>[poster presentation; EASL travel grant]<br>**The nucleoprotein High-mobility group box 1 critically regulates the immune response to bacterial infection**<br>Volmari A, Luecke K, Mittruecker HW, Lohse AW, Huebener P |

# VII. Acknowledgements

Mein Dank gilt zunächst Prof. Dr. Lohse dafür, dass ich diese Doktorarbeit in seinem Labor anfertigen durfte.

Bei Dr. Peter Hübener möchte ich mich dafür bedanken, dass er dieses Thema ausgeschrieben und damit diese Doktorarbeit möglich gemacht hat. Darüber hinaus möchte ich mich für die Betreuung während der letzten Jahre bedanken.

Ich bedanke mich bei Prof. Dr. Johannes Herkel für die Begutachtung meiner Arbeit und die stets offene Tür bei Fragen und Problemen. Ebenso möchte ich mich bei Prof. Dr. Wolfgang Streit für die Begutachtung meiner Dissertation bedanken.

Ich möchte mich bei allen Mitarbeitern im Labor für die tolle Arbeitsatmosphäre bedanken. Mein besonderer Dank geht dabei an Katharina Fölsch, Stephanie Kondratowiscz und Karlotta Bartels für die super Zusammenarbeit sowie ihre unermüdliche Hilfsbereitschaft und Unterstützung über die letzten Jahre. Außerdem danke ich Karsten Yan für seine Hilfe bei den Infektionen.

Besonders danke ich auch bei Jennifer Wigger, Sabrina Kreß, Anja Koop, Daria Krzikalla, Stephanie Stein und Katja Giersch für den Austausch, die Aufmunterung und die Freundschaft. Außerdem möchte ich mich bei meinen Freunden außerhalb des Labors bedanken, insbesondere Steffeni Mountford, für ihr Verständnis und ihre Unterstützung.

Abschließend bin ich meiner Familie, meinen Eltern Birgit und Heinz Volmari, sowie meinen Geschwistern Wiebke und Henrik Volmari, dankbar, dass sie mich auf all meinen Wegen immer unterstützt haben